Aus dem Department für Augenheilkunde Tübingen

Forschungsinstitut für Augenheilkunde

Direktor: Professor Dr. M. Ueffing

Molecular mechanisms in inherited retinal degeneration: Exploring three routes towards understanding Retinitis pigmentosa

Inaugural-Dissertation
zur Erlangung des Doktorgrades
der Humanwissenschaften

der Medizinischen Fakultät
der Eberhard Karls Universität
Tübingen

vorgelegt von

Pietro Farinelli

aus Comacchio

2013

Dekan:	Professor Dr. I. B. Autenrieth
1. Berichterstatter:	Professor Dr. Dr. h. c. E. Zrenner
2. Berichterstatter:	Professor Dr. Dr. P. Ruth

To my two families

TABLE OF CONTENTS

Abbreviations

5hmC	5-hydroxymethylcytosine
5mC	5-methylcytosine
ABCR	ATP binding cassette transport
AC	Amacrine cell
AIF	Apoptosis-inducing factor
Akt	Protein kinase B
ALAS1	Aminolevulinic acid synthase1
BBS	Bardet-Biedl's disease
BC	Bipolar cell
BSA	Bovine serum albumin
CaMKII	Calmodulin kinase II
CBP	CREB-binding-protein
ChR2	Channelrhodopsin-2
cGMP	Cyclic GMP
CNG	cGMP cation-gated channel
CNTF	Ciliary neurotrophic factor
CRALBP	Cellular retinaldehyde binding protein
CREB	Cyclic AMP-response-element-binding
CRX	Cone-rod-homeobox
DIV	Days *in vitro*
DMSO	Dimethyl sulphoxide
DNMT	DNA methyltransferase
ERG	Electroretinogram
ERK	Extracellular-signal-regulated kinase
FGF	Fibroblast growth factor
FGF15	Fibroblast growth factor 15
GAPDH	Glyceraldehyde 3-phosphate dehydrogenase
$G\alpha_t$	Transducin
GC	Guanylate cyclase
GCAP	Guanylate cyclase activating protein
GCs	Ganglion cell
GCL	Ganglion cell layer

GGA	Geranylgeranylacetone
GPCR	G protein-coupled receptor
HC	Horizontal cell
HDAC	Histone deacetylase
HE	Hematoxilin-eosin
HPLC	High performance liquid chromatography
HSF1	Heat shock factor 1
Hsp40	Heat shock protein 40 kDa
Hsp70	Heat shock protein 70 kDa
Hsp90	Heat shock protein 90 kDa
IGF-1	Insulin-like growth factor 1
INL	Inner nuclear layer
IPL	Inner plexiform layer
IRBP	Interphotoreceptor retinoid binding protein
IS	Inner segment
LCAT	lecithin:retinol acyltransferase
Lctl	Klotho/lactase-phlorizin hydrolase-related protein
MC	Müller cell
MeDIP	Methylated DNA immunoprecipitation
MS	Mass spectrometry
NAD^+	Nicotinamide dinucleotide
NAM	Nicotinamide
NFL	Nerve fibre layer
NO	Nitric oxide
OLM	Outer limiting membrane
ONL	Outer Nuclear layer
OPL	Outer plexiform layer
OS	Outer segment
PARP	Poly (ADP-ribose) polymerase
PBS	Phosphate saline buffer
PCR	Polymerase-chain reaction
PDE6	Phosphodiesterase 6
PFA	Paraformaldeheyde
PKCθ	Protein kinase C theta

PKG	cGMP-activated protein kinase
PN	Post natal day
pPKCα/βII	Phosphorylated Protein kinase C α and βII
PRPH2	Peripherin 2
PR	Photoreceptor
PT	Phototransduction
PTX	PBS-triton X100
qPCR	Quantitative PCR
RD	Retinal degeneration
RDH	all-*trans*-retinol dehydrogenase
Rec	Recoverin
Rho	Rhodopsin
RIG-I	Retinoic-acid-inducible gene-I
RK	Rhodopsin kinase
RP	Retinitis Pigmentosa
RPE	Retinal pigment epithelium
RPE65	Retinal pigment epithelium-specific 65 kDa protein
RPGR	Retinitis Pigmentosa GTPase regulator
RT	Room temperature
RT-PCR	Reverse transcriptase PCR
SD	Standard deviation
SDS-PAGE	Sodium-dodecyl-sulphate Polyacrylamide gel electrophoresis
SEM	Standard error of the mean
TET	Ten-eleven translocation
TBS	Tris-buffered saline
TSA	Trichostatin A
TUNEL	Terminal dUTP nick-end labeling
UPR	Unfolded protein response
USH	Usher’s disease

1. Introduction

1.1 Retinitis Pigmentosa

The retina is the photosensitive organ at the back of the eye and it is crucial for our ability to see. Retinal degeneration (RD) represents a process in which photoreceptors (rods and cones) and/or other retinal cells die. This condition groups together a number of independent inherited diseases including retinitis pigmentosa (RP) and Leber's congenital amaurosis, as well as non-inherited diseases or conditions such as retinal detachment and diabetic retinopathy. All share the common feature of loss of vision, although in different forms and likely by different mechanisms. The work presented in the present thesis specifically investigates RP, which is therefore the focus of this introduction. RP refers to a group of diseases that provoke a slow but irreversible loss of vision, and represents the leading cause of inherited blindness in the developed world, where it affects about 1.5 million people, and with a prevalence of about 1:4000. There are already many mutations in many genes known to cause the disease, and more are expected to be identified in the future. Despite this vast knowledge, the mechanisms leading to photoreceptor degeneration as a result of the mutations are still largely unknown and there is currently no treatment available.

Typically, the disease progression in RP has a two-step form; first there is death of rod photoreceptors (PR) in a mutation-dependent fashion, which is followed by a secondary degeneration of cone photoreceptors, even though these cells may not be primarily affected by the mutation. This pattern of photoreceptor cell death (rod-cone) initially leads to a loss of night vision and then, secondarily, to a restriction of the visual field followed by complete blindness. The disease can be inherited as an autosomal-dominant (AD), autosomal-recessive (AR), or X-linked trait (Hartong et al., 2006), the first of which is usually the mildest form. RP is generally inherited by mendelian ratios, but in a few cases mutations in certain genes can lead to both the AD and the AR form (Hamel, 2006).

Many researchers categorize RP into two main groups: isolated (confined to the eye) and syndromic (when mutations can additionally lead to abnormalities in other organ systems). It is generally considered that 70-80 % of all RP cases fall into the category of nonsyndromic (isolated) rod-cone degeneration, or dystrophy. However, some syndromic forms of RP valid a mention here. Usher's disease (USH) groups together

a family of autosomal recessive diseases (Usher, 1914), clinically and genetically highly heterogeneous but all related by dysfunctions of cilia. They are characterized by loss of vision due to RD as well as hearing loss during late childhood due to degeneration of inner ear cells. Together with USH, Bardet-Biedl's syndrome (BBS) is the major cause of syndromic retinal dystrophy. Being classified as a cone-rod dystrophy (*i.e.* RD characterized by primary cone cell loss or by concomitant loss of both photoreceptors types), BBS is a highly disabling ciliopathy. The RD in BBS patients is very quick, with complete blindness occurring within the second decade of life, and the clinical features also include obesity, polydactily, renal failure, hypogonadism and cognitive impairment (Mockel et al., 2011).

Although RP is a highly variable disorder, most patients having the isolated form fall into a classic pattern of night blindness and difficulties with dark adaptation in adolescence and loss of mid-peripheral visual field in young adulthood. Some patients however, remain asymptomatic until adulthood, whereas others develop symptomatic visual loss already during infancy. Either way, as the disease advances patients develop restriction of the visual field (tunnel vision), and finally lose central vision (Hartong et al., 2006).

The reason for why cone photoreceptors die in a mutation-independent fashion in RP is still an open question, but a number of theories have been proposed. Cone degeneration may be a consequence of the release of some detrimental molecule or the loss of a survival factor due to the ongoing death of rods (Mohand-Said et al., 1998, Leveillard et al., 2004), or perhaps oxidative stress is a contributing factor (Komeima et al., 2006). For the latter, during rod degeneration the oxygen supply from the choroid blood vessels via the retinal pigmented epithelium (RPE) to photoreceptors remains constant, which thus could overload the remaining cones with oxygen (Yu and Cringle, 2005).

While there for decades have been clinical trials for RP treatments, there is today still no therapy or cure available for RP patients. At the experimental level, however, scientists have recently used gene therapy (Beltran et al., 2012, Koch et al., 2012, Wert et al., 2013), stem cells (Li et al., 2012) and optogenetics derived strategies (Tomita et al., 2009, Busskamp and Roska, 2011), and some of these are likely to advance into the clinic in the foreseeable future. Neuroprotection is a different strategy based on use of drugs, growth/neurotrophic factors or antioxidants in order to

counteract retinal degeneration. One of the most successful and promising neuroprotective approaches refers to the use of ciliary neurotrophic factor (CNTF) delivered by cells transfected with the human CNTF gene (Sieving et al., 2006), which is currently in clinical trials. The body of work of this thesis will focus on the finding and molecular analysis on new targets for retinal neuroprotective strategies.

1.2 General anatomy of the eye

In order to understand and visualize what occurs during RP, it is necessary to be aware of the anatomy and physiology of the human eye, and the next chapters will give a brief overview of these topics.

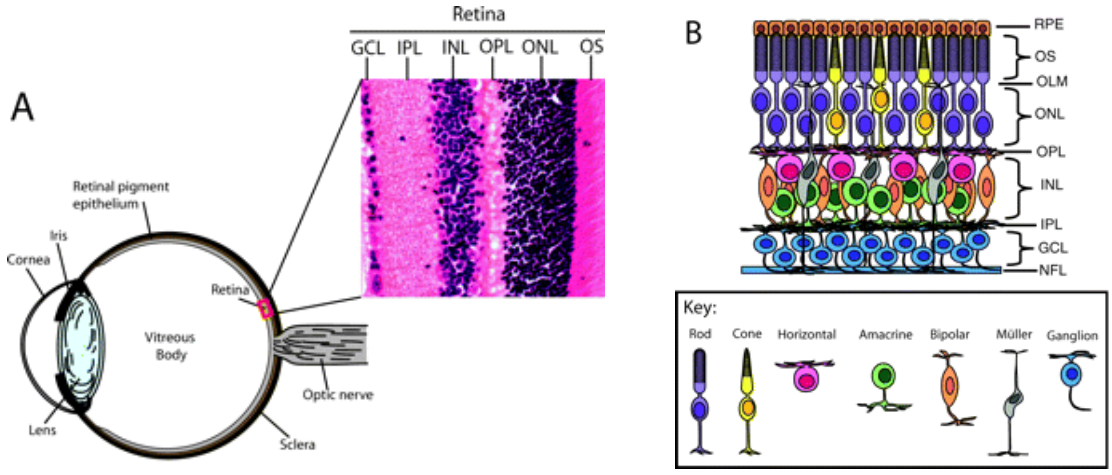

***Figure 1.1**. A) Representation of a sagittal section of a human eye and retina. B) Drawing of the layout of a human retina*. RPE = retinal pigment epithelium; OS = outer segments; OLM = outer limiting membrane; ONL = outer nuclear layer; OPL = outer plexiform layer; INL = inner nuclear layer; IPL = inner plexiform layer; GCL = ganglion cell layer; NFL = nerve fibre layer. (Poché and Reese, 2009)

The vertebrate eye is a roughly spherical-shaped, complex organ that enables vision by channelling and focusing light on its photosensitive retina. Figure 1.1 shows a schematic diagram of a human eye. At the outermost side there is the cornea, a transparent structure that covers the inner tissues and eye components and refracts the light entering into the eye. Continuous with the borders of the cornea is the sclera, which is a fibrous, protective tissue that in humans has a characteristic white, opaque colour. It provides protection to the eye and an attachment for the extraocular muscles, which allow eye movements. The visible part of the sclera and the inner part

of the eyelids are covered by the conjunctiva, a mucous membrane that lubricates the eye and acts as immune barrier. The iris, which is visible through the cornea, is a circular coloured structure composed of smooth muscle and connective tissue. In response to light intensity, the iris can contract or relax and therefore modify the size of the pupil, a round aperture by which photons can enter the eye, so that the amount of light passing through the eye is regulated. Immediately behind the iris sits the crystalline lens, which is a transparent structure held in position by suspensory ligaments. By changing its shape the refractive lens allows light to be correctly focused on the retina. Between the cornea and the iris and between the iris and the lens there are the anterior and posterior chambers, respectively, which are both filled with a clear and gelatinous fluid, the aqueous humour. The eyeball cavity, between the crystalline lens and the back of the eye, is filled with vitreous humour, a gelatinous transparent fluid primarily composed of water with minimal cell content, and which maintains the retina in position. The vitreous reaches back to the photosensitive organ of the eye, the retina. This is a very complex organ composed of several neuronal cell types and synaptic terminals, finely organized in layers with a range of interconnections. The retina is the focus of this thesis and is therefore discussed in greater detail below. Finally, between the retina and the sclera lies the choroid, a vascular and connective tissue layer, which provides nutrients and oxygen to the outer layers of the retina, a task which for the inner layers is served by vessels running within the eye.

1.3 Functions of the retina

The retina is organized in several layers with different but functionally interconnected cell types (Figure 1.1 B). This organization allows the neuronal impulse initiated by the photoreceptors to be suitably processed by the other retinal cells and transmitted to the optic nerve. Via the latter, the electro-chemical signal finally reaches the visual cortex of the brain, where it creates a representation of the environment, *i.e.* what we refer to as vision.

Retinal Pigment Epithelium

The outermost part of the retina, in contact with the choroid, is the retinal pigment epithelium (RPE), which consists of a single layer of epithelial cells (Caldwell et al.,

1982). The RPE performs functions in support of the photoreceptors. It is the center of the visual cycle, a group of biochemical reactions aimed at the regeneration of the consumed retinal co-factor (see "Visual Cycle" below). The RPE also provides nourishment to the PRs and allows ion buffering (Steinberg et al., 1983) as well as contains phagocytic organelles, that play a role in the turnover of the outer segment of the PRs (Sparrow et al., 2010). By means of the pigment melanin the RPE absorbs scattered light, improving the quality of the optical system (Bülow, 1968) and it expresses and secretes a wide range of neuroactive factors (Strauss, 2005). Finally it offers immune privilege to the inner eye (Streilein et al., 2002).

Photoreceptors

The photoreceptors (PRs) are the main light capturing cells of the retina. The PRs are contained in the outer nuclear layer (ONL), with their inner and outer segments (IS and OS, respectively, figure 1.1 B) pointing outwards from this. They are roughly classified in function of the intensity of light they are able to detect: rods that work in dim light and play a role in night vision; cones, which work in bright light and allow distinction of colours and provide visual acuity. Also cone PRs can be sub-classified depending on the wavelength they can absorb: L-, M- and S-cones, which absorb long, medium and short wavelength radiations, respectively. Both types of PRs also have a cell body and a synaptic termination.

The OS of a PR is a cilium modified in order to maximize light detection. The rod OS is cylindrical, about 1,4 μm in diameter and 24 μm in length, and filled with around 1,000 lamellar-shaped membrane discs (Sung and Tai, 2000, Carter-Dawson and Lavail, 1979). The rhodopsin (Rho) visual pigment accounts for about 95 % of the disc proteins in rods (Sung and Chuang, 2010). The organization of the OSs and the huge density of Rho together make rods very sensitive, to the extent that they are able to detect a single photon of light. Cone OSs have a different morphology in that they are shorter (Carter-Dawson and Lavail, 1979), and the membrane discs are continuous with the membrane of the OS itself (Mustafi et al., 2009).

The membrane discs require constant turnover. The distal portion of an OS is in direct contact with the apical processes of an RPE cell, and this arrangement allows the tips of aged OSs to be phagocytosed by the neighboring RPE cells in a mechanism still not fully elucidated. The OS of a vertebrate PR cell is connected to its IS by the so

called connecting cilium, which harbours a component of the cytoskeleton of the OS and represents the major route by which various components from other parts of the cell can reach the OS (Liu et al., 1999).

The IS is the sub-compartment of a PR in which the majority of the metabolic, biosynthetic and endocytotic functions take place. In fact, the PR has an extraordinary energy need and a huge population of mitochondria are present in the IS. Biosynthesis of visual pigments takes place in the Golgi apparatus of IS from where they are transported in vesicles to the connecting cilium, which uses myosin VIIa as a molecular motor for transportation into the OS (Deretic et al., 1995). The cell body of the PRs essentially contains the nucleus with very limited cytoplasm.

Outer plexiform layer

The task of PRs is of course to detect light and to convert this light into an electro-chemical signal (described below), but they must additionally transmit this signal to second order retinal neurons in the inner nuclear layer (INL). This transfer takes place in the outer plexiform layer (OPL), which is the first transmission/integration point for the visual signal. It is represented by the synaptic terminations of the PRs and their contacts with cells of the INL. Rods and cones differ in the number of connections they have with the inner retinal neurons (Rao-Mirotznik et al., 1995, Sterling and Matthews, 2005, Ahnelt and Kolb, 1994).

Inner nuclear layer

The INL holds the cell bodies of horizontal cells, bipolar cells and amacrine cells as well as Müller glial cells.

Horizontal cells (HCs). The HCs lie in the outermost part of the INL and represent the smallest cellular population of the neuroretina (Strettoi and Masland, 1995, Jeon et al., 1998). HCs laterally interconnect a large number of neurons using γ-aminobutyric acid (GABA) as a neuromodulator. This helps integrating the PRs input and allows fine regulation in both dim and bright light. HCs produce lateral inhibition adjusting the overall level of illumination (Masland, 2001) and may as such help creating contrast.

Bipolar cells (BCs). BCs are composed of a central cell body and two diametrically opposed processes that receive information from the PRs and transmit it to the

innermost retinal layers, respectively. Their cell bodies are situated in the outer portion of the INL and they synapse with rods, cones and HCs. While there is just one subtype of BC that connects with rods, in mammals ten different cone BCs are known. Functionally the BCs are subdivided into ON and OFF (Miller, 2008), because they express two different types of receptors for the neurotransmitter glutamate released by the PRs: an ionotropic glutamate receptor that opens cation channels and depolarizes the cell (OFF), and a metabotropic glutamate receptor, which hyperpolarizes the cell when stimulated (ON) (Nawy and Jahr, 1990, Nawy and Jahr, 1991). Rod BCs themselves release glutamate as an excitatory neurotransmitter to the next neuron in the chain (see "Ganglion cell layer").

Amacrine cells (ACs). The ACs are interneurons synaptically active in the inner plexiform layer, where they communicate between BCs and ganglion cells (below), contributing to signal integration. There are a wide range of AC types, which contact other retinal neurons with a variety of different neurotransmitters. The primary function of ACs is the fine tuning of retinal responsiveness in both dim and bright light (Ehinger, 1983).

Inner plexiform layer

The inner plexiform layer (IPL) consists of a tangle of processed coming from the processes of the INL cells as well as the ganglion cells (see next section). The resulting synaptic connections are regulated by many kinds of neurotransmitters/neuromodulators, with very individual functions and messages. Probably the most dominant is glutamate, the prototypical neurotransmitter of the vertical, straightforward pathway through the retina used by all PR types (Massey and Redburn, 1987) and by BCs as well. Others identified include GABA, glycine, dopamine, acetylcholine, serotonin, adenosine, and various neuropeptides (Wässle et al., 2009, Djamgoz and Wagner, 1992, Famiglietti Jr, 1983, Vaney and Young, 1988, Marc et al., 1995, Blazynski and Perez, 1991, Sagar, 1987, Marshak, 1989).

Ganglion cell layer

Ganglion cells (GCs) are the predominant cellular population (in mouse retina one can find displaced ACs) of the ganglion cell layer (GCL), the innermost retinal layer, and they represent the final retinal output. The dendrites of GCs receive the information from the PRs via the INL cells and forward this through the optic nerve.

The latter is composed of GC axons, which terminate in the lateral geniculate nucleus and the superior colliculus of the brain. The GCs are heterogeneous (Wassle and Boycott, 1991) and every sub-type can execute a separate and specific task. Generally, GCs provide information on contrast, colour and visual acuity (Sernagor et al., 2001).

Retinal glial cells

In addition to the RPE cells, there are three different non-neuronal cell types within the retina. They are all glial cells and their main characteristics are described below.

Müller cells (MCs). These are derived from the same progenitor cells as retinal neurons (Turner and Cepko, 1987) and represent the main glial cell of the retina. They provide structural support extending radially throughout the layers of the retina (Newman and Reichenbach, 1996). At the position between the IS and PR cell body, there are gap junctions between individual MCs and between MCs and PRs, and these form the outer limiting membrane (OLM). The innermost ends of MCs display conical endfeet, which give rise to the inner limiting membrane (ILM). The apical part of the MCs, facing the RPE, extends with villi outgrowths into the subretinal space. As well as structural support, MCs have several other essential functions for the health of the retina (Reichenbach and Robinson, 1995), including the supply of components for the production of energy, the clearing of waste products and the recycling of neurotransmitters, which protects the neurons from the excess of glutamate. The MCs are additionally involved in the release of neuroactive substances and in ionic buffering, and may also work as optical fibers conveying the light to the PRs (Franze et al., 2007).

Astrocytes. Astrocytes enter the developing retina from the brain along with the development of the optic nerve (Stone and Dreher, 1987). Astrocyte cell bodies and processes are almost entirely restricted to the nerve fiber layer of the retina (Schnitzer, 1988), which is the innermost part of the retina. The astrocytes function as nerve and vascular glial sheaths enveloping GC axons and blood vessels and they form part of the blood-brain barrier (here the blood-retina barrier). Like MCs, they are a source of glycogen and may provide raw material for the production of energy in the retinal neurons. Moreover, astrocytes are able to control the ionic homeostasis and the metabolism of the neurotransmitter GABA.

Microglia (Mgs). Mgs are phagocytic sentinels in the central nervous system and in the retina, required for neuronal homeostasis and innate immune defense and represent the resident mononuclear phagocytes of the nervous system. They infiltrate the retina during development (Kaur et al., 2001), colonizing every layer. Mgs can take on different morphologies as a function of the position and activity they are carrying out, and in retina they are usually found in a quiescent state in the IPL. In the situation of PR degeneration (Langmann, 2007), the Mgs migrate towards the ONL, where they can phagocyte cellular debris, producing pro-inflammatory chemokines and in the long term possibly provoking chronic inflammation (Karlstetter et al., 2010)

1.4 Phototransduction

According to the International Lighting Vocabulary, light is defined as "*Any radiation capable of causing a visual sensation directly*". For humans, visible light is in the wavelength range of 380-740 nm, *i.e.* between the invisible infrared (IR) and the invisible ultraviolet (UV) wavelengths. Visible light may be absorbed in "quanta", referred to as photons. The human retina is not sensitive to IR because at these wavelengths there is not enough energy for the activation of visual pigments, whereas UV radiation cannot be seen as other tissues of the eye absorb this.

Vision is the final outcome of phototransduction (PT), a process by which a photon of light is converted into an electro-chemical signal by photosentive cells. This requires visual pigments, and for the rod PRs this was discovered during the end of the 19th century and named visual purple (Kuhne, 1879). Later this was renamed rhodopsin (Rho) and acknowledged as the first identified G protein-coupled receptor. Rho in turn consists of a protein, opsin, and a chromophore, retinal, which is the actual light sensitive molecule. The PT cascade in both types of PRs is produced by a transient decrease in cGMP concentration, mediated by four finely regulated molecular events: cascade activation, amplification, cascade inactivation, and cGMP restoration. The interplay among these reactions determines the dynamics of the photoreceptive cells in response to light. As this thesis is primarily concerned with rods, the rod PT pathway will be described below.

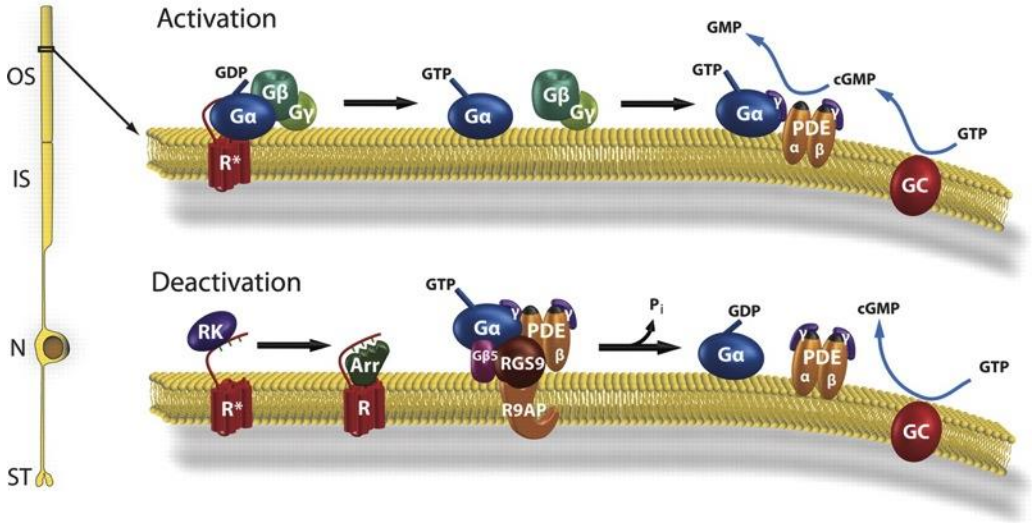

***Figure 1.2**. Activation and deactivation of the phototransduction cascade (Arshavsky and Burns, 2012).*

Activation. In complete darkness, the balance between cGMP synthesis, by guanylyl cyclase (GC), and hydrolysis, by cGMP phosphodiesterase 6 (PDE6), produces a steady level of cGMP. The inward current through cGMP-gated cation channels (CNG) maintains a partial depolarization of the PRs, and the synaptic endings of such unstimulated PRs release Glu. In the classical and straightforward information pathway through the retina (the so called ON-pathway), the released glutamate has an inhibitory action on the postsynaptic inner retinal neurons. When a photon of light hits the photosensitive pigment Rho, it causes the rapid isomerization of the chromophore from the 11-*cis*-retinal to the all-*trans*-retinal configuration (Wald, 1968). This puts Rho in a state where it is able to promote activation of the G protein transducin ($G\alpha_t$), which in turn binds the γ inhibitory subunit of PDE6 (Arshavsky et al., 2002). The γ subunit is then released from the catalytic subunits α and β of the PDE6, which quickly hydrolyzes cGMP to GMP, thereby provoking the closure of CNG. The consequent reduction of cation influx causes an electro-chemical signal represented by membrane hyperpolarization and depression of glutamate release at the synaptic termination. The inhibitory glutamate action is thus lifted and the visual signal can propagate to second order neurons in the INL for further transmission to the visual cortex of the brain.

Amplification. The hallmark of the PT cascade is a high degree of signal amplification, which is indispensable for generating a sizable response to the absorption of a single quantum of light. The amplification of PT signalling is achieved

by means of four components: Rho, $G\alpha_t$, PDE6 and CNG channels. A single Rho has the ability to activate a large number of $G\alpha_t$ molecules (Heck and Hofmann, 2001), which in turn works at a rate greatly higher than any other G protein signaling pathway (Bhandawat et al., 2005). The extent of signal amplification provided by PDE6 is not less important. Studies on amphibian retina showed that a single $G\alpha_t$-PDE6 interaction provokes the hydrolysis of more than 600 cGMP molecules per second (Leskov et al., 2000). Last, cGMP-gated channels give an additional and final amplification, due to the steep concentration gradient of the extracellular cations that can now enter the cell.

Inactivation. In order to allow photoreceptors to respond to subsequent photons, the inward current must rapidly return to basal level, but the PT persists until all the components of the cascade are properly inactivated and recycled. The first step toward inactivation occurs when Rho is phosphorylated by Rhodopsin kinase (RK), a membrane-associated enzyme. In the dark, RK is associated with the Ca^{2+} binding protein Recoverin (Rec), which inhibits the RK (Chen et al., 1995). After photo-activation, the intracellular levels of Ca^{2+} plummet, thus decreasing the affinity of the Rec-RK complex allowing RK to phosphorylate Rho. Phosphorylated Rho is then bound at high-affinity by a protein called arrestin, which prevents residual $G\alpha_t$ activation (Vishnivetskiy et al., 2000).

cGMP restoration. In order to reset the system, the restoration of cGMP to the higher basal level is necessary and this is accomplished by retinal GCs. As light provokes dramatic reduction of Ca^{2+} in the OSs, this is detected by another family of Ca^{2+} binding proteins called GC activating proteins (GCAPs) (Palczewski et al., 1994). In the dark these proteins are bound with abundant Ca^{2+}, and inhibit GC activities. When illumination occurs and Ca^{2+} declines, the GCAPs release this inhibition, and the GC rapidly restores the cGMP level.

1.5 Visual Cycle

Anytime a photon of light activates the photosensitive molecules, the retinal is released from the visual pigment and it is recycled through the visual cycle (Fig. 1.3). The removal of all-*trans*-retinal from the interdiscal space to the cytosolic face of the OS is performed by the retina specific ATP binding cassette transporter (ABCR). Once released it is reduced to all-*trans*-retinol by all-*trans*-retinol dehydrogenase

(RDH), after which it can exit the cell and enter the interphotoreceptor matrix. Here it is bound by the interphotoreceptor retinoid binding protein (IRBP), which carries the modified retinal into the RPE. Once in an RPE cell, three crucial enzymes metabolize the retinal. The first of these is the lecithin:retinol acyltransferase (LCAT), which esterifies the retinal to all-*trans*-retinyl esters. The RPE65 enzyme then hydrolyses the all-*trans*-retinyl esters to 11-*cis*-retinol, which is then bound by cellular retinaldehyde binding protein (CRALBP) and delivered to 11-*cis*-retinol dehydrogenase (11-*cis*-RDH), the last enzymatic step within the RPE. Finally, the regenerated retinal crosses the membrane and is in the sub-retinal space again bound by IRBP, which delivers it to the OSs of the PRs where it can bind and restore the functional opsin protein.

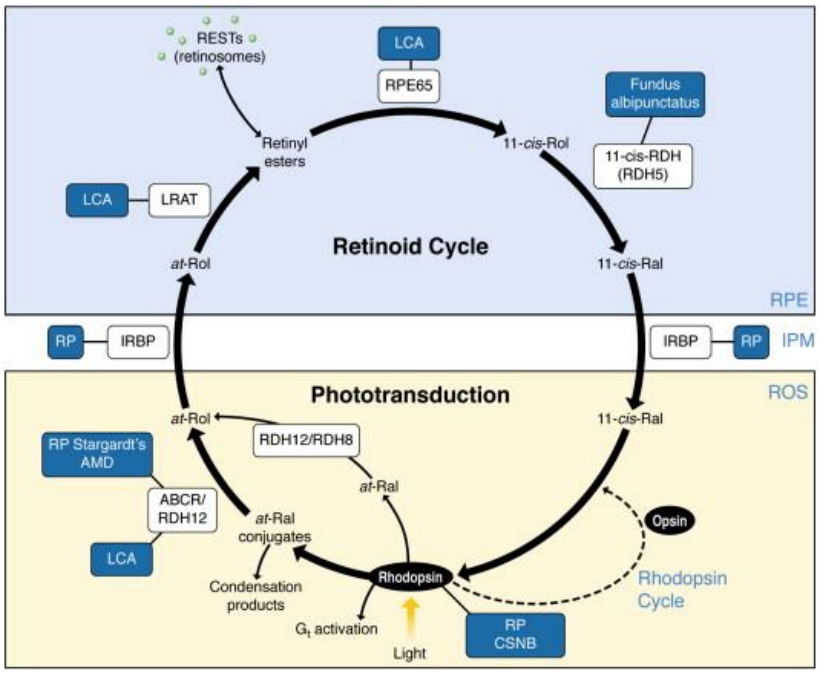

Figure 1.3. *Visual cycle (Kiser et al., 2012).*

1.6 Approach – Animal models

Following this introduction to human RP and the vertebrate visual system, it is now necessary to introduce the animal models that allow the study of RP and form such an important basis for the work in this thesis.

rd1. The most characterized model for RD is the *rd1* (retinal degeneration 1) mouse (Keeler, 1966). The *rd1* mouse carries a mutation in exon 7 of the β subunit of rod specific PDE6 (PDE6β). PDE6 is composed of two small inhibitory units (γ) and two larger catalytic subunits (α and β). As figure 1.4 shows, the mutation relates to the

catalytic β subunit and results in a nonfunctional protein leading to the neurotoxic accumulation of cGMP within the photoreceptor (Paquet-Durand et al., 2009). Since a similar mutation has been observed in a number of human conditions (Bayés et al., 1995), the *rd1* mouse has become a valuable model for the study of human RP.

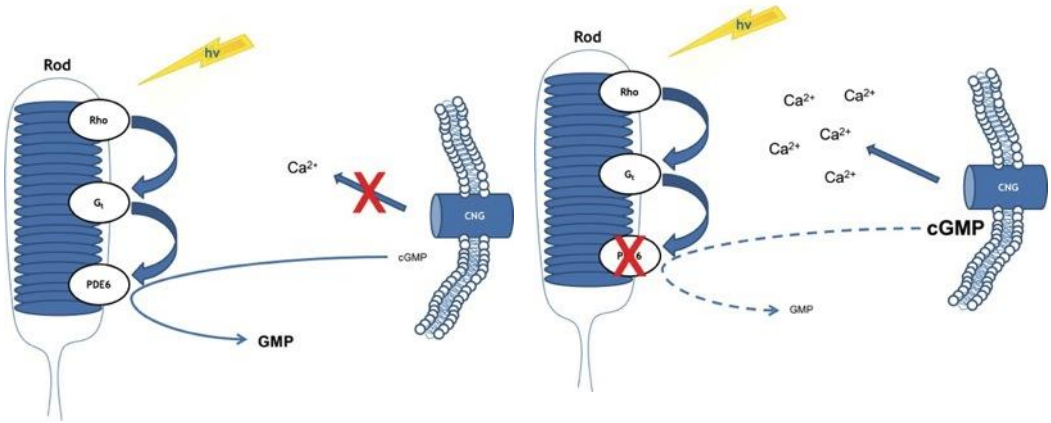

Figure 1.4. *Phototransduction changes provoked by mutated PDE6β.* Normal phototransduction (on the left) begins when a photon of light hits and activates Rho, which in turn activates $G\alpha_t$ and PDE6. This enzyme then hydrolyzes cGMP to GMP, closing CNG channels and reducing the influx of cations. When PDE6 is mutated (on the right), cGMP accumulates allowing massive calcium influx and provoking cellular stress that eventually promotes cell death pathways.

The *rd1* phenotype is inherited in an AR fashion and homozygous mice display very early onset and rapid rod degeneration, which is completed by the third week of life. The loss of rods promotes subsequent cone degeneration within six months (Lavail et al., 1997). The degeneration of both types of PRs induces an extensive remodeling of the inner retina and subsequent degeneration of other retinal neurons.

The PDE6β mutation leads to degeneration of the photoreceptors by triggering a caspase independent cell death pathway (Zeiss et al., 2004). More in detail, the accumulation of cGMP in this model of RP promotes the activation of cGMP-activated protein kinase (PKG). The down-stream substrates of PKG have not yet been identified, but it is clear that PKG inhibition contributes to neuroprotection (Paquet-Durand et al., 2009). It is also possible that the cGMP accumulation could lead to a supranormal opening of CNGs, which could aggravate the situation (Frasson et al., 1999). Furthermore, an increase of oxidatively damaged DNA (Sanz et al., 2007) and a reduction in the expression of DNA repair enzymes (Azadi et al., 2006) is also observed in the *rd1* retina. This may contribute to the dramatic activation of poly (ADP-ribose) polymerase (PARP) (Paquet-Durand et al., 2007), which could lead to energy collapse. Alongside the up-regulation of cGMP signaling, histone deacetylases

(HDACs) of class I & II are overactivated in *rd1* mouse and the blockade of this regulative class of enzymes promotes neuroprotection under different *in vitro* treatment paradigms (Sancho-Pelluz et al., 2010). Hence, the RD observed in the *rd1* phenotype is multifactorial and intricate and is as such likely to mimic the complexity of degeneration observed in human RP.

rd2. The *rd2* mouse suffers from a RD slower than in *rd1*. As described previously, the OSs are formed by stacks of membrane disks piled up on top of each other. Peripherin-2 (PRPH2) is a protein that localizes within the membrane disks (Molday et al., 1987) of the PRs and is involved in OS formation and homeostasis of both rods and cones, therefore the *rd2* mutation affects both types of PRs. The mutation was thought to be inherited in AR fashion, but it is now known that the heterozygous mouse also develops abnormalities (Hawkins et al., 1985). The *rd2* model is important as different mutations within the gene encoding for the PRPH2 gene have been shown to lead to diverse retinal diseases (Boon et al., 2008), making it an obvious target for further investigation and clinical approaches.

Rat rhodopsin mutants

The role of Rho in vision has been discussed above and mutations in the Rho gene are a major contributor to a wide range of visual impairment conditions. According to Retnet, a database on inherited retinal degenerations (https://sph.uth.edu/RetNet/), more than 100 mutations within the Rho gene have been linked to RP. There are several mechanisms by which Rho mutation could lead to RD and they have been assigned to six different classes (Mendes et al., 2005). For the research presented here two Rho mutants were routinely used, S334ter and P23H, which may represent mechanisms of class I and II, respectively.

P23H. The most common RP-causing mutation within the Rho gene is the substitution of histidine 23 for a proline (P23H) (Dryja et al., 1990), and patients carrying this mutation suffer from relatively mild visual problems (Oh et al., 2003). P23H Rho shows mislocalization and uncorrect folding which are common causes implicated in neurodegenerative diseases (Muchowski, 2002). In the retina, misfolded proteins can provoke endoplasmic reticulum (ER) stress and activate the unfolded protein response (UPR), which in turn can promote activation of cell death pathways (Alfinito and Townes-Anderson, 2002). The P23H retina has been widely studied and

several lines of research suggest aberrancies at different levels. Firstly, misfolded P23H Rho mutants lack oligosaccharide complexes that are normally added to Rho in the Golgi. Additionally, Rho is not able to bind chromophore, resulting in a shift of the spectrum of absorbance (Sung et al., 1991). Normally, misfolded proteins are ubiquitinated and directed to the proteasome for degradation, but it has been reported that P23H Rho is unstable and accumulates in the ER (Saliba et al., 2002). On the other hand, mutant Rho can form oligomers and the co-expression of wild-type (wt) and P23H mutant Rho increases the proteasome-mediated degradation (Rajan and Kopito, 2005), suggesting that P23H Rho mutants have a dominant negative influence. The cell death pathway in the photoreceptors of P23H rats appears to be caspase-independent. Recently the overactivation of calpain, led by the reduction of the cytoplasmatic level of its endogenous inhibitor calpastatin, has been reported in these cells, as have increased PARP activity (Kaur et al., 2011), just as is the case in several other RP models (Sancho-Pelluz et al., 2008). The P23H rat is a valuable RP model, both for its protein misfolding and mislocalization and for the fact that a large number of people are affected by this mutation.

S334ter. S334ter rats carry a 15-residue deletion in the C-terminal of the Rho gene due to the presence of a premature stop codon. This mutation results in a defect in Rho trafficking and transport to the OSs, highlighting the critical role for the C-terminal of Rho in this process (Tai et al., 1999). S334ter mutants show more severe phenotypes than mutations in other domains of the same gene. The molecular mechanisms by which S334ter retina degenerate follows a classical apoptotic pathway, involving the activation of caspases 3 and 9, cytochrome C leakage and overactivation of cysteine protease calpain and PARP enzymes (Liu et al., 1999, Kaur et al., 2011). Recently, it has been suggested that ER stress plays a pivotal role in RD in S334ter rat models (Shinde et al., 2012) and selective activation of ER stress signaling pathways prevents the accumulation of Rho in the retina (Chiang et al., 2012a). In conclusion, the S334ter rat is an excellent model for studying multi-phenotypical RD, showing distinguishing morphological and molecular features.

2. Experimental procedures

2.1 Animals

Animals used included C3H *rd1*/*rd1* (*rd1*), C3H *rd2/rd2* (*rd2*) and control C3H wild-type (wt) mice (Sanyal and Bal, 1973) which were all kept in colonies in Lund or Tübingen. Homozygous P23H and S334ter Rho transgenic rats (produced by Chrysalis DNX Transgenic Sciences, Princeton, NJ) of the line Tg(P23H)1Lav and Tg(S334ter)3Lav (P23H and S334ter-3), were all kindly provided by Dr. M. M. LaVail (University of California, San Francisco, CA) and bred in the Tübingen laboratory animal housing facility. Heterozygous P23H and S334ter rats were obtained by crossing with wild-type, CD rats (CD® IGS Rat; Charles River, Germany) to reflect the genetic background of ADRP. CD rats were used as controls.

Model	Mutation	Genetics	Phenotype	Degeneration
rd1	PDE6β	AR; Homozygous	cGMP accumulation	Fast
rd2	PHP	AR; Homozygous	Lack outer segments	Slow
S334ter	Rho (C-terminal deletion)	Autosomal negative dominant; Transgenic	Defective trafficking; rhodopsin continuously activated	Fast
P23H	Rho (single amino acid substitution)	Autosomal negative dominant; Transgenic	Unfolded rhodopsin	Slow

Table 2.1. *Characteristics of the animal models used in this thesis.*

All procedures were performed in accordance with either the Swedish National Animal Care and Ethics Committee (*rd1* and *rd2*, wt mice; permits # M242/07, -M220/09, M172/12), or the Tübingen University committee on animal protection (S334ter, P23H and CD rats), and protocols compliant with § 4 paragraph 3 of the German law on animal protection were reviewed and approved by the "Einrichtung für Tierschutz, Tierärztlichen Dienst und Labortierkunde" (Anzeige/Mitteilung nach § 4 vom 28.04.08 and 29.04.10). All efforts were made to minimize the number of animals used and their suffering and the experiments conformed to the ARVO statement for the use of animals in ophthalmic and visual research. Animals were kept

in their respective animal housing under standard white cyclic lighting, with free access to food and water, and were used irrespective of gender.

To minimize any bias from loss of retinal tissue mass due to the degeneration, comparisons of *rd1* and healthy wt retinae were typically performed at postnatal day (PN) 11 (although other time-points were included in some experiments). At PN11 degenerating photoreceptors are frequent in the *rd1* retina, but their death has not yet resulted in any considerable thinning of the photoreceptor layer (Sancho-Pelluz et al., 2008). For the other models we chose time-points that would serve the same purpose, *i.e.* for *rd2* mice PN19, P23H rats PN15 and S334ter rats PN12.

2.2 Organotypic retinal explant culture

For *in vitro* experimentation, PN5 *rd1* animals were sacrificed by decapitation, after which retinal explants were generated and cultured as described previously (Caffé et al., 2002). In short, immediately after killing of the animals the eyes were enucleated. To allow preparation of retinal explants for culturing with the retinal pigment epithelium (RPE) still attached, the eyes were incubated in R16 serum-free culture medium (Invitrogen Life Technologies, Paisley, UK; 07490743A), that contained 0.12 % proteinase K (MP Biomedicals, Solon, OH, USA; 193504), at 37 ºC for 15 min. The proteinase K was then inactivated with R16 medium containing 10 % fetal calf serum (Invitrogen Life Technologies; PET10108165), after which the eyes were dissected aseptically in a Petri dish with R16 medium. The R16 powder is composed by 41 ingredients that can be classified in salts, amino acids (except the potentially neurotoxic Glu and Asp), sugars and vitamins (Table 2.2). R16 is dissolved in Millipore water and then completed by addition of bovine serum albumin BSA, hormones and vitamins (Table 2.3) in order to make a full nutrient medium.

The dissection consisted of careful removal of the anterior segment, lens, vitreous, sclera, the choroid, and accessible vessels, after which the retina was subjected to four cuts perpendicular to its rim, which resulted in a cloverleaf-like shape of the explant. The latter was subsequently transferred to a Millicell culture dish filter insert (Millipore Billerica, Massachussets, USA; PIHA03050), where the explant was placed with the RPE layer facing the culturing membrane. The insert was then put into a six-well culture plate and incubated in R16 nutrient medium at 37 ºC. The full

volume of nutrient medium, 1.5 ml per dish, was replaced with fresh medium every second day during the culturing period.

Ingredient	Concentration		Ingredient	Concentration
L-Alanine	23 µM		Glucose	19.1 mM
L-Arginine HCl	494 µM		D(+)-Galactose	83 µM
L-Asparagine H_2O	23 µM		D(+)-Mannose	56 µM
L-Cystine Na_2	134 µM		Choline chloride	43.5 µM
L-Glycine	292 µM		Pyridoxal HCl	13.4 µM
L-Histidine HCl.H_2O	158 µM		$CaCl_2.2H_2O$	1.28 mM
L-Isoleucine	546 µM		$Fe(NO_3)_3.9H_2O$	0.17 µM
L-Leucine	562 µM		$FeSO_4.7H_2O$	0.68 µM
L-Lysine HCl	585 µM		KCl	4.29 mM
L-Methionine	142 µM		$MgSO_4.7H_2O$	680 µM
L-Phenylalanine	276 µM		$NaH_2PO_4.2H_2O$	610 µM
L-Proline	68 µM		Na_2HPO_4	230 µM
L-Serine	292 µM		$ZnSO_4.7H_2O$	0.70 µM
L-Threonine	562 µM		Folic acid	6.79 µM
L-Tryptophan	55 µM		i-Inositol	48.7 µM
L-Tyrosine	275 µM		Nicotinamide	22.2 µM
L-Valine	562 µM		Hypoxanthine	6.75 µM
Putrescine	180 µM		Riboflavine	0.74 µM
L-Carnitine	12.4 µM		Thymidine	0.67 µM
Cytidine 5'-diphospho ethanolamine	1.28 mg/ml		NaCl	103 mM
Cytidine 5'-disphospho choline	2.56 mg/ml		D-calcium pantothenate	5.77 µM
			Sodium phenol red	5.0 mg/ml

Table 2.2. *Composition of R16 medium.*

	Components	Amount (in ml) required to make 100 ml
1	Basal R16	80.0
2	BSA 10 %	2.0
3	Transferrin	0.1
4	Progesterone	0.1
5	Insulin	0.1
6	T3	0.1
7	Corticosterone	0.1
8	Thiamine HCl	0.1
9	Vitamin B12	0.1
10	(±)-α-Lipoic acid	0.1
11	Retinol / Retinylacetate	0.2
12	DL-Tocopherol / Tocopheryl acetate	0.2
13	Linoleic acid / Linolenic acid	0.2
14	L-Cysteine HCl	0.1
15	Glutathione	0.1
16	Na-pyruvate	0.1
17	Glutamine + Vitamin C	1.0
18	Distilled H2O	15.3
	Total volume	100 ml

Table 2.3. *Supplements for R16 medium.*

2.3 Fixation and sectioning

Mouse eyes (or explanted retinae still attached to the culturing filters) were fixed in 4 % paraformaldehyde (PFA) for 2 h in phosphate buffered saline (PBS, NaCl 145 mM, NaH_2PO_4 x H_2O 1.86 mM, Na_2HPO_4 8.3 mM). Rat tissues were fixed in PFA in PBS for 5 min in room temperature (RT) and 55 min in 4 °C. This was followed by thorough rinses with PBS, after which the preparations were placed in sucrose containing PBS to prepare for cryosectioning. Tissue was sectioned on cryostat which yielded 8-12 μm frozen sections, used as indicated.

Primary Antibody	Source	Provider	Cat. No.	IF	WB
α-Klotho	Rabbit	Abcam	ab18131	1:400	1:2.000
α-Klotho	Rabbit	Abcam	ab75023	1:200	1:1.000
α-Klotho	Rat	Santa Cruz	sc-74205	1:100	na
β-Klotho	Goat	Santa Cruz	sc-74343	1:200	1:1.000
Rhodopsin	Mouse	Chemicon	MAB5316	1:500	Na
pPKCα/βII	Rabbit	Cell Signalling	#9375	1:200	n.a.
FGF15	Goat	R&D Systems	AF6755	1:25	na
FGFR4	Mouse	Santa Cruz	sc-136988	1:200	1:1000
α-Tubulin	Mouse	Abcam	ab7291	1:2.000	1:20.000
5-methylcytosine	Sheep	Novus Biologicals	NB100-744	1:200	na
5-methylcytidine	Mouse	Abcam	ab10805	1:1.000	na
5-methylcytidine	Mouse	Abcam	ab51552	1:100	na
DNMT1	Rabbit	Abcam	ab16632	1:1.000	1:10.000
DNMT3A	Rabbit	Novus Biologicals	NB100-265	1:1.000	1:20.000
DNMT3B	Rabbit	Novus Biologicals	NB100-266	1:1.000	1:10.000
Hsp70	Mouse	Abcam	Ab47455	1:500	na
Cone-Arrestin	Rabbit	Gift	-	1:2.000	na
F4/80	Rat	Serotec	MCA497	1:500	na
cGMP	Sheep	HWM Steinbusch, Dept. Translational Neuroscience, Univ. Maastricht, The Netherlands	-	1:500	na
HSF1	Rabbit	Cell Signalling	#4356	1:50	na

Table 2.4. *List of primary antibodies used*

2.4 Microscopy

Morphological observations and routine light microscopy were performed on a Zeiss Axiophot microscope equipped with a Zeiss Axiocam digital camera. Fluorescence excitation was provided by a HBO 100W halogen lamp. Images were captured using Zeiss Axiovision 4.2 software, and image overlays and contrast enhancement were

done utilizing Adobe Photoshop CS. Confocal microscopy was performed with a Leica TCS SP2 (Solms, Germany).

2.5 Histological staining / Immunofluorescence

PFA fixed sections were stained for general histological light microscopic analysis with hematoxylin-eosin (HE) or underwent immunostaining. For the latter, the sections were washed 3 x 5 minutes each in PBS containing 0.25 % Triton X100 (PTX) plus 1 % BSA. Blocking solution containing PTX and 5 % normal serum from the host animal, from which the secondary antibody was obtained, was applied for 45 minutes. Primary antibodies (see Table 2.4) were diluted in PBS with 1 % BSA and 0.25 % Triton X100, and applied overnight at 4° C. Sections were then washed 3 x 5 min in PTX and incubated with appropriate secondary antibodies diluted in PTX (see Table 2.5) for 45 minutes. After 3 more washing steps in PBS, the sections were mounted with Vectashield DAPI (Vector, Burlingame, CA, USA). Controls consisted of sections processed in parallel without primary antibody and application of the fluorescence detection system.

Secondary Antibody	Provider	Type and Wavelength	Cat. No.	Dilution
Goat anti mouse	Molecular Probes	Alexa fluor 488	A11001	1:200
Goat anti mouse	Abcam	Dylight 594	Ab96873	1:500
Goat anti rabbit	Molecular Probes	Alexa fluor 488	A11008	1:200
Goat anti rabbit	Molecular Probes	Alexa fluor 594	A11037	1:200
Goat anti rat	Molecular Probes	Alexa fluor 488	A11006	1:200
Goat anti rat	Molecular Probes	Alexa fluor 594	A11007	1:200
Donkey anti goat	Molecular Probes	Alexa fluor 488	A11055	1:200
Donkey anti mouse	Molecular Probes	Alexa fluor 488	A21020	1:200
Donkey anti sheep	Jackson Immunoresearch	Texas Red 615	713-076-147	1:200
Donkey anti sheep	Jackson Immunoresearch	FITC 521	713-095-147	1:200

***Table 2.5**. List of the secondary antibodies used.*

Counterstaining	Provider	Emission wavelength	Cat. No.	Diluition
DAPI	Vector Labs	460 nm	H-1200	Ready to use
TO-PRO-3	Invitrogen	661 nm	T-3605	1:1000

***Table 2.6.** Nuclear counterstainings used.*

HE staining was performed according to the following protocol: sections were immersed in hematoxylin for 3 minutes and washed in running water for 5 minutes, after which they were rinsed in distilled water and immersed in eosin for 1 minute. Sections were afterward rinsed in distilled water, in 70 % and 96 % ethanol and then 2 x 1 minute in absolute alcohol. Last, they were washed 3 x 5 minute in Tissue Clear (Histolab, Gothenburg, Sweden), following which the HE labeled sections were finally mounted with Pertex.

For some immunofluorescence stainings antigen retrieval processing was performed by means of Na-Citrate-Tween-20 buffer (10 mM sodium citrate, 0.05 % Tween-20, pH 6.0) for up to 40 minutes in sub-boiling, prior to the above-mentioned protocol.

2.6 Terminal dUTP nick-end labelling (TUNEL)

Sections of PFA fixed preparations were washed three times in PBS. TUNEL staining was performed using an in situ cell death detection kit (Roche, Mannheim, Germany) conjugated with TMR red were carried out as by manufacturer's instructions. Controls with this kit and similar preparations have been performed in previous studies (Paquet-Durand et al., 2007), by omitting the terminal deoxynucleotidyl transferase enzyme from the labelling solution (negative control), and by pretreating the sections for 30 min with DNAse I (Roche, 3U/ml) in 50 mM Tris-HCl, pH 7.5, 1 mg/ml BSA to induce DNA strand breaks throughout the tissue (positive control).

2.7 Cell counting

Although there were minor modifications in the counting protocol for each of the separate projects, the following general guidelines were followed. Pictures taken of the marker of interest, as well as DAPI for nuclear labeling were merged together using Adobe Photoshop. The resulting pictures were opened in the Axiovision software, and the region of interest (photoreceptor layer) was outlined obtaining an area value (in pixel^2). The positive cells were counted and area was reported. From some randomly selected pictures the average area of a cell body (in pixel^2) was estimated from DAPI stained sections. To do so random areas within those pictures

were outlined and total cells were counted after which the percentage of positive cells (% (+) cells) was calculated as follows:

$$A_c = A_o / C_{DAPI}$$

$$\downarrow$$

$$C_t = A_t / A_c$$

$$\downarrow$$

$$\% (+) \text{ Cells} = (+) \text{ cells} / C_t$$

Here (+) cells is the total number of the positively labelled cells, C_t is the overall number of cells taken into account, A_t is the total area analyzed, A_c is the average area of a cell, A_o is the random area expressed in pixel^2 and C_{DAPI} represents the total DAPI positive cells in A_o.

2.8 Immunofluorescence quantification

Immunofluorescence in the outer segments of the photoreceptors (F_{os}) was in study 1 (see 4.2) quantified using the ImageJ program according to a protocol developed by Burgess (sciencetechblog.com/2011/05/24/measuring-cell-fluorescence-using-imagej/), with minor modifications. In brief, fluorescent areas of the whole segments, inner segments and blank (a random area close, but external, to the tissue) were outlined, after which values corresponding to integral density (ID) and area (A) of the whole segments (ID_s, A_s) and the inner segments alone (ID_{is}, A_{is}), as well as mean value (M) of the blank, were calculated.

2.9 Collection of conditioned medium

Retina explants were processed and cultured as described above. For study 1 (4.2) conditioned medium was collected at different time points reflecting the onset and progress of cell death (PN9, 11, 13, 15) for *rd1* and wt animals. The medium used contained 0.2 % bovine serum albumin (BSA), which may interfere with measurements of other proteins and thus a number of strategies were adopted to deplete BSA in collected medium: i) HiTRAP Blue HP (GE Healthcare, Uppsala, SE), ii) ProteaPrep Albumin Depletion Sample Prep Kit (Protea, Morgantown, WV, USA),

iii) as described by Colantonio (Colantonio et al., 2005). The first two are affinity columns which retain BSA and were used according to the manufacturer's instructions, whereas the third was performed as summarized: NaCl was added to the cultured medium to reach 0.1 M; this was then incubated with gentle rotation 1 h at 4˚C, followed by centrifugation at 16,000 x g for 45 min at 4˚C, after which the supernatant was transferred and pellet number 1 collected. The supernatant was set to pH 5.7 using cold 0.8 M Na-acetate, pH 4.0, and was incubated with gentle rotation for 1 h at 4˚C, followed by centrifugation at 16,000 x g for 45 min at 4˚C. The supernatant containing albumin was then discarded while pellet number 2 was retained and combined with pellet number 1 and finally resuspended in 10 mM Tris buffer pH 6.8 with 1 M urea for further analysis.

2.10 Western blot

Retinae from PN11 animals were removed in dissecting buffer (10 mM Tris, 1 mM EDTA, 150 mM NaCl, 1 mM Na_3VO_4, 50 nM okadaic acid, pH 7.3) supplemented with a protease inhibitor mixture (Roche). The tissue was homogenized in sample buffer [2 % sodium dodecyl sulphate (SDS), 10 % glycerol, 0.0625 M Tris-HCl, pH 6.8] by mechanical force. The sample was centrifuged for 10 min at 14,000 x *g*, and the supernatant was then removed and stored at -20°C. Bio-Rad (Hercules, California, USA) DC Protein Assay kit was used to determine protein concentrations, and either 10 or 20 µg of protein from each sample were separated by SDS-PAGE on 12 % gels, which were then transferred onto Immobilon-P polyvinylidene difluoride membranes (Millipore, Billerica, MA, USA). Membranes were incubated for 2 h in blocking buffer (5 % non-fat dried milk in PBS with 0.1 % Tween 20) and then kept overnight at 4°C with antibodies of interest. The day after, the membranes were washed, treated for 1 h with horseradish peroxidase-conjugated secondary antibodies (Table I), and visualized using the ECL Plus Western Blotting Detection system (Amersham Biosciences, Sunnyvale, CA) and Hyperfilm (Amersham Biosciences).

2.11 Quantitative RT-PCR

Although there were significant modifications in the qRT-PCR protocol for each of the separate projects (see Material and Methods in the respective chapters), the following general guidelines were followed. Tissues were extracted and quickly stored at -80 °C. Then total RNA was extracted either with Trizol or with the use of

RNA isolation kits, according to manufacturer's instructions. Quality of RNA was assessed and reverse-transcription was performed to obtain cDNA. Real Time PCR was done with the use of Sybr Green or TaqMan probes. Changes in gene expression were calculated by the ΔC_T, $\Delta\Delta C_T$ method or according to Pfaffl (Pfaffl, 2001).

2.12 Methylated DNA immunoprecipitation (MeDIP)

MeDIP was performed in Project 2 (4.3) according to the protocol provided from NimbleGen (http://www.nimblegen.com/). In brief: DNA was extracted from the retina of wt and *rd1* animals at PN11 with DNeasy kit (Qiagen, Hilden, Germany, 69504) according to the manufacturer's instructions and digested with *MseI* restriction enzyme (New England Biolabs, Ipswich MA, USA, R0525S) overnight at 37 °C. The digested DNA samples were then purified using QIAquick PCR Purification Kit (Qiagen, 28104) according to the manufacturer's instructions. Following this, 1,25 µl of purified DNA was diluted in 300 µl of TE buffer (10mM Tris HCl, pH 7,5; 1 mM EDTA) and heat denatured at 95 °C for 10 min. Of this volume, 250 ng were then removed and stored as input control, while 60 µl of 5x IP buffer (100 mM Na-phosphate, pH 7,0; 5 M NaCl; 10 % Triton X-100; ddH_2O until final volume) were added to the remaining DNA. Samples were then immunprecipitated using a mouse anti 5mC antibody (Abcam, Cambridge, UK, Ab10805) on a rotating platform overnight 4 °C. Next, antibody conjunction to beads of Protein A-agarose (Invitrogen, Carlsbad CA, USA, 15918-014) was performed for 2 h at 4 °C by gentle rotation. Samples were washed in 1x IP buffer and centrifuged at 6000 rpm for 2 min at 4 °C and the supernatant was discarded. The washing step was repeated twice and the beads were resuspended in 250 µl digestion buffer (1M Tris HCl, pH 8,0; 0,5M EDTA; 10 % SDS; ddH_2O until final volume). Proteinase K (Roche Applied Science, Penzberg, Germany, 03115836011) at the concentration of 10 mg/ml was added in order to resuspend the beads. Microcentrifuge tubes containing the antibody-beads complex and DNA were then placed in 50 ml Falcon tubes and incubated overnight on a rotating platform at 55 °C. In order to purify the samples, 250 µl of phenol (Sigma Aldrich, P-4557) was added. Methylated DNA samples were then vortexed for 30 seconds and centrifuged at 14000 rpm for 5 minutes at RT. The aqueous supernatant was collected and transferred to a sterile microcentrifuge tube. After addition of 250 µl of chloroform:isoamyl alcohol (Sigma Aldrich, C0549), the previous step was repeated. To pellet the DNA purified samples, 1 µl of glycogen

(Roche Applied Science, 10901393001), 20 µl of 5 M NaCl and 500 µl of ethanol were added. Precipitation was reached after incubation of the samples for 30 min in -80 °C. The pellets were centrifuged at 14000 rpm for 15 min at 4 °C; the supernatants were discharged and the samples washed in 500 µl of cold 70 % ethanol. The centrifugation step was repeated and samples were dried in SpeedVac and resuspended in 30 µl of 10 mM Tris-HCl (pH 8,5). Immunoprecipitated and input DNA was then amplificated using the GenomePlex Complete Whole Genome Amplification (WGA) kit (Sigma Aldrich, WGA2-50RXN) according to the manufacturer's instructions. Finally, each sample was purified with the Qiagen QIAquick PCR purification Kit according to the manufacturer's protocol. On those samples microarray analysis was then performed.

2.13 High-performance liquid chromatography/Mass spectrometry/Mass spectrometry (HPLC/MS/MS)

Project 2 also used HPLC/MS/MS analysis. After extraction the DNA was enzymatically digested to its nucleosides and subsequently analyzed by LC-ESI-MS. Samples (97 µl injection volume) were chromatographed by a *Dionex* Ultimate 3000 HPLC system with a flow of 0.15 ml/min over an Uptisphere UP3HDO-150/21 column (3 µm, 2.1 mm x 150 mm) from Interchim (Montluçon, France). The column temperature was maintained at 30 °C. The gradient (buffer A: 0.01 % formic acid in H_2O; buffer B: 0.01 % formic acid in 95 % MeCN / 5 % H_2O) was as follows: 0 → 12 min; 0 % → 1 % buffer B; 12 → 20 min; 1 % → 2 % buffer B; 20 → 30 min; 2 % → 10 % buffer B; 30 → 35 min; 10 % → 80 % buffer B; 35 → 41 min; 80 % buffer B; 41 → 51 min; 80 % → 0 % buffer B; 51 → 60 min; 0 % buffer B. Sample elution was monitored at 260 nm (*Dionex* Ultimate 3000 Diode Array Detector). The effluent from the first 5 minutes (total run time of 60 min) was diverted to waste by a *Valco* valve in order to protect the mass spectrometer. The subsequent chromatographic effluent was directly injected into the ion source of a *Thermo Finnigan* LTQ Orbitrap XL without prior splitting. Ions were scanned using a positive polarity mode over a full-scan range of *m/z* 100-500 with a resolution of 30000. The absolute amounts of mC was determined by a stable isotope dilution method and then related to the dG

content by UV-detection giving the relative values in percentage. Two technical replicates per sample were performed (Schiesser et al., 2012, Münzel et al., 2010, Globisch et al., 2010).

LC-ESI-MS was carried out on a *Thermo Finnigan* LTQ Orbitrap XL coupled to a *Dionex* Ultimate 3000 HPLC system.

2.14 Mathematical modelling

To interpolate between the data points we used the Interpolation function of the Mathematica computer software, which employs the Hermite interpolation method (http://reference.wolfram.com/mathematica/ref/Interpolation.html). This method returns a piecewise polynomial, in our case of degree three that goes through all the given data points. If the interpolated function is regular, the Hermite interpolation gives a good approximation inside the interval of data points.

2.15 Statistical evaluation

Statistical significance was tested using t-tests, ANOVA or two way ANOVA test, as indicated, and a p-value < 0.05 was considered statistically significant. Calculations were made using Graph Pad Prism.

3. Aim of the thesis

The general aim of this thesis is to help filling in the knowledge gaps in the understanding of the molecular mechanisms leading to RP. This is done by investigating the participation of several novel and distinct players in the context of RP, combined with the use of relevant animal models.

Thus, the specific aims of the thesis include the study of:

- The association of the anti-aging protein Klotho in retinal degeneration.
- The contribution of HDACs and DNA methylation, which are cellular processes aimed at the control of the gene expression, to the degeneration of the photoreceptors.
- The cellular expression and possible neuroprotective tasks of the stress induced heat shock protein Hsp70.

In order to achieve these aims, I have employed techniques such as immunofluorescence/immunohistochemistry, western blot, immunoprecipitation, qRT-PCR and pharmacological treatments on organotypic retinal cultures.

4.1 Retinitis Pigmentosa: Over-expression of anti-ageing protein Klotho in degenerating photoreceptors

J Neurochem. 2013, Jun 24

Pietro Farinelli[1,2], Blanca Arango-Gonzalez[2], Jakob Völkl[3], Ioana Alesutan[3], Florian Lang[3], Eberhart Zrenner[2], François Paquet-Durand[2*], Per A.R. Ekström[1]

[1]Division of Ophthalmology, Department of Clinical Sciences, Lund, University of Lund, Lund, 22184 Sweden; [2]Division of Experimental Ophthalmology, Institute for Ophthalmic Research, University of Tübingen, 72076 Tübingen, Germany; [3]Department of Physiology, University of Tübingen, 72076 Tübingen, Germany.

Rationale

In a previous study, micro-array analysis revealed that the transcript of member of the anti-ageing protein family Klotho has been found up-regulated in *rd1* mouse retina compared to control. Moreover, degeneration of the photoreceptors of the retina may be considered as to a very early form of ageing. The following study was aimed at understanding whether any Klotho proteins are involved in the pathways leading to photoreceptor cell death in different rodent models of RP.

Introduction

The inheritable disease Retinitis Pigmentosa (RP) leads to loss of vision via degeneration of rod and cone photoreceptors: typically rods die via mutation-induced mechanisms, after which cones degenerate secondarily (Pierce, 2001). Although today over 60 genes have been linked to RP (RetNet: http://www.sph.uth.tmc.edu/RetNet), the mechanisms behind the degeneration are largely unclear, and there is currently no treatment available.

The Klotho protein – named after the Greek goddess Klotho, who spins the thread of life – is a player in longevity, and defective Klotho expression provokes rapid ageing and early death in mouse (Kuro-o et al., 1997). Apart from the prototypical α-Klotho, there are other Klotho family members, including β-Klotho and Klotho/lactase-phlorizin hydrolase-related protein [Lctl or γ-Klotho] (Ito et al., 2000). The *Klotho*

gene encodes a 1014 amino acid, transmembrane protein (Matsumura et al., 1998), with homology to β-glucuronidases and is found mainly in kidney distal tubules, parathyroid gland, and brain choroid plexus, but also in other tissues including urinary bladder (Kuro-o et al., 1997) and inner ear (Kamemori et al., 2002). Both membrane and soluble forms (Imura *et al.* 2004) are known, with shedding of α-Klotho ectodomain (fragments) from the cell membrane via various secretases (Bloch et al., 2009). The connection between Klotho and the demise of various cell types warrants a consideration of an involvement also in the retina and RP. Current Information on retinal Klotho is sparse. High mRNA expression levels of Lctl have been reported in adult mouse eyes (Fon Tacer et al., 2010), with α-Klotho and β-Klotho expression either absent or limited, respectively. However, a previous, microarray based study suggested elevated levels of β-Klotho mRNA in retinae of the *rd1* mouse model for RP (Azadi et al., 2006).

The altered β-Klotho mRNA in *rd1* retina and the α-Klotho connection to ageing and death triggered us to investigate Klotho isoforms in different RP animal models. These included the *rd1* mouse, which carries a mutation in the gene coding for the β-subunit of phosphodiesterase-6 (PDE6β) (Farber and Lolley, 1974), giving a rapid degeneration, and the *rd2* mouse, with a mutation in the photoreceptor disk protein peripherin-2 (prph-2) gene (Goldberg, 2006) and in which the retinal degeneration is slower. Both models represent human RP forms (Bayés et al., 1995; Kajiwara et al., 1991). Rhodopsin mutations are frequent in RP patients, and hence we also used two rhodopsin mutant rats that display fast (*S334ter*; Liu et al., 1999) and slow (*P23H*; Sung et al., 1991) rod degeneration, respectively. The *rd2* mutation affects both rod and cone photoreceptors, while the other mutations are rod specific. The unique characteristics of the four models, from two different species, make them well suited to address the possible involvement of Klotho in inherited photoreceptor cell death.

Here, we demonstrate a strong upregulation of several Klotho isoforms in degenerating retinae, as well as an effect on retinal morphology by addition of exogenous Klotho to retinal cultures. The findings suggest a link between Klotho and the process of retinal degeneration.

Materials and Methods

Animals

Animals included C3H *rd1*/*rd1* (*rd1*), C3H *rd2*/*rd2* (*rd2*) and control C3H wild-type (*wt*) mice (Sanyal and Bal, 1973). Homozygous P23H and S334ter rhodopsin transgenic rats of the line Tg(*P23H*)1Lav and Tg(S334ter)3Lav (*P23H* and *S334ter-3*), were kindly provided by Dr. M. M. LaVail (University of California, San Francisco, CA). Heterozygous *P23H* and *S334ter* rats were obtained by crossing with *wt*, *CD* rats (*CD*® IGS Rat; Charles River, Germany) to resemble autosomal dominant RP. *CD* rats were used as controls.

Ethics statement: All procedures were performed in accordance with permits granted by either the "Malmö/Lunds Djurförsöksetiska nämnd" (*rd1* and *rd2*, *wt* mice; permits # M242/07, M220/09), or the Tübingen University committee on animal protection (*S334ter*, *P23H* and *CD* rats). Protocols compliant with § 4 paragraph 3 of the German law on animal protection were reviewed and approved by the "Einrichtung für Tierschutz, Tierärztlichen Dienst und Labortierkunde" (Anzeige/Mitteilung nach § 4 vom 28.04.08 and 29.04.10). All efforts were made to minimize the number of animals used and their suffering. Animals were kept in the animal house under standard white cyclic lighting, with free access to food and water, and were used irrespective of gender.

To minimize any bias from loss of retinal tissue due to the degeneration, comparisons of *rd1* and healthy *wt* retinae were typically performed at postnatal day (PN) 11. At PN11 degenerating photoreceptors are frequent in *rd1* retina, but ONL thickness is not significantly affected (Sancho-Pelluz et al., 2008). For the other models, we typically chose time-points corresponding to the respective peaks of degeneration, *i.e.* PN19 for *rd2* mice, PN15 for *Rho P23H* rats and PN12 for *Rho S334ter* rats.

Organotypic retinal explant culture

For *in vitro* experimentation, PN5 *rd1* animals were sacrificed by decapitation, after which retinal explants were generated and cultured in principle as detailed previously (Caffé et al., 2002, Sancho-Pelluz et al., 2010). Briefly, the enucleated eyes were dissected aseptically in a Petri dish with R16 serum-free culture medium (Invitrogen

Life Technologies, Paisley, UK; 07490743A) (Caffé et al., 2002), to yield a retinal explant devoid of other eye tissue except for the retinal pigment epithelium (RPE). The retina had four cuts perpendicular to its rim, resulting in a propeller-like shape of the explant, which was then transferred to a Millicell culture dish filter insert (Millipore AB, Solna, Sweden; PIHA03050), where it was placed with the RPE layer facing the culturing membrane. Inserts were put into six-well culture plates, and each well given 1.5 ml serum-free R16 medium. Plates were incubated at 37º C with medium replacement generally every second day (except for one day treatments described below).

Prior to treatment, PN5 explants were allowed to adjust to control culture conditions for 2 or 5 days *in vitro* (DIV), after which a 4 or 1 day treatment, respectively, was performed. The end point of both of these experiments (PN5+2DIV+4DIV alt. PN5+5DIV+1DIV) thus corresponded to PN11. Treatment used either 1 nM or 2.5 nM (stock was x μg/ml in PBS 50% (v/v) Glycerol and 0.1 mM EDTA, pH 6.8) of the recombinant ectodomain of Klotho protein (R&D Systems, Abingdon, UK; 1819-KL; representing 948 of 1044 amino acids of full length protein), or appropriate concentration of vehicle. These concentrations clearly exceeded the physiological levels of the circulating form in *wt* (100 pM) or in α-Klotho overexpressing strains (200 pM) (Kurosu et al., 2005).

In separate, long-term experiments *wt* retinae were cultured from PN5 for 2 days without any treatment, and subsequently treated for 15 days (PN5+2 DIV+15 DIV; *i.e.* to PN22) with either 1 nM Klotho or vehicle.

At the end of experiments, preparations were fixed and sectioned, as described below.

Fixation, sectioning and microscopy

Mouse retinal samples were fixed in 4% paraformaldehyde (PFA) for 2h in phosphate buffered saline (PBS). Rat tissues were fixed in PFA in PBS for 5 min in room temperature (RT) and 55 min in 4°C. This was followed by thorough rinses with PBS, after which the preparations were placed in sucrose containing PBS to prepare for cryosectioning, which yielded 8 or 12 μm frozen sections, used as indicated.

Morphological observations and light/fluorescence microscopy were performed and recorded on a Zeiss Axiophot microscope with a HBO 100W halogen lamp and a

Zeiss Axiocam digital camera (Jena, Germany). Images were captured using Zeiss Axiovision 4.2 software; image overlays and contrast enhancement were done utilizing Adobe Photoshop CS (San Jose, California, USA).

TUNEL staining

TUNEL (Terminal deoxynucleotidyl transferase dUTP nick-end labelling) staining was performed on PBS washed sections using the In Situ Cell Death Detection Kit (TMR Red, Roche, Mannheim, Germany). Controls, including omitting the terminal deoxynucleotidyl transferase enzyme from the labelling solution (negative control), or pre-treatment of the sections with DNAse I to induce strand breaks (positive control), have been performed earlier with similar kits and preparations, giving no staining at all (negative) or general staining of all nuclei in all retinal layers (positive) (Paquet-Durand et al., 2007).

Histological staining/Immunofluorescence

Fixed sections were stained for general histological light microscopy with haematoxylin-eosin (HE) according to standard protocols, or underwent immunostaining. For the latter, the sections were washed 3 x 5 minutes each in PBS containing 0.25% Triton X100 (PTX) plus 1% bovine serum albumin (BSA). Blocking solution containing PTX and 5% normal serum from the secondary antibody host species was applied for 45 minutes. Primary antibodies were diluted in PBS with 1% BSA and 0.25% Triton X100, and applied overnight at 4°C. Following 3 x 5 min washing in PTX, sections were incubated with appropriate secondary antibodies in PTX for 45 minutes, washed thrice in PBS and mounted with Vectashield DAPI (Vector, Burlingame, CA, USA). Controls were processed in parallel without primary antibody. Antibodies are listed in Supplemental Table I.

Some stainings required antigen retrieval processing, performed by means of Na-Citrate-Tween-20 buffer (10 mM sodium citrate, 0.05% Tween-20, pH 6.0) for up to 40 minutes in sub-boiling, followed by the above-mentioned protocol.

Counting of cells and tissue parameters

The number of TUNEL or α-Klotho-positive (+) cells was assessed and calculated as reported previously (Paquet-Durand et al., 2006, Sancho-Pelluz et al., 2010). For each animal at least three non-contiguous sections were quantified to yield an average value, with at least three independent animals analysed for each experimental situation. Values are given as TUNEL (+) cells relative to control ± standard deviation (SD).

Some HE stained sections were analysed with respect to surviving rows (perpendicular to the radius of the retina) of photoreceptors or to disorganization of the retinal structure. For the former, six pairs of treated and untreated retinae represented the samples and three non-contiguous sections per sample were analysed. In every section three random central, but non-contiguous, areas were selected, inside of which the rows of photoreceptor nuclei were manually counted in the microscope. The mean values of every section were averaged giving the number of surviving rows of photoreceptor nuclei per sample. For the disorganization analysis, the combined length (in the horizontal aspect) of disorganized retina in both of the edges of the stained sections was measured in the microscope. Normal, non-disorganized length of retina was also recorded, which together with disorganized length equalled each section's total length. Four sections were analysed on each of three non-contiguous slides for each preparation, which gave rise to an average value for that slide. The three observed slides were then averaged to yield one, final value.

Immunofluorescence quantification

The FGF15 immunofluorescence in photoreceptor OS (F_{os}) was quantified using the ImageJ program following a protocol developed by Burgess (http://sciencetechblog.com/2011/05/24/measuring-cell-fluorescence-using-imagej), with some minor modifications. In brief, fluorescent areas of the whole segments, inner segments (IS) and blank (a random external area close to the tissue) were outlined, after which values corresponding to integral density (ID) and area (A) of the whole segments (ID_s, A_s) and the IS alone (ID_{is}, A_{is}), as well as mean value (M) of the blank, were calculated. The following equation then gave a reliable approximation of

the expression of FGF15 in the OS of the photoreceptors: $F_{os} = ID_s – (A_s \times M) - [ID_{is} – (A_{is} \times M)]$.

Western blot

PN11 retinae were prepared in dissecting buffer (10 mM Tris, 1 mM EDTA, 150 mM NaCl, 1 mM Na_3VO_4, 50 nM okadaic acid, pH 7.3) supplemented with protease inhibitor mixture (Complete Mini, Roche) and homogenized in sample buffer [2% sodium dodecyl sulphate (SDS), 10% glycerol, 0.0625 M Tris-HCl, pH 6.8] by mechanical force. After centrifugation for 10 min at 14,000 x *g*, the supernatant was removed and stored at -20°C. Bio-Rad DC Protein Assay kit (Hercules, CA, USA) was used to determine protein concentrations, and either 10 or 20 µg of protein from each sample were separated by SDS-PAGE on 12% gels, and blotted onto Immobilon-P polyvinylidene difluoride membranes (Millipore, Billerica, MA, USA). Membranes were incubated for 2h in blocking buffer (5% non-fat dried milk in PBS with 0.1% Tween 20) and then kept overnight at 4°C with antibodies of interest. The membranes were then washed, treated for 1h with horseradish peroxidase-conjugated secondary antibodies (Supplemental Table I), and immunoreactions visualized using the ECL Plus Western Blotting Detection system (Amersham Biosciences, Sunnyvale, CA) and Hyperfilm (Amersham Biosciences).

qRT-PCR

After enucleation, PN11 retinae were immediately snap frozen in liquid nitrogen. Total RNA was isolated by using Trifast Reagent (Peqlab, Erlangen, Germany) according to the manufacturer's instructions. Reverse transcription of 2 µg total RNA was performed using oligo$(dT)_{12\text{-}18}$ primers (Invitrogen, Karlsruhe, Germany) and SuperScriptIII Reverse Transcriptase (Invitrogen, Karlsruhe, Germany). cDNA samples were treated with RNaseH (Invitrogen, Karlsruhe, Germany). Quantitative real-time PCR was performed with the iCycler iQ™ Real-Time PCR Detection System (Bio-Rad Laboratories, Hercules, CA) and iQ™ Sybr Green Supermix (Bio-Rad Laboratories, Hercules, CA) according to the manufacturer's instructions.

The following primers were used (5'→3' orientation):

α-Klotho	fw:	CCCTGTGACTTTGCTTGGG;
α-Klotho	rev:	CCCACAGATAGACATTCGGGT;
β-Klotho	fw:	TGTTCTGCTGCGAGCTGTTAC;
β -Klotho	rev:	TTATCCCATATTGCTTTCCCGTC;
Lctl	fw:	GTGACTATGCTGACCTATGCTTT;
Lctl	rev:	TGTGAGCCAATGCTTCACTCG;
Gapdh	fw:	AGGTCGGTGTGAACGGATTTG;
Gapdh	rev:	TGTAGACCATGTAGTTGAGGTCA;

The specificity of the PCR products was confirmed by analysis of the melting curves and by agarose gel electrophoresis. The results were derived from analyses of five independent samples per group and all PCRs were performed in duplicate. Fold changes of mRNA were calculated by the $2^{-\Delta\Delta Ct}$ method using glyceraldehyde 3-phosphate dehydrogenase (Gapdh) as internal reference, and analysed by Student's t-test.

Statistical analyses

Statistical significance was tested using unpaired, two-tailed, Student's t-test, Student's paired t-test, Student's one-group t-test or two-way ANOVA test, as indicated. When Student's one-group t-test was used, the treated/untreated ratios were compared with a ratio of 1.00. For all tests, a p-value < 0.05 was considered to indicate a statistically significant difference.

Results

Klotho mRNA expression in rd1 retina

Quantitative RT-PCR analysis revealed an increase of α-Klotho mRNA levels in postnatal day (PN) 11 *rd1* retinae (3.74 ± 2.49 a.u. [arbitrary units]) compared with age matched *wt* (wild type) tissue (1.07 ± 0.46 a.u.; $p < 0.05$). The mRNA levels for β-Klotho and Lctl were numerically, but not significantly, higher in *rd1* than in *wt* samples (*rd1* 1.46 ± 0.69 a.u.; *wt* 1.14 ± 0.57 a.u., and *rd1* 1.29 ± 0.55 a.u.; *wt* 1.07 ± 0.43 a.u., respectively; mean ± SD; n = 5; n.s. [not significant]).

Immunofluorescence of Klotho proteins in RP models

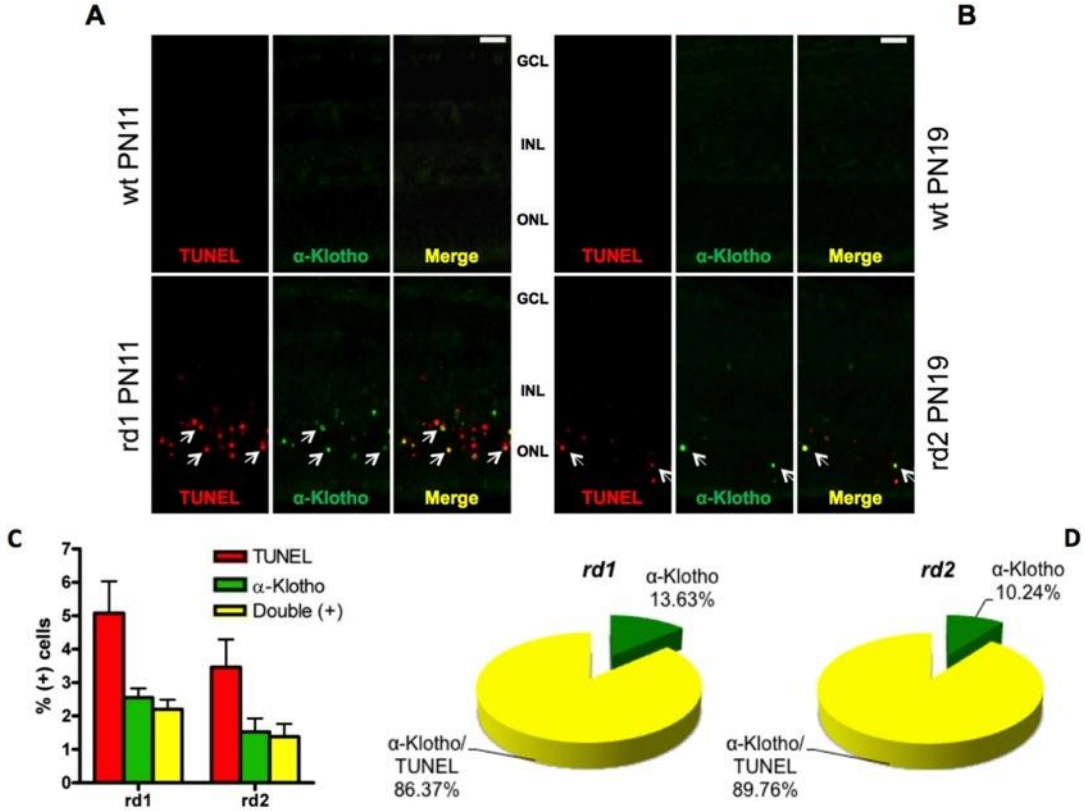

Figure 4.1.1. *α-Klotho and cell death in degenerating mouse retina.* Immunostaining with α-Klotho antibody ab18131 (green) and TUNEL cell death staining (red) of PN11 *rd1* and *wt* (A), or PN19 *rd2* and *wt* (B), retinal sections. Pictures are from subcentral positions, *i.e.* close to the optic nerve exit. In *wt* specimens α-Klotho was only very rarely found in the outer nuclear layer (ONL), whereas a subset of photoreceptors in the *rd1* and *rd2* ONL showed a distinct nuclear staining. The percentages of cells positive for either TUNEL, α-Klotho or both are given in (C) (mean ± SD; n = 3-5), indicating a major TUNEL on α-Klotho overlap (C, D). Weak but noticable α-Klotho immunoreactivity was found in inner nuclear and ganglion cell layers (INL, GCL), both in *wt* and *rd1* retinae. The staining is representative for at least three independent animals of each type. Scale bar = 20 µm.

α-Klotho – At PN11, at the onset of the *rd1* degeneration, the α-Klotho ab18131 antibody revealed a high number of strongly positive nuclei in *rd1* outer nuclear layer (ONL) (see Supplemental Table I for antibodies), but not in PN11 *wt* ONL (Fig. 4.1.1). The higher number of positive cells in the central *rd1* retina (not shown) resembled the known centre to periphery degeneration in this model (Carter-Dawson *et al.* 1978). Co-staining with the TUNEL (Terminal deoxynucleotidyl transferase dUTP nick-end labelling) assay (Fig. 4.4.1 A, C, D) confirmed that α-Klotho positive nuclei indeed belonged to degenerating photoreceptors. Furthermore, α-Klotho co-localised with markers for oxidatively damaged DNA and overactivation of PARP enzymes (Fig. 4.1.2 A and B), which are known to label dying photoreceptors (Paquet-Durand *et al*. 2007). Validation of the α-Klotho staining (Fig. 4.1.2C and D) was done by two other antibodies (ab75023, sc-74205).

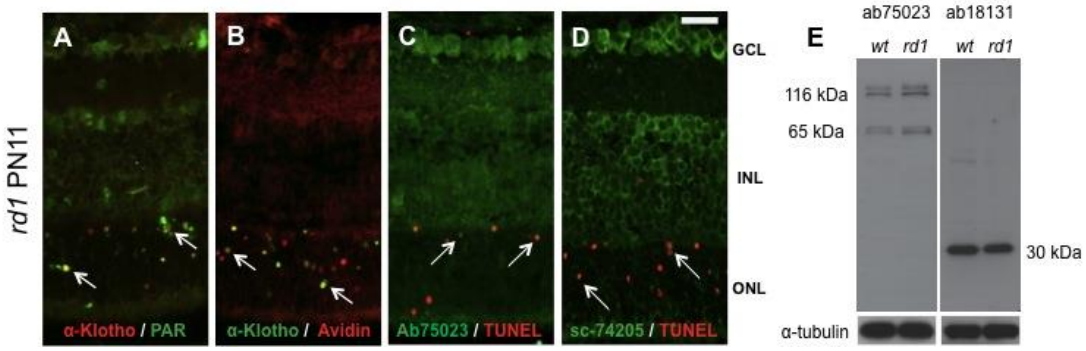

Figure 4.1.2. *α-Klotho co-localizes with stress markers.* Immunostaining for α-Klotho with A) poly(ADP-ribose) (PAR) and B) avidin, which labels 8-hydroxydeoxyguanosine (a marker for oxidatively damaged DNA), shows a linkage between α-Klotho and both cellular stress markers. In order to validate the result with the ab18131 antibody, we stained degenerating *rd1* retinae with two other antibodies (ab75023, sc-74205) for α-Klotho, both of which required antigen retrieval treatment (see Methods) in order to produce a signal. The resulting staining was similar to the ab18131 antibody, including the co-localisation with TUNEL, although the absolute number of α-Klotho positive cells appeared lower. Western blot of *rd1* and *wt* retinal proteins for α-Klotho with the ab75023 antibody detected α-Klotho full length and approximately half length forms, whereas the ab18131 antibody labelled a 30 kDa band, probably representing a cleavage product. There were no obvious differences between the genotypes. The Western blot (E) results are representative of at least four runs of independent sample pairs. Each applied sample pair consisted of either 10 or 20 µg proteins per sample from a pool made of two retinae. Lower insets show that *wt* and *rd1* samples contained similar amounts of protein, as judged by the anti-α-tubulin control run on a separate blot. GCL = ganglion cell layer; INL = inner nuclear layer; ONL = outer nuclear layer. Scale bar = 20 µm.

To determine whether the retinal α-Klotho increase represents a more generalised phenomenon, the same analyses where performed in *rd2* mouse and *P23H* and *S334ter* rat retinae. Figures 4.1.1 B and D show that the other mouse model, *rd2*, had

α-Klotho/TUNEL co-staining qualitatively similar to *rd1*, as did both rat models (Fig. 4.1.3 A and D), suggesting a common situation across species and mutations. The more aggressive degeneration in the *S334ter* retina, with a higher percentage of dying cells at the peak time-point studied (Kaur *et al.* 2011), seemed to coincide with less α-Klotho/TUNEL co-labelling (Fig. 4.1.3 C and D). This difference in α-Klotho *vs* TUNEL staining may relate to the fact that photoreceptor cell death in the *S334ter* model shows an extensive activation of caspase-3 which is not seen in *P23H* rats (Kaur *et al.* 2011) and *rd1* mice (Sahaboglu *et al.* 2013).

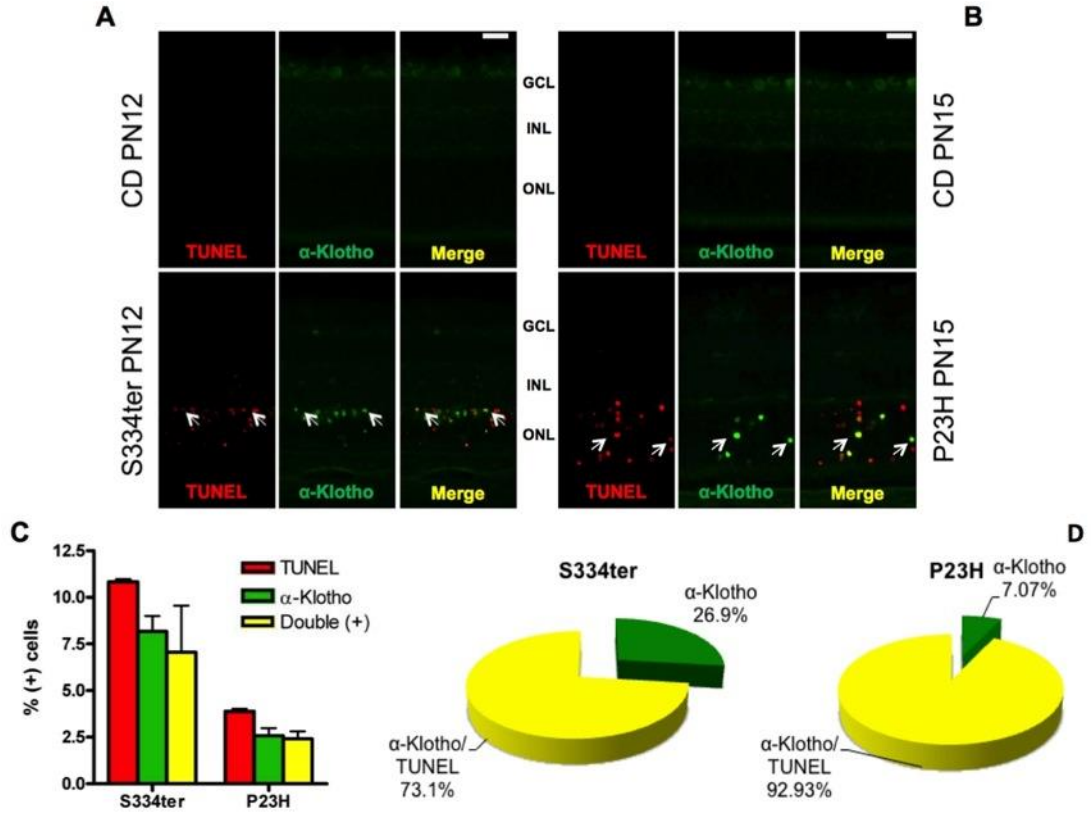

Figure 4.1.3. *α-Klotho and cell death in degenerating rat retina.* Immunostaining for α-Klotho and TUNEL in retinal sections from PN12 *S334ter* (A), and PN15 *P23H* (B) rats plus appropriate controls (Methods). Both models displayed strong α-Klotho labelling in ONL cells, as well as weak INL and GCL staining. In each situation, the ONL α-Klotho staining overlapped with TUNEL-positivity (C, D). Labels and other features are as in Fig. 1. Scale bar = 20 μm.

β-Klotho - β-Klotho staining was also increased in rd1 ONL cells (Fig. 4.1.4). While the absolute number of β-Klotho positive cells was lower than seen for α-Klotho (0.85% ± 0.17; Table 4.1.1), over 90% of the β-Klotho positive cells were also TUNEL positive.

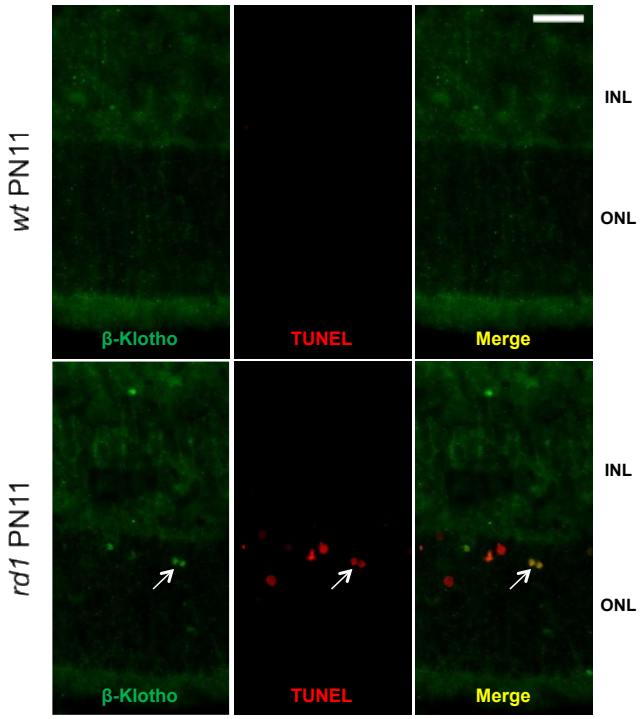

Figure 4.1.4. *Expression of β-Klotho in* wt *and* rd1 *retina* Both C3H *wt* mice and *rd1* mutants showed weak β-Klotho immunoreactivity in the inner retina. In the *rd1* retina a proportion of photoreceptors was β-Klotho positive and more than 90% of those cells were positive for TUNEL as well. The pictures were taken in subcentral positions, and the staining is representative for at least three independent animals. Labels are as previous figures. Scale bar = 20 μm.

Model; Age	***TUNEL (+) cells (%)***	***α-Klotho (+) cells (%)***	***α-Klotho and TUNEL (+) cells (%)***
rd1; PN 11	5,07 (± 0,96)	2,55 (± 0,28)	2,20 (± 0,28)
rd2; PN 19	3,46 (± 0,83)	1,53 (± 0,40)	1,38 (± 0,39)
S334ter; PN 12	10,83 (± 0,14)	8,17 (± 0,82)	6,05 (± 0,79)
P23H; PN 15	3,88 (± 0,14)	2,59 (± 0,39)	2,41 (± 0,40)
Model; Age	**TUNEL (+) cells (%)**	**β-Klotho (+) cells (%)**	**β-Klotho and TUNEL (+) cells (%)**
rd1; PN11	*4,57 (± 0,58)*	*0,85 (± 0,17)*	*0,79 (± 0,16)*

Table 4.1.1. Co-localization of Klotho immunostaining with TUNEL positivity. Values are given as mean ± SD, n =3-5. See Material and Methods for other details.

Western blot

In Western blot tests the ab75023 antibody yielded a double band of around 116 kDa plus bands of about 65 kDa (Fig. 4.1.2 E). This is compatible with the expected molecular-weight-range for α-Klotho, *i.e.* two full-length protein bands around 116 kDa (with/without glycosylation; Kamemori *et al.* 2002), as well as some weaker bands of about 65 kDa, which may be α-Klotho fragments (Chen *et al.* 2007). The ab18131 consistently revealed only an approximately 30 kDa band, perhaps similar to that previously reported in mouse tissue by a different and non-commercial antibody

(Chen *et al.* 2007). Neither antibody revealed significant differences in signal strength between the two genotypes. The cells with increased α-Klotho expression (as in the immunostainings) likely represent only a small fraction of the tissue mass of the global retina samples, and hence any increase might have been masked at the Western blot level.

Cultured rd1 retinae and exogenous α-Klotho

Klotho proteins can be released (Kurosu *et al.* 2005; Imura *et al.* 2007), but Western blot analysis of *rd1* retinal explant conditioned medium failed to detect extracellular α-Klotho (not shown). Still retinal cells may respond to extracellular protein, and we therefore added recombinant α-Klotho protein to *rd1* retinal explants and analysed the outcome by TUNEL staining of preparations corresponding to PN11. Early cellular responses to α-Klotho have been seen in other systems (Kurosu *et al.* 2005), and we thus tested a one day treatment with either 1 or 2,5 nM α-Klotho (PN5+5DIV+1DIV; culturing from PN5 for 5 days *in vitro* [DIV] without treatment, followed by 1 DIV treatment). However, this gave no effect on *rd1* TUNEL positivity (TUNEL positive cells in treated *vs* untreated [set to 1.0] = 0.96 ± 0.14 for 1 nM; 0.85 ± 0.14 for 2.5 nM, respectively; mean ± SD; n = 4; n.s.), and neither did an extension of treatment to four days (PN5 + 2DIV + 4DIV) (1.20 ± 0.20 for 1 nM; 1.12 ± 0.22 for 2.5 nM, respectively; n = 5; n.s.).

Cultured wt retinae and exogenous α-Klotho

We then treated *wt* retinal explants, which do not have a degenerative phenotype, and increased the treatment duration to encompass ages PN7 to PN22 (PN5 + 2 +1 5). Such α-Klotho treatment did not affect the number of surviving rows of photoreceptors at the end of culturing (Fig. 3A: α-Klotho treated 8.5 ± 0.8, untreated 9.0 ± 0.8; mean ± SD; n = 6; n.s.).

The explant culturing regularly leads to a slight disorganization of the retinal layering at the very edges of the preparations, and cell row and TUNEL analyses *etc*., are therefore regularly performed using the more central parts of the specimens. While lacking any effect on central cell rows (Fig 4.1.5 A), the treatment of *wt* explants consistently caused a disorganization at the edges of the retinal explants, that was much more extensive than in the untreated specimens (Fig. 4.1.5 C and D;

disorganized edge lengths: α-Klotho treated 1506 ± 708 µm, untreated 780 ± 340 µm; mean ± SD; n = 12; $p < 0.01$; Student's paired t-test). The total length of an explant section usually ranges between 4000 and 5000 µm, but this parameter was not different between treated and untreated (ratio total length; treated/untreated: 0.98 ± 0.05; n = 12; n.s., Student's one-group t-test).

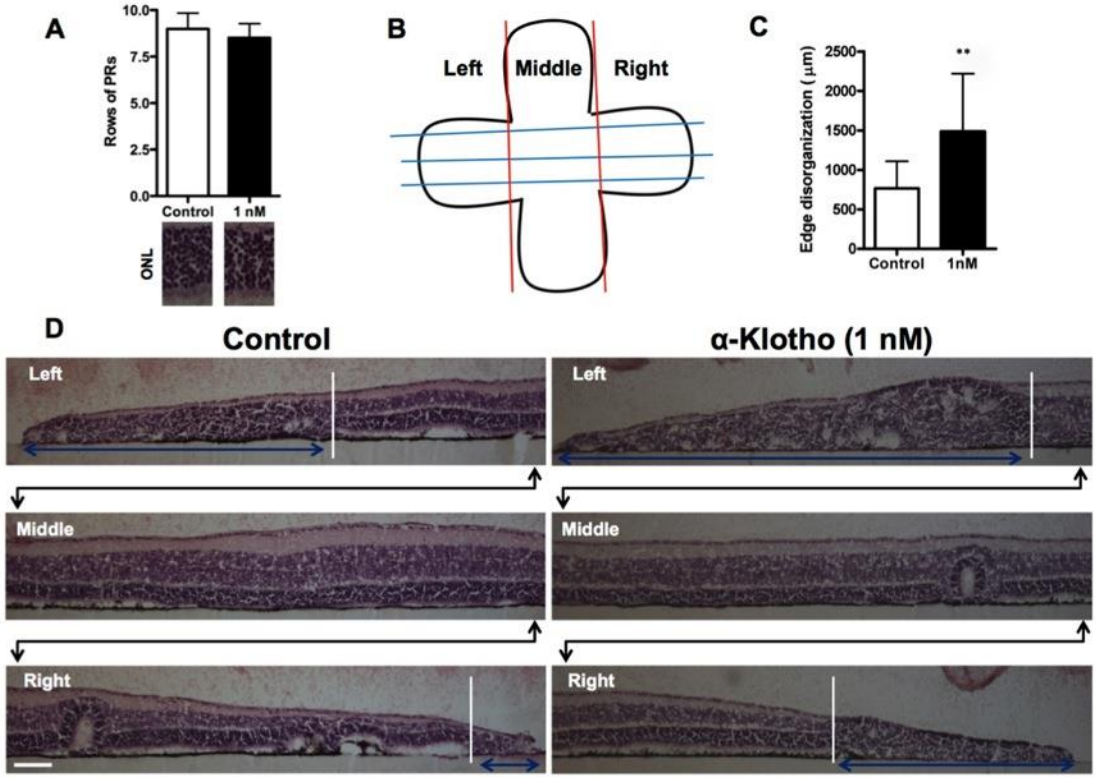

Figure 4.1.5. *α-Klotho treatment causes retinal disorganization.* Quantification of surviving rows of *wt* photoreceptors after the PN5+2+15 α-Klotho treatment paradigm is shown in (A). No significant difference was seen (mean ± SD; n = 12.) PRs = Photoreceptors. Micrographs below the bar diagram show examples of the hematoxylin-eosin histology of the corresponding ONL areas. The sketch in (B) depicts the typical propeller-like explant outline, with blue lines indicating approximate positions of the sections that are generally analysed in explant based experiments. The captions Left, Middle, Right indicate how the tissue in the micrographs below was situated in the explants, while the red lines indicate the approximate splitting points for these partitions. Panels in (D) show the histology of full and representative sections (split into Left, Middle and Right parts, respectively) of long-term *wt* retinal explants, untreated or treated with 1 nM α-Klotho. Note the treatment induced increase of disorganized area, as marked out by blue arrowed lines. The measurements of the disorganized lengths are summarized in the diagram in (C) (mean ± SD; n = 12; $p < 0.01$). Scale bar = 100 µm.

Immunostaining for rhodopsin showed compromised photoreceptors throughout the disorganized area of the α-Klotho treated *wt* retinae (Fig. 4.1.6). Moreover, immunoreactivity for bipolar cells (phosphorylated PKCα/βII; Zhang and Yeh 1991) was dramatically decreased in the same area. The α-Klotho treatment thus affected

both inner and outer retina integrity. However, TUNEL positive cells were seen predominantly at the outermost part of the edges, suggesting that not all cells in the disorganized area were actively undergoing cell death (Fig. 4.1.6).

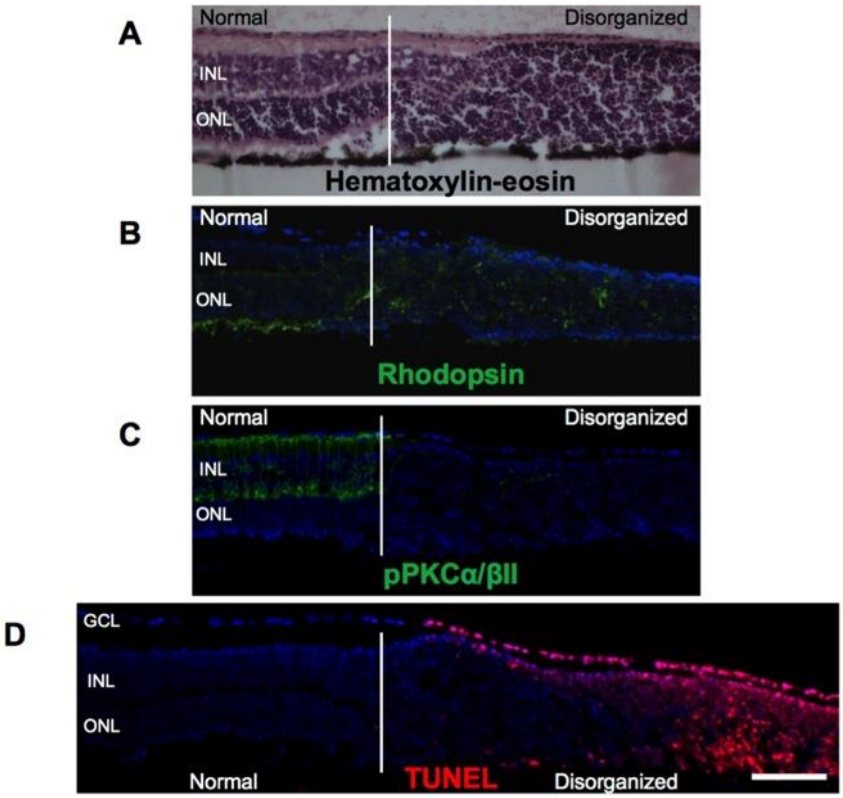

Figure 4.1.6. *Markers for rods and bipolar cells and TUNEL staining in α-Klotho peptide treatment of* wt *retinae.* The disorganized retinal areas (right side of white vertical bars in A to D), can be seen by hematoxylin-eosin staining (A), and shows a lack of ordered rhodopsin staining (B, rod photoreceptors) and severe reduction of pPKCα/βII (C, bipolar cells) staining, underscoring the disturbance of both outer and inner retina. The frequency of TUNEL positive cells decreased from the very edges towards the central parts of the explant (D), and there were (with the exception of ganglion cells) only very few TUNEL positive cells close to the border between the normal and disorganized retina. Staining results are representative of at least six independent samples. Layer labels are as in Figure 1. Scale bar = 100 μm.

FGF 15 in rd1 retina

An interesting feature of both α- and β-Klotho proteins is that they can associate with the four fibroblast growth factor (FGF) receptors (FGFR1-4), to act as co-receptors for the FGF19 subfamily members (FGF15/19, FGF21 and FGF23) (Kurosu *et al*. 2006; Liu *et al.* 2008). The Klotho proteins increase the atypical FGFs otherwise low FGFR affinity (Zhang *et al.* 2006) and enable activation of FGFR and downstream components (Kurosu *et al*. 2006; Wu *et al.* 2007). FGF15 represents the mouse orthologue to human FGF19, which has neuroprotective properties on adult

mammalian photoreceptors (Siffroi-Fernandez *et al.* 2008), and is expressed by various cell types in the developing mouse retina (Kurose *et al. 2004)*. We therefore studied the expression of FGF15 in post-natal *wt* and *rd1* retinae. PN11 retinae displayed FGF15 immunostaining in both the nerve fibre layer (NFL; not shown) and the photoreceptor outer segments (OS) (Fig. 4.1.7 and 8). With respect to the temporal dynamics, the expression of FGF15 in OS was in PN7 and PN9 specimen low in both *wt* and *rd1* genotypes, after which it increased, but then preferentially in the *wt* retinae. The comparably low expression in *rd1* OS at PN10 and PN11 suggests that low FGF15 expression in *rd1* photoreceptors may have caused an imbalance in any possible Klotho-FGF interactions. The *rd2* retina also shows a weaker FGF15 staining than corresponding *wt,* although the lack of OS here makes the analysis difficult (Fig. 4.1.7).

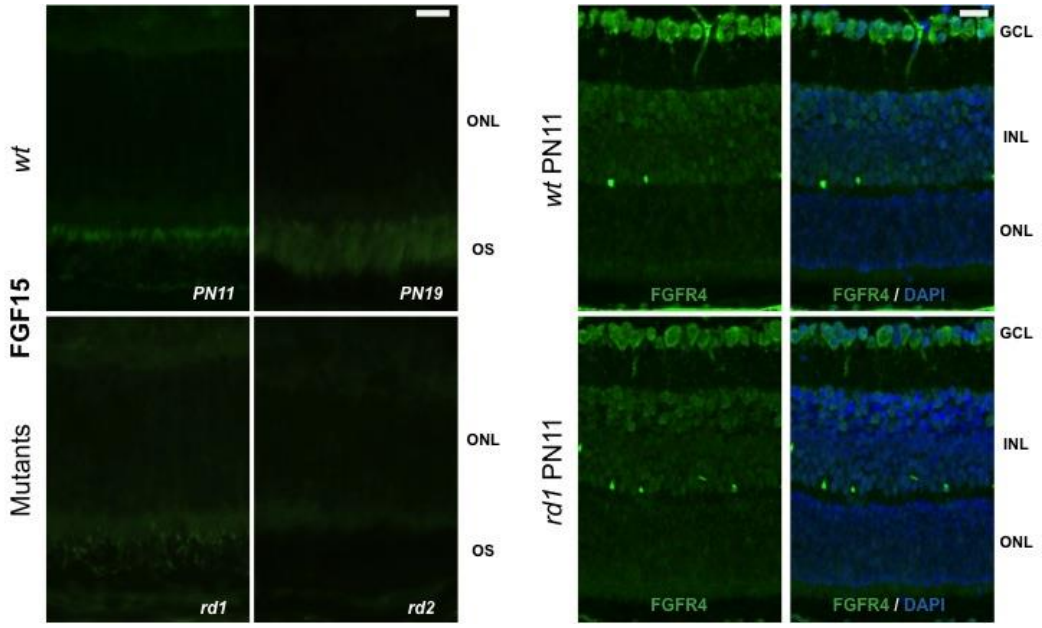

Figure 4.1.7. *FGF15/19 and FGFR4 expression mouse mutants.* Immunofluorescence staining of FGF15 in *wt* and *rd1* retinae at PN11, and in *wt* and *rd2* retinae at PN19. The staining is typical for at least three independent experiments. FGF15 is clearly expressed in photoreceptor outer segments (OS) of *wt* retinae, while it was much lower in corresponding areas of *rd1* samples. A similar situation may be present in the *rd2* retina, but here the OS are underdeveloped, making analysis difficult. FGFR4 is expressed throughout the retina. In particular ganglion cells appear strongly labelled. Cells in the INL are more weakly labelled and staining in photoreceptors is faint. FGFR4 seems to be primarily localised in the nuclei of all retinal cells. Labels are as for previous figures. Scale bar = 20 μm.

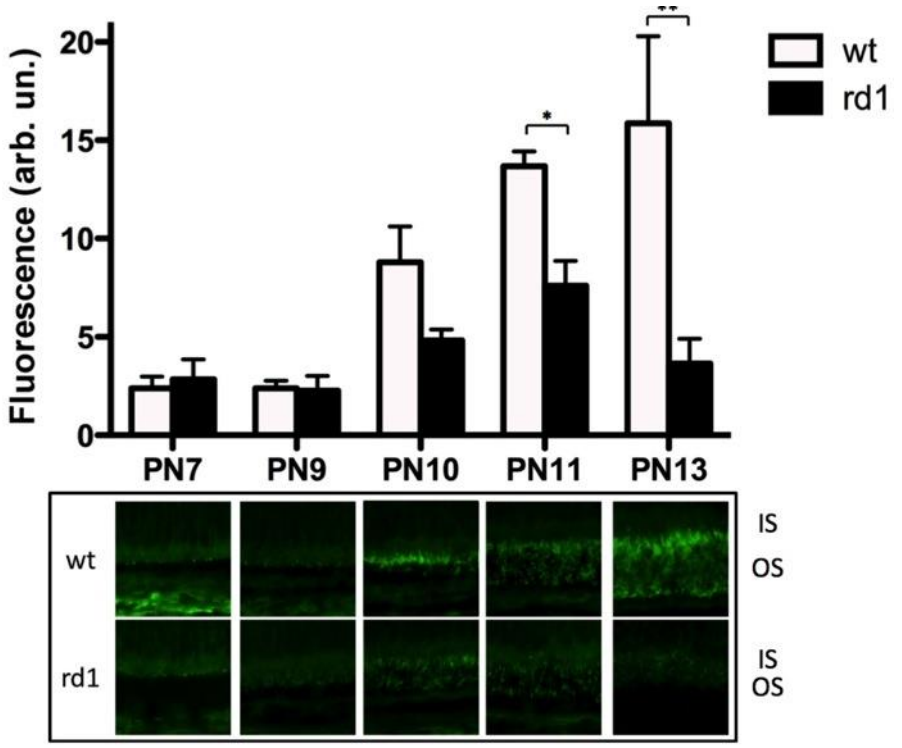

Figure 4.1.8. *Expression of FGF15 is reduced in degenerating retina.* Immunostaining of retinal tissue sections for FGF15 in the OS of *wt* and *rd1* retinae during the PN7-13 period. While *wt* FGF15 expression shows a strong increase after PN10, FGF15 in the *rd1* situation remains at low levels. The PN11 sections were 8 µm, all others 12 µm. Values are given as mean ± SD and represent analyses of three independent samples. Statistical significance was tested using two way ANOVA test (p-value < 0.05 = *; < 0.01 = **). OS = outer segments; IS = inner segments. Scale bar = 20 µm.

Discussion

The Klotho protein is recognized as an important factor for cellular ageing and survival (Kuro-o *et al.* 1997; Kurosu *et al*. 2005), but a clear connection between high Klotho expression and neuronal cell death, as shown here, has to our knowledge not been demonstrated before. Our results also suggest that overexpression of Klotho proteins, particularly α-Klotho, serves as a marker for hereditary photoreceptor cell death, and that the protein as such may act towards disorganization of photoreceptors and other retinal cells.

Klotho expression in the retina

Immunostaining using three independent antibodies identified a sub-population of photoreceptors in the *rd1* retina with a highly increased nuclear α-Klotho protein expression. Nuclear Klotho has previously been shown in both brain (*e.g.* Purkinje cells; German *et al.* 2012) and inner ear sensory cells (Takumida *et al.* 2009). α-

Klotho is known to assist the atypical FGF family in binding to the FGFRs and has been mainly found in the nuclei of dying photoreceptors. FGFRs are membrane proteins, although alternative spliced transcripts may lose the hydrophobic transmembrane domain and can then also be found as a soluble form (Guillonneau et al., 1998b). Since retinal FGFR4 could be detected in cellular nuclei (Fig. 4.1.7) one of the possible Klotho interaction partners may reside in this compartment.

The degeneration also affected α-Klotho mRNA, which was higher in *rd1* retinal samples than in *wt* material. This increase may have occurred over a low steady-state transcription of the α-Klotho gene, since a screen for Klotho mRNA showed its expression to be low or not detectable in several (adult) mouse tissues, including the eye (Fon Tacer *et al.* 2010). In contrast to immunostainings and mRNA measurements, our comparisons at the Western blot level did not show an *rd1 vs. wt* difference. However, the Western data suggested *wt* retinal α-Klotho protein levels to be sustained at a detectable level at the PN11 age, and an increase in a small, select number of cells, as in the *rd1* situation, would then be difficult to distinguish in a global sample.

Klotho and cell death

Each of the three α-Klotho antibodies revealed an extensive co-localisation with dying, TUNEL positive photoreceptors in the *rd1* retina. This confirms that the antibodies identified the same population of cells, and suggests that the α-Klotho increase connects with the *rd1* degeneration process. Moreover, this connection was not restricted to a certain model or species, since comparable co-localisation results were readily detected in the *rd2* mouse and in the *P23H* and *S334ter* rats. Taken together, these data argue for α-Klotho upregulation as an integrated and general event of photoreceptor degeneration, regardless of how the pathological processes start. Interestingly, this notion extends also to the β-Klotho protein, which showed increased expression, and broad TUNEL co-localisation, in a subset of *rd1* photoreceptors. We could not identify a significant increase in β-Klotho mRNA in *rd1* samples compared with control tissue, even though this was suggested in a previous microarray study (Azadi *et al.* 2006). The discrepancy might be attributed to the distinctive technologies used (microarray *vs.* qRT-PCR) or to other methodological differences. At any rate, Klotho expression is unequivocally associated with

photoreceptor cell death and may thus serve as a novel diagnostic marker for RP and related neurodegenerative diseases.

Is Klotho protective or destructive?

α-Klotho is linked to anti-ageing and has potential cellular protection capacities. In this role it may act extracellularly either on its own or as a co-receptor for members of the FGF19 subfamily, such as FGF23 (Wang and Sun 2009), although intracellular effects have also been described (Liu *et al.* 2011). Lack of α-Klotho appears to promote senescence (Kuro-o *et al.* 1997) and weaken the oxidative stress defence (Nagai *et al.* 2002). Conversely, oxidative stress, old age, inflammation, and cellular senescence lead to, or coincide with, reduced α-Klotho levels (Takumida *et al.* 2009; Liu *et al.* 2011; Mitani *et al.* 2002; Mitobe *et al.* 2005; Thurston *et al.* 2010). Furthermore, α-Klotho gene over-expression or addition of α-Klotho protein may counteract or reduce oxidative stress, inflammation, cellular senescence, cellular dysfunction, or even cell death in various systems (Liu *et al*. 2011; Saito *et al.* 2000; Yamamoto *et al.* 2005; Sugiura *et al.* 2010; Haruna *et al.* 2007). Since oxidative stress, in particular DNA oxidation, is involved in *rd1* degeneration (Paquet-Durand *et al.* 2007) the upregulation of α-Klotho in photoreceptors could thus be part of a protective response to such insults.

As an alternative scenario α-Klotho could instead be part of the neurodegeneration mechanism as such. This notion appears novel, since many investigations rather suggest α-Klotho to *counteract* neurodegeneration, in that α-Klotho reduction leads to signs of neurodegeneration and/or loss of cells in several areas of the CNS (Kuro-o *et al.* 1997; Nagai *et al.* 2002; Anamizu *et al.* 2005; Kosakai *et al.* 2011; Shiozaki *et al.* 2008). However, these reports identify neurodegeneration in a situation of experimentally altered α-Klotho, whereas we detected altered α-Klotho in a situation of disease-induced neurodegeneration, which represents a completely different setting. Judging from the distinct co-localisation of α-Klotho (and β-Klotho) with TUNEL, *i.e.* a clear connection with cell death, we are tempted to speculate that Klotho proteins may be involved in the later stages of the degeneration process. The fact that photoreceptor degeneration was not promoted by exogenous α-Klotho would then point to a preferential intracellular degeneration involvement of α-Klotho,

although the lack of effect might also be a result of Klotho co-effectors (*e.g.* FGF15) being low in *rd1* photoreceptors.

At any rate our study implies that degenerating photoreceptors experience a distinct imbalance in the Klotho-FGF system, which is interesting not the least because of the benign effects of FGF signalling on photoreceptor survival and maintenance (Green et al., 2001, Guillonneau et al., 1998a, Lau et al., 2000). Perhaps future experimental manipulation of the interaction between α- and/or β-Klotho and FGF15 protein family can shed light on the exact importance of the Klotho/FGF axis for the retinal degeneration process.

Furthermore, α-Klotho has been reported to confer resistance to oxidative stress through the expression of mnSOD (manganese supeoxide dismutase), led by FOXO (FoxO forkhead transcription factors) a downstream effector of the insulin intracellular signaling (Yamamoto et al., 2005). The activation of FOXO is negatively regulated by Akt (also known as PKB)-dependent phosphorylation. It is known that Akt is overactivated in *rd1* retinae (Johnson et al., 2005), therefore we can suggest that α-Klotho fails to confer protection in degenerating retina possibly because of its inability to induce expression of mnSOD.

Klotho and post-natal retinal development

Interestingly, exogenously added α-Klotho protein resulted in a structural disorganization of both inner and outer retinal elements at the edges of the preparations. For one thing this underlines that the lack of effect by Klotho on the degeneration was not likely to be due to methodological problems in those experiments. Furthermore, with respect to the mechanisms behind the disorganization**,** the treatment of the explants started at a time-point when the retina is still undergoing development in a centre-to-periphery fashion (Young 1985), making it possible that Klotho interfered with normal tissue development. Since retinal precursors are present in the retinal margin (Willbold and Layer, 1992), one should also not disregard the possibility that these may have been re-activated and contributed for instance to the loss of markers such as PKCα/βII. However, the fact that the treatment did not increase the size of the treated explants, a re-activation and significant growth of such stem cells seem not to have occurred.

In conclusion, the present report introduces α-Klotho as a novel player in the context of retinal health and disease, and particularly so in inherited retinal degeneration. While Klotho proteins are increased in degenerating *rd1* photoreceptors, FGF15 is reduced, suggesting an imbalanced α-Klotho-FGF axis as part of the disease characteristics. Furthermore, the disorganization of the developing mouse retina by α-Klotho is compatible with a role for this protein in retinal cell differentiation and/or layer formation.

Acknowledgements

The authors declare no conflict of interest. This study has been supported financially by grants from Torsten och Ragnar Söderbergs Stiftelser, Kronprinsessan Margaretas Arbetsnämnd för synskadade, Stiftelsen Olle Engkvist Byggmästare, The Swedish Research Council 2009-3855, Stiftelsen för Synskadade i f.d. Malmöhus län, Ögonfonden, Charlotte and Tistou Kerstan Foundation, Deutsche Forschungsgemeinschaft (DFG; PA1751/4-1). We like to extend our thanks to Dragana Trifunović for help with retinal samples for mRNA measurements, and to Birgitta Klefbohm and Hodan Abdshill for expert technical assistance regarding retinal explant experiments.

4.2 Excessive HDAC activation is critical for neurodegeneration in the *rd1* mouse

Cell Death Dis. 2010 February; 1(2): e24.

Sancho-Pelluz Javier[1,2], Alavi Marcel V.[3,4], Sahaboglu Ayse[1], Kustermann Stefan[1], Farinelli Pietro[4], Azadi Seifollah[5], van Veen Theo[1,4], Romero Francisco J.[2], Paquet-Durand François[1] and Ekström Per A. R.[4]

[1]Division of Experimental Ophthalmology, Institute for Ophthalmic Research, University of Tübingen, 72076 Tübingen, Germany; 2Fundacion Oftalmologica del Mediterraneo, Universidad Cardenal Herrera-CEU, Valencia, Spain; [3]Molecular Genetics Laboratory, Institute for Ophthalmic Research, University of Tübingen, Tübingen, Germany; [4]Division of Ophthalmology, Department of Clinical Sciences, Lund, University of Lund, Lund, 22184 Sweden; [5]Department of Biochemistry and Molecular Biology, University of British Columbia, BC, Canada

Rationale

Literature data support the notion of profound modification in the gene expression profile in *rd1* mouse. Furthermore, PARP enzymes that play a pivotal role in the DNA repair machinery are also involved in the epigenetic modification of the structure of the chromatin, are overactivated contributing to photoreceptor degeneration. The following paper is aimed at the study of histone deacetylases (HDACs), a family of protein able to remove acetyl groups on target proteins, regulating the gene expression through the control of the balance of chromatin compaction/relaxation.

Introduction

Retinitis pigmentosa (RP) is a group of inherited neurodegenerative diseases that result in selective cell death of retinal photoreceptors. Usually the mutations first lead to degeneration of the rod photoreceptor cells followed by a mutation-independent secondary degeneration of cone photoreceptors. With a prevalence of about 1 : 3500, RP is considered as the main cause of blindness among the working age population in

the developed world. At least 40 RP causing mutations have been identified so far, but the metabolic pathways leading to photoreceptor cell death have not been resolved, and no adequate RP treatment is available (Sancho-Pelluz et al., 2008).
The *rd1* mouse is one of the most studied human homologous RP animal models and carries a loss-of-function mutation in the gene encoding for the *β*-subunit of rod photoreceptor cGMP phosphodiesterase-6 (Bowes et al., 1990). This leads to an accumulation of cGMP, which eventually causes photoreceptor cell death. (Farber and Lolley, 1974, Paquet-Durand et al., 2009). In microarray experiments, others and we found *rd1* degeneration to be accompanied by extensive changes in gene expression (Azadi et al., 2006, Hackam et al., 2004, Rohrer et al., 2004). Although some changes may result from direct and specific effects of cGMP on defined genes (Pilz and Broderick, 2005), it is likely that also more generalized alterations of the transcriptional machinery are involved. Previously, we have shown that *rd1* photoreceptor degeneration is in part caused by a strong activation of poly-ADP-ribose-polymerase (PARP) (Paquet-Durand et al., 2007), which may have a bearing on transcriptional activity (Schreiber et al., 2006). However, as PARP activity was found to occur only relatively late during *rd1* degeneration, we hypothesized that there might be yet other mechanisms causing dysregulation of gene expression.

Gene regulation is to a large extent governed by epigenetic mechanisms, among which acetylation of histones (Egger et al., 2004) appears to be one of the most important (Morrison et al., 2007). Histone acetylation and deacetylation is mediated by histone acetyltransferases (HATs) and histone deacetylases (HDACs), respectively (Haberland et al., 2009). The HDAC family is subdivided into three main classes (HDAC I, II, and III), depending on their similarity with homologous yeast genes. Class I (HDAC 1–3 and 8) and class II (HDAC 4–7, 9, and 10) are inhibited by trichostatin A (TSA) (Haberland et al., 2009). Class III HDACs, also referred to as sirtuins (isoforms: sirt1–7) form a structurally distinct class of NAD+-dependent enzymes that can be inhibited by nicotinamide (NAM) (Kruszewski and Szumiel, 2005).

Although a number of studies have related transcription of photoreceptor genes and photoreceptor viability with histone acetylation (Chen and Cepko, 2007, Peng and Chen, 2007, Wallace et al., 2006), information regarding whether and how HDAC activity connects to degenerating photoreceptors is lacking. Here, we analyzed

enzymatic activities of different HDAC classes *in situ* on retinal tissue sections and studied how various inhibitors affect retinal cell viability. Activity of HDACs I/II was strongly elevated in *rd1* photoreceptors and causally related to their death, suggesting HDAC inhibition as a novel approach for neuroprotection in retinal degeneration.

Material and methods

Animals

Animals were housed under standard white cyclic lighting, had free access to food and water, and were used irrespective of gender. C3H *rd1*/*rd1* (*rd1*) and control C3H *wt* mice were used (Sanyal and Bal, 1973). All procedures were performed in accordance with the local ethics committee in Lund (permits M225-04 and M242-07), the Tübingen University (§4 registration from 23–01–08), and the ARVO statement for the use of animals in ophthalmic and visual research. All efforts were made to minimize the number of animals used and their suffering. Because of the critical changes at P11 (Hauck et al., 2006, Paquet-Durand et al., 2006), most comparisons between *rd1* and *wt* were carried out at this age. Day of birth was considered as P0.

Microarray analysis

Details of the transcription assay performed on a custom-made mouse gene chip were described in Azadi *et al.* (Azadi et al., 2006). Two times up- or downregulation in at least three out of five hybridizations was considered as significant variation. Results not pertaining to this study are published elsewhere.

In vitro retinal explant cultures

Retinae from P5 *rd1* and *wt* animals were used to generate retinal explants as described before (Paquet-Durand et al., 2009, Sanz et al., 2007). In brief, animals were killed and the eyes enucleated in an aseptic environment. Afterwards, the entire eyes were incubated in R16 serum-free culture medium (Invitrogen Life Technologies, Paisley, UK; 07490743A) containing 0.12% proteinase K (MP Biomedicals, Solon, OH, USA; 193504) at 37 °C for 15 min, to allow preparation of retinal cultures with RPE attached. Proteinase K was inactivated with 10% fetal calf serum (Invitrogen Life Technologies; PET10108165) in R16 medium, and the eyes dissected aseptically in a Petri dish containing R16 medium. The anterior segment,

lens, vitreous, sclera, and choroids were carefully removed, and the retina was cut perpendicular to its edges, resulting in a cloverleaf-like shape. Subsequently, the retina was transferred to a Millicell culture dish filter insert (Millipore AB, Solna, Sweden; PIHA03050) with the retinal pigment epithelium layer facing the membrane. The insert was put into a six-well culture plate and incubated in R16 nutrient medium at 37 °C. Every second day, the full volume of nutrient medium, 1.5 ml per dish, was replaced with fresh medium.

The first 2 days, the retina was left in R16 culture medium without treatment to adapt to culture conditions. At P7, cultures were either exposed to different treatments (TSA 1 μM, Scriptaid 6 μM, NAM 200 μM, and 1000 μM; all from Sigma, Munich, Germany), or kept as untreated control. NAM is a constituent of the culturing medium and present at about 22 μM, which should be less than half the reported IC50 value in cell-free studies (Bitterman et al., 2002). Explants were cultured until P11 for short-term cultures (P5+2+4), or until P28, for long-term cultures (P5+2+21). Culturing was stopped by 2 h fixation in 4% paraformaldehyde (PFA), washed 4 × 15 min in phosphate-buffered saline (PBS), then cryoprotected first with PBS +10% sucrose, and subsequently with PBS +25% sucrose. Explants were frozen and embedded in Jung tissue freezing medium (Leica Microsystems, Nussloch, Germany) for cryosectioning (12 μm).

HDAC assay

HDAC activity assays were performed on cryosections of 4% PFA P11 fixed eyes. The assay is based on an adaptation of the Fluor de Lys Fluorescent Assay System (Biomol, Hamburg, Germany). Retinal sections were exposed to different concentrations of Fluor de Lys-SIRT2 deacetylase substrate (Biomol) with 2 or 100 μM TSA (Sigma, Steinheim, Germany), 2 mM NAM (Sigma), and 500 μM NAD+ (Biomol) in assay buffer (50 mM Tris/HCl, pH 8.0; 137 mM NaCl; 2.7 mM KCl; 1 mM MgCl2; 1 mg/ml BSA) and 0.1% NP40 and 0.5 × Developer II (Biomol). Images were captured at indicated time points with a fixed exposure time of 2 s using a Zeiss (Jena, Germany) Axiophot microscope (× 20 magnification) and Zeiss Axiovision 4.2 software; densitometry was performed with the aid of ImageJ (National Institutes of Health, Bethesda, MD, USA). The reaction rate was determined in at least four independent experiments, as the slope of the linear regression fitted to the data points

in the linear range of a time course, using SigmaPlot (Systat software, Erkrath, Germany) software. For the calculation of *K*m values, the slope of time courses with different substrate concentrations was plotted against the corresponding substrate concentrations; a hyperbolic regression fitted to the data points revealed *K*m values and *V*max.

In situ deacetylation activity was determined on retinal sections incubated for 3 h with 200 μM Fluor de Lys-SIRT2 deacetylase substrate in assay buffer with/without inhibitors. Sections were then washed in PBS and fixed in methanol at −80 °C for 20 min. × 0.5 developer (Biomol) in assay buffer was applied and pictures taken immediately in an Apotome microscope (Zeiss), at × 20 using the DAPI filter.

TUNEL assay

The terminal deoxynucleotidyl transferase dUTP nick end labeling (TUNEL) assay was performed on cryosections from treated and untreated *rd1* retinas, using an *in situ* cell death detection kit conjugated with tetra-methyl-rhodamine or fluorescein isothiocyanate (Roche Diagnostics, Mannheim, Germany). For controls, terminal deoxynucleotidyl transferase enzyme was either omitted from the labeling solution (negative control), or sections were pretreated for 30 min with DNAse I (Roche Diagnostics, 3 U/ml) in 50 mM Tris-HCl, pH 7.5, 1 mg/ml BSA to induce DNA-strand breaks (positive control). Negative control showed no staining at all, whereas positive control stained all nuclei in all layers of the retina (Paquet-Durand et al., 2007).

Immunostaining

Frozen retinal sections from P11 animals or cultured retinae were dried for 30–60 min at 37 °C. Subsequently, the tissue was rehydrated in PBS, and preincubated for 1 h at room temperature (RT) in blocking solution, containing 10% normal serum, and 0.1 or 0.3% Triton in PBS (PBST). Immunohistochemistry was performed overnight at 4 °C, using primary Abs (acetylated lysine; acetylated H2A, H2B, H3, H4; Sirt2; HDAC2; HDAC5; PAR) diluted 1 : 100 in blocking solution. Primary Abs were purchased from Cell Signaling (Danvers, MA, USA) except PAR Ab (Alexis Biochemicals, Lörrach, Germany) and Rhodopsin Ab (Millipore, Schwalbach, Germany). The tissue was rinsed with PBST, and incubated for 1 h with a

corresponding secondary Ab, Alexa 488 (1 : 200–1 : 750, Invitrogen), diluted in PBST. Sections were rinsed in PBS, and mounted in Vectashield with DAPI (Vector Laboratories, Burlingame, CA, USA).

Western Blot

Retinae from P11 animals were enucleated and stored at −80 °C. Later on, the tissue was homogenized in buffer (10 mM Tris, 1 mM EDTA, 150 mM NaCl, 1 mM Na3VO4, 50 nM okadaic acid, 2% SDS, 10% glycerol, 0.0625 M Tris-HCl, and protease inhibitor cocktail 10 μl/ml (Calbiochem, Darmstadt, Germany); pH 6.8) with a Heidolph DIAX 600 homogenizer (Heidolph, Schwabach, Germany) or a manual homogenizer (glass to glass). Retinal explant cultures, both treated and untreated with TSA, from *wt* and *rd1* mice were homogenized using the same process. Bradford assay was used to measure protein concentration. Proteins were then separated by SDS-PAGE 4–12% gradient gel (at 55 V), and transferred to a PVDF membrane (Amersham Biosciences, Buckinghamshire, UK). Membranes were incubated in Roti block (Roth, Karlsruhe, Germany) blocking buffer for 3 h at RT. After washing, primary Abs (acetylated lysine; acetylated H2A, H2B, H3, H4; actin) were added at a dilution of 1 : 1000 in buffer containing TBS-T and 5% dried milk (Roth), and incubated overnight at 4 °C. Primary Abs were purchased from Cell Signaling, except for actin Ab which was from Chemicon (Schwalbach, Germany). After washing, the membranes were treated with buffer containing HRP-conjugated secondary Ab (Amersham Biosciences) overnight at 4 °C. The membranes were developed using Hyperfilm (Amersham Biosciences) detection system. Quantification was performed after film scanning using ImageJ (NIH).

Microscopy, cell counting, and statistics

Morphological observations and routine light microscopy were performed on a Zeiss Imager Z1 Apotome Microscope, equipped with a Zeiss Axiocam digital camera. Images were captured using Zeiss Axiovision 4.7 software; image overlays and contrast enhancement were performed using Adobe Photoshop CS3. Images shown in figures are representative for least three different animals for each genotype/treatment. Percentages of TUNEL-positive cells were assessed and calculated in a blinded manner as reported previously (Paquet-Durand et al., 2009,

Paquet-Durand et al., 2007). The mean value for photoreceptor rows in the ONL after *in vitro* culture was determined using DAPI nuclear counterstaining. Values are given as mean ± S.E.M. Statistical significance was tested using one-way ANOVA with Bonferroni correction and Prism (GraphPad Software, San Diego, CA, USA), significance levels were $P<0.05$ (*), $P<0.01$ (**), and $P<0.001$ (***).

Results

Expression of HDACs in wt and rd1 retina

Microarray analysis of the expression of 13 different HDAC genes did not identify any significant differences between wild type (*wt*) and *rd1* (Figure 4.2.1 A). Immunohistology revealed that HDACs representing all three major classes were present in *wt* and *rd1* retina at post-natal day (P) 11. Both class I HDAC2 (Figure 4.2.1 A and D) and class II HDAC5 (Figure 4.2.1 B and E) were prominently expressed in nuclei of the outer nuclear layer (ONL), inner nuclear layer (INL), and ganglion cell layer. In contrast, class III HDAC Sirt2 (Figure 4.2.1 C and F) was expressed predominantly in non-nuclear structures including photoreceptor segments, neuritic processes in the ONL, and different INL cells. No obvious differences in expression or localization between *wt* and *rd1* at P11 were detected for any of the HDACs.

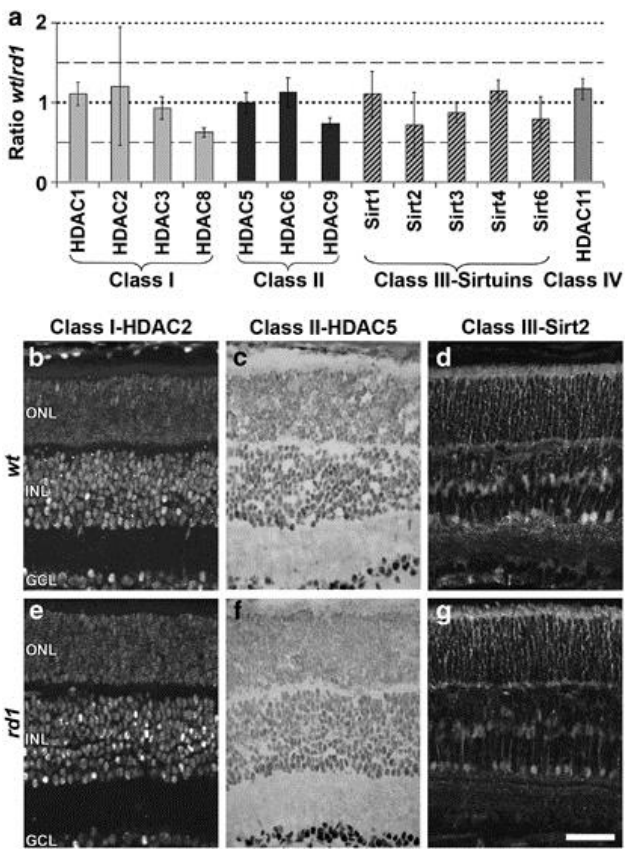

Figure 4.2.1. *Micro-array analysis and immunodetection of different HDAC isoforms in wt and rd1 retinae at P11 in vivo.* mRNA expression for 14 different HDAC isoforms pertaining to all 4 HDAC classes was assessed using micro-array analysis. For all studied HDAC isoforms, the ratio of mRNA expression wt/rd1 was not significantly different from 1, indicating that expression was not changed. Values are mean ± SEM from five independent hybridization experiments, each containing retinae from four male wt and four *rd1* animals. Immunostaining was performed for 3 different HDAC isoforms representing HDAC classes I-III HDAC2 (**B**, **E**) and HDAC5 (**C**, **F**) were expressed in nuclei of ONL, INL, and GCL,

while Sirt2 (**D**, **G**) was expressed in photoreceptor segments, neuritic processes in the ONL and different INL cell types. No obvious differences between *wt* (**B**-**D**) and *rd1* (**E**-**G**) were found. Scale bar: 50 µm.

rd1 photoreceptor nuclei show hypoacetylation

Acetylation of lysine residues was studied in *wt* and *rd1* retinae using acetylation-specific antibodies (Abs). In the ONL of *wt* mice at P11, an Ab detecting general acetylation of lysine residues showed homogeneous staining of the photoreceptor population (Figure 4.2.2 A - C). In contrast, the P11 *rd1* ONL presented staining ‘gaps' that contained unlabeled photoreceptor nuclei (Figure 4.2.2 D - F). Such lack of staining encompassed decreased histone acetylation, as confirmed by several Abs directed against specific acetylated histones (Figure 4.2.3). No obvious signs for hypoacetylation for any of the Abs used were found in the inner retina of neither *wt* nor *rd1*. Western blot (WB) of P11 *in vivo* retinae with the acetyl-lysine Ab (Figure 4.2.2 G) mainly revealed bands between 12 and 17 kDa that corresponded to the reported molecular weights of different histones and showed numerically decreased acetylation levels in the *rd1* retina (*wt*: 100 % *rd1*: 89.8 % ± 40, *n* = 3).

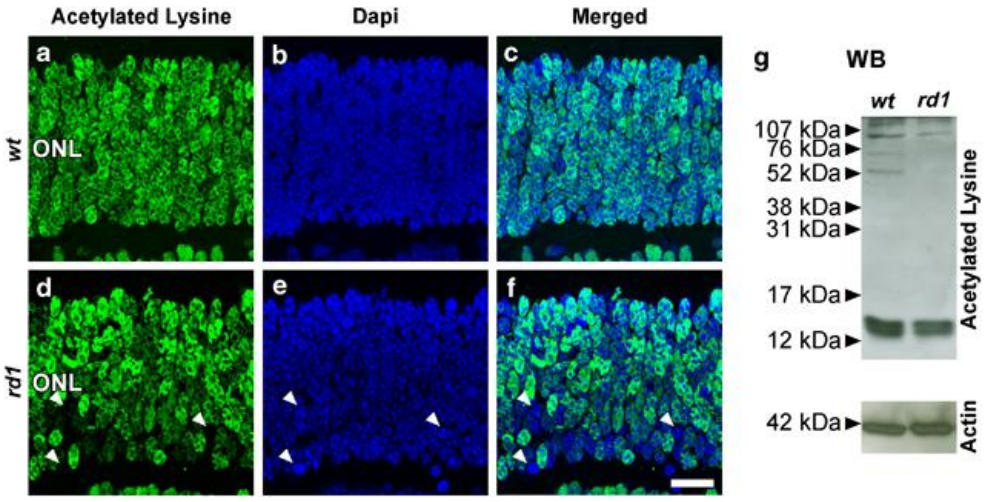

Figure 4.2.2. *Decreased acetylation in rd1 photoreceptors in vivo.* At P11 immunofluorescence for acetylated lysine residues (green) on wt (**a**) and rd1 (**d**) retinae revealed a number of DAPI-stained rd1 photoreceptor nuclei (**b**, **e**; blue) with very low levels of protein acetylation. (Merged pictures in **c**, **f**, arrowheads indicate nuclei showing low acetylation levels.) WB with the same Ab mainly labeled bands corresponding to the molecular weight of histones (**g**). Scale bar: 20 µm.

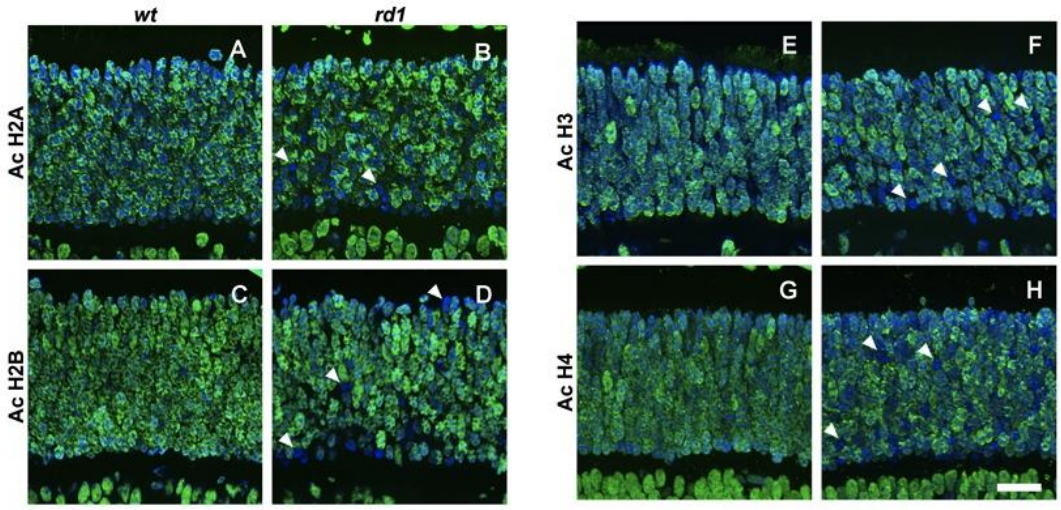

Figure 4.2.3. *Histone acetylation patterns in wt and rd1 retina***.** Antibodies against the acetylated forms of four major histones (H2A, H2B, H3, and H4) showed strong immunoreactivity (green) in *wt* photoreceptor nuclei. Similar staining was observed in *rd1* retina, however, a number of photoreceptor nuclei were not stained for acetylated histones (arrowheads), suggesting an imbalance in acetylation/deacetylation in these cases. DAPI (blue) was used as nuclear counterstain; pictures shown are representative for images obtained from retinae from at least 3 different animals for each genotype; scale bar=20 µm.

HDAC activity is increased in rd1 photoreceptors

To investigate whether the decreased *rd1* photoreceptor acetylation was related to increased activity of HDACs, we adapted a technique originally intended to measure tissue homogenates (Wood et al., 2004) for the use on retinal tissue sections.

Whole fixed retinal cryosections revealed deacetylation activity. By specifically blocking either HDACs I/II with TSA or HDAC III with NAM, we were able to distinguish the relative contributions of different classes of HDACs to the total activity, and to follow their kinetics with different substrate concentrations. As proof of principle for the HDAC assay, we determined the *K*m values for total HDAC activity on retinae of *rd1* and *wt* mice (Figure 4.2.4). The *K*m value for the fluorogenic substrate of 83 μM at 500 μM NAD+ is in good agreement with previous reports (Fan et al., 2009). When studied with cellular resolution, both *wt* and *rd1* tissue displayed HDAC activity in photoreceptor segments. All nuclear layers of *wt* retina were essentially devoid of visible activity (Figure 4.2.5 A). In contrast, the *rd1* ONL carried a subset of cells, displaying typical nuclear morphology of photoreceptors, with highly elevated HDAC activity (Figure 4.2.5 B). Inhibition of either class I/II HDACs (Figure 4.2.5 C) or HDAC III (Figure 4.2.5 D) suggested that

most of the excessive HDAC activity in *rd1* photoreceptor originated from HDAC I/II. Together, these results implied that *rd1* photoreceptor hypoacetylation was due to an excessive activation of HDACs, and most likely HDAC I/II.

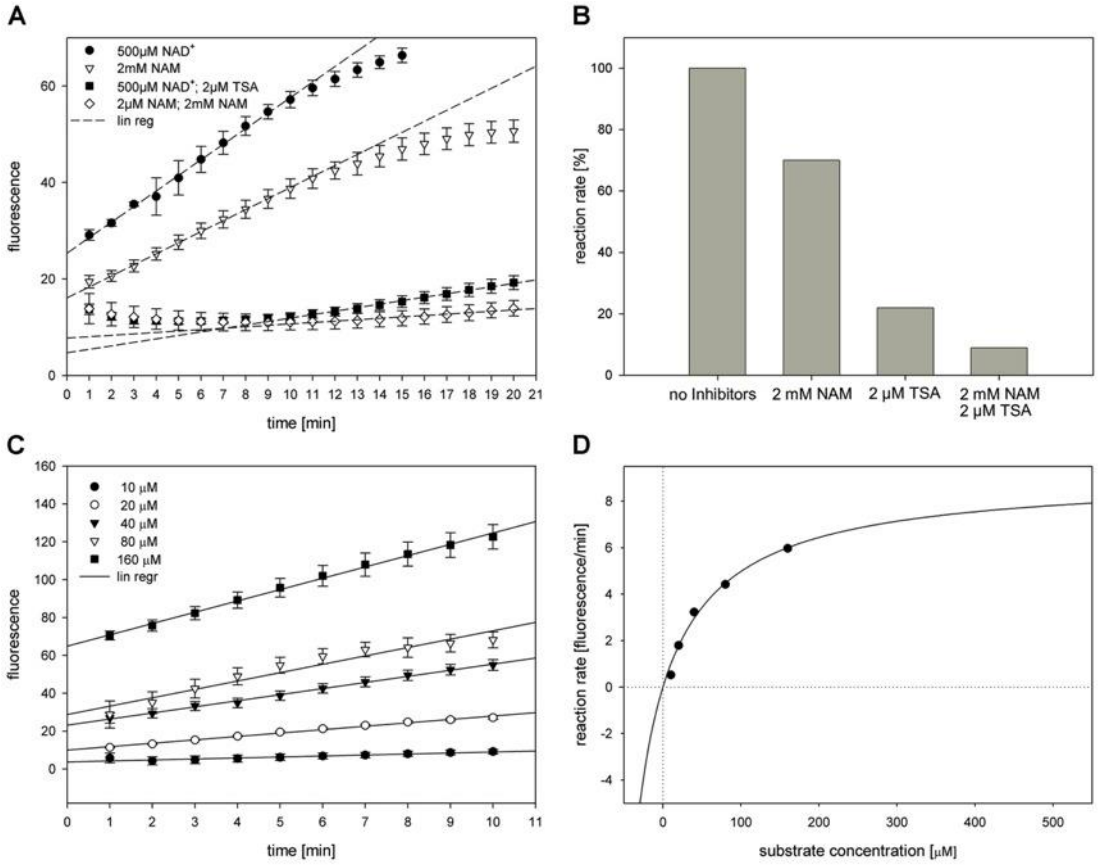

Figure 4.2.4. *HDAC activity in the retina in vivo.* HDAC activity reaction rates were measured on rd1 retinal tissue sections in the presence/absence of inhibitors specific to different HDAC classes. (TSA for HDAC class I/II; NAM for HDAC class III). The strong inhibition demonstrated by TSA suggested that measured activity was predominantly caused by HDACs I/II (**A**). Relative contributions of different HDACs to the general activity are shown in (**B**). Note that the assay has an auto-deacetylase activity of approx. 10% that could not be inhibited by NAM and TSA. Reaction rates with different substrate concentrations are shown in (**C**). To confirm that the observed signals were indeed caused by enzymatic activity, the dependency of reaction rate on substrate concentration was plotted and fitted to the Michaelis-Menten equation (**D**). Auto-fluorescence (t=0) was subtracted for all time points, n=4; lines in **A**, **C** indicate calculated regression for the linear reaction phase.

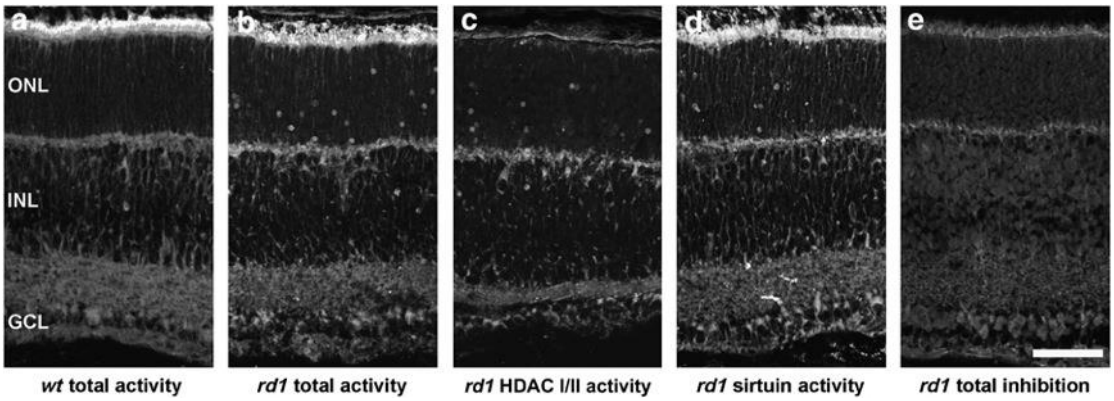

Figure 4.2.5. *HDAC activity in the retina in vivo*. HDAC activity was detected in situ in particular in the segment layers of both wt (**a**) and rd1 (**b**) retina. In contrast to wt, rd1 retina displayed a subset of ONL cells with strongly increased HDAC activity. Activity of HDAC I/II (**c**) was studied by inhibition of HDAC III with NAM. Conversely, sirtuin activity (**d**) was assessed by inhibiting HDACs I/II with TSA. Combined inhibition with TSA and NAM was used as negative control (**e**). Scale bar: 50 µm

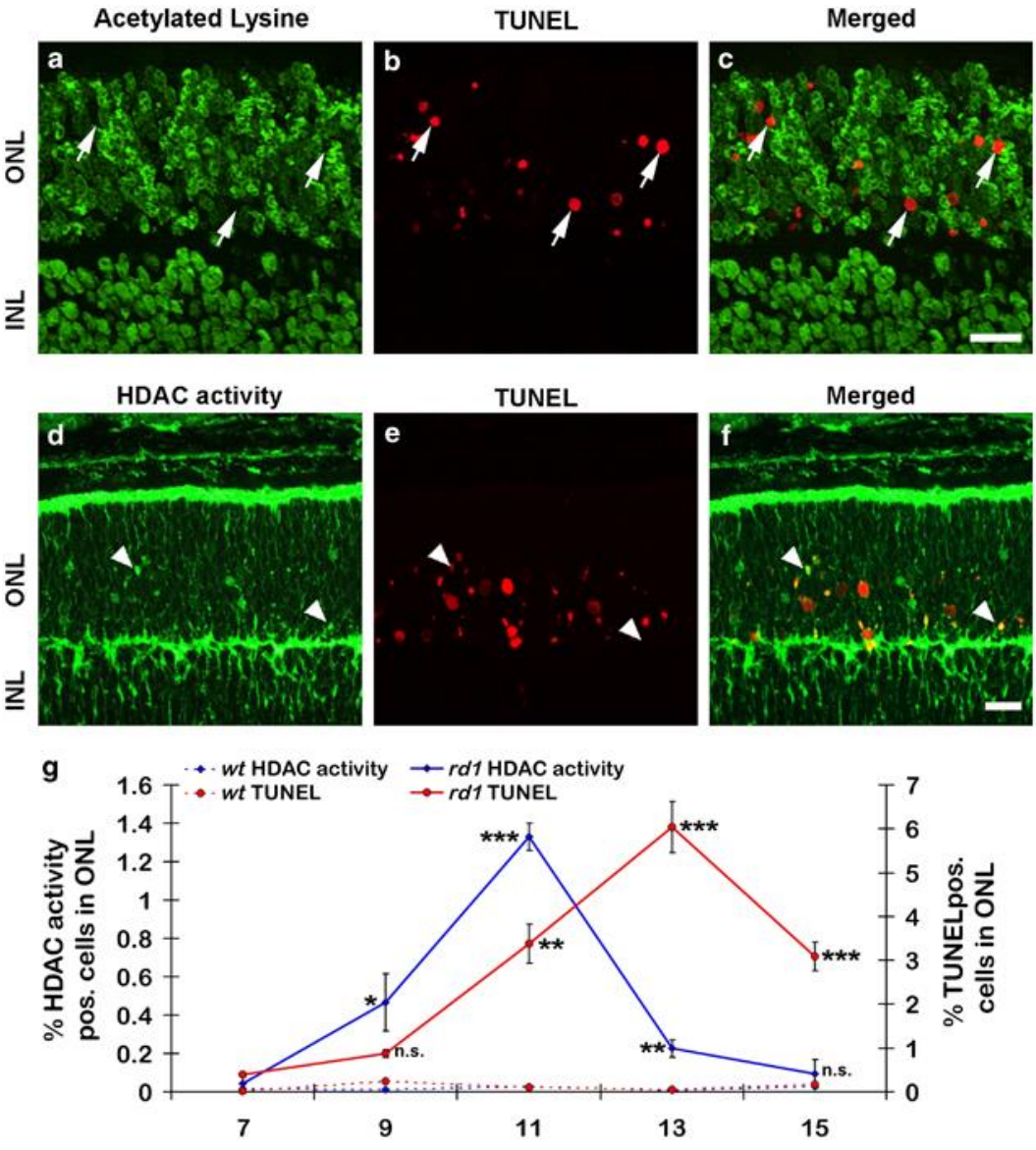

Figure 4.2.6. *Protein acetylation and temporal progression of HDAC activity and cell death* in vivo. At P11, immunostaining for acetylated lysine residues (**a**, green) in rd1 ONL showed characteristic "gaps", which were partly filled by TUNEL staining (red) for dying cells (**b**) (merged in **c**), suggesting hypoacetylation to contribute to photoreceptor cell death. Conversely, the HDAC activity assay (**d**, **f**) colocalized in part with TUNEL staining at P11 (**e**) in the rd1 ONL (merged in **f**). Scale bar: 20μM. The graph in **g** shows the temporal progression of HDAC activity (blue line) in wt and rd1 ONL during the second postnatal week, and relates it to the time-course for TUNEL-positive cells (red). Note that the peak of HDAC activity markedly precedes the peak of TUNEL. n >3 for each time point and genotype, data for TUNEL assay were previously published in Paquet-Durand et al., 2007 and are shown here for reference purposes only.

HDAC activity and cell death

To test whether the high HDAC activity observed in *rd1* photoreceptors was related to their degeneration, staining for acetylated lysine was combined with the TUNEL assay for dying cells. Most of the cells lacking acetylation (94.3 % ± 7.3 S.E.M., n = 3) were also TUNEL positive (Figure 4.2.6 A - C). In another co-labeling experiment, *rd1* HDAC activity colocalized only partially (32.5 % ± 6.7 S.E.M., n = 3) with TUNEL-positive cells (Figure 4.2.6 D - F) implying that the activity generally preceded the final stages of cell death. To confirm this hypothesis, we assessed the number of HDAC activity positive cells in the ONL of *wt* and *rd1* retinas at various time points during the second post-natal week (i.e., during onset and peak of *rd1* degeneration). The analysis of the temporal progression of HDAC activity showed a marked increase in the number of HDAC activity positive cells at P9, with a peak in activity already at P11 (Figure 4.2.6 G). Comparison with previously published data on cell death (TUNEL assay) and PARP activity (Paquet-Durand et al., 2007) indicated that the peak in HDAC activity preceded the peak of the degeneration by ~2 days. Overall, this suggested that an acetylation/deacetylation imbalance might have an important role in *rd1* photoreceptor degeneration.

HDAC I/II inhibitors protect rd1 photoreceptors

We then exposed retinal explants in a short-term culture paradigm (until P11) to inhibitors specific for the three main classes of HDACs and evaluated the outcome on photoreceptor viability using the TUNEL assay.

The HDAC I/II inhibitor TSA (1 μM) did not affect the number of TUNEL-positive cells in the ONL of P11 *wt* retinal cultures (TSA: 1.6 ± 0.2 %, n = 6 retinal cultures

from six different animals *versus* vehicle controls: 1.7 ± 0.2 %, *n* = 9; Figure 4.2.10 A and B). In the *rd1* retina, however, 1 μM TSA significantly decreased the rate of cell death (TSA: 2.2 ± 0.4 %, *n* = 12 *versus* vehicle: 3.5 ± 0.2 %, *n* = 27, *P* < 0.001; Figure 5c, d; quantification in panel e). A second HDAC I/II inhibitor, Scriptaid (6 μM), also conferred a significant neuroprotective effect to *rd1* photoreceptors (Scriptaid: 2.6 ± 0.1 %, *n* = 6, *versus* vehicle: 3.5 ± 0.2 %, *n* = 27, *P* < 0.05). The HDAC III inhibitor NAM (200 μM and 1 mM) had no measurable effect on photoreceptor viability (NAM 200 μM: 3.9 ± 0.2 %, *n* = 5 *versus* vehicle: 3.5 ± 0.2 %, *n* = 27; Figure 4.2.7 E). Neither of the above treatments affected the number of photoreceptor rows (quantification in Figure 4.2.7 E). Successful *in vitro* HDAC inhibition by TSA was confirmed using both a tissue-based analysis (WB for acetylated lysine; Figure 4.2.7 F) and an *in situ* approach (HDAC activity; Figure 4.2.8).

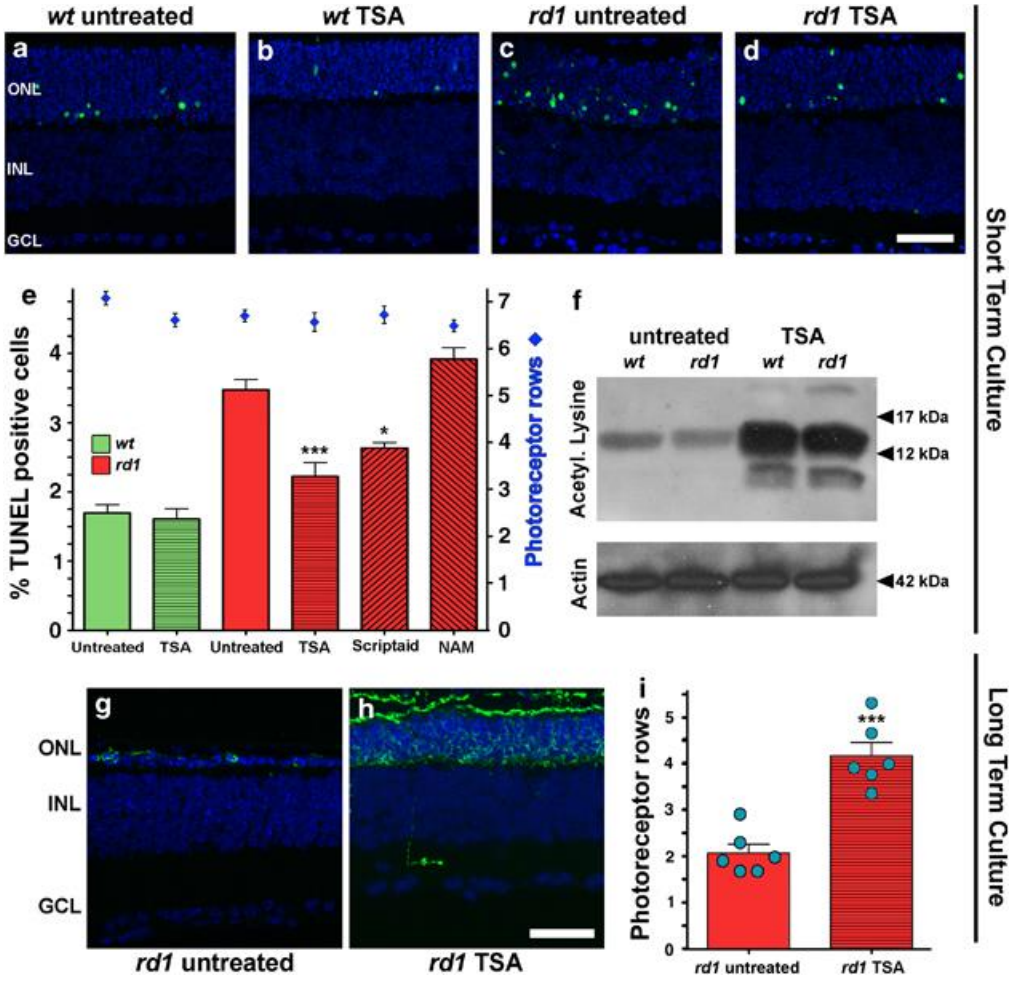

Figure 4.2.7. *HDAC inhibition reduces photoreceptor cell death* in vitro. Short-term retinal explant cultures from rd1 and wt animals were exposed to control conditions or 1 μM TSA from P7 to P11 (**a**-**d**). In untreated specimens (**a**, **c**), TUNEL assay (green) showed the characteristic increase of dying cells in rd1 ONL compared with wt. TSA treatment (**b**, **d**) reduced the number of degenerating photoreceptors in rd1, but did not alter viability of wt. The bar graph (**e**) summarizes effects of TSA, 6 μM Scriptaid, and 200 μM NAM on photoreceptor viability. HDAC I/II inhibitors, TSA and Scriptaid, significantly reduced the amount of dying cells, whereas HDAC III inhibitor NAM had no effect on cell survival. Immunoblotting for acetylated lysine residues (**f**) showed an increase in protein acetylation after TSA treatment in both wt and rd1 retinae. Long-term cultures of rd1 retinae (until P28; **g**, **h**) treated with TSA showed a marked increase in the number of rhodopsin-positive cell bodies and overall size of their ONL when compared with untreated situation (quantification in **i**). DAPI (blue) was used as nuclear counterstain; actin immunoblotting was used as loading control in **f**; n > 6, Scale bars in **d** and **h** are 50 and 20 μM respectively.

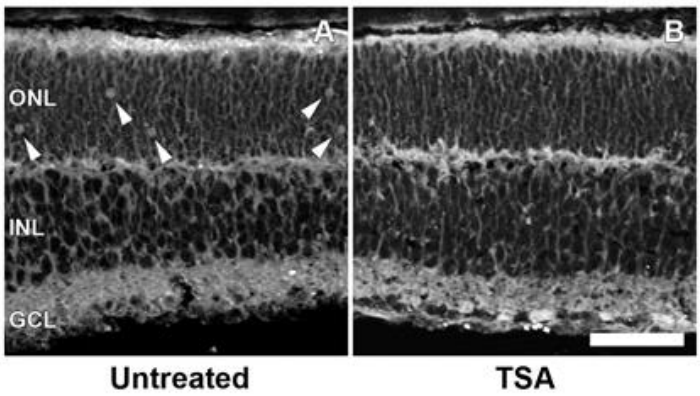

Figure 4.2.8. *TSA treatment reduces HDAC activity in rd1 photoreceptors*. After short-term culture with/without 1 μM TSA an HDAC activity assay was performed. While HDAC activity positive nuclei are present in untreated *rd1* ONL (**A**), they are undetectable in TSA treated specimens (**B**). Pictures shown are representative for images obtained from retinae from at least 3 different animals; scale bar=50 μm.

Although we did not observe any negative properties of TSA in our cultures, a previous study on acute *wt* retinal explants showed proapoptotic effects of TSA at early developmental stages (Wallace et al., 2006). To address the possibility of a transient TSA effect on retinal cell viability, we treated P5 *rd1* retinal explants with 1 μM TSA for 24 h, but this did not affect the percentage of TUNEL-positive cells in the P6 *in vitro* retina (TSA: 1.7 ± 0.2 %, vehicle: 1.5 ± 0.3 % n = 3; Supplementary Figure 4). Furthermore, when extending the culture period for another 5 days without TSA (P5 + 1 + 5 = P11), to match with the end point used in our previous experiments, the treated *rd1* retina again showed a markedly reduced number of TUNEL-positive cells (TSA: 1.0 ± 0.2 % vehicle: 3.8 ± 0.5 %, n = 3, $P < 0.05$). At the same time, the number of photoreceptor rows was not significantly affected by the treatment (TSA: 7.1 ± 0.2, vehicle: 7.5 ± 0.1; n = 3).

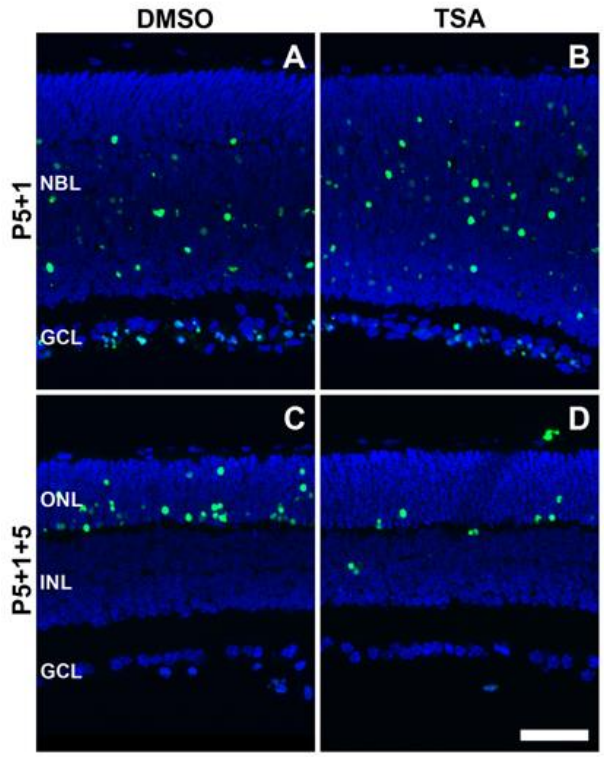

Figure 4.2.9. *TSA treatment reduces cell death in rd1 photoreceptors.* In *rd1* retinal cultures acutely treated with TSA from P5 to P6, control (DMSO; **A**) and TSA treated (**B**) specimens exhibit similar numbers of dying, TUNEL positive cells in the neuroblastic layer (NBL). However, when the culture period is prolonged for another 5 days beyond the TSA treatment (**C**, **D**), the number of dying cells in the ONL is markedly reduced in treated specimens (**D**; for quantification see main text). Pictures shown are representative for images obtained from retinae from at least 6 different animals; scale bar=50 µM.

paradigms would translate into improved long-term survival of photoreceptors, *in vitro* treatment was prolonged until P28. TSA treatment almost doubled the number of surviving *rd1* photoreceptor rows (TSA: 4.1 ± 0.3; vehicle: 2.1 ± 0.2, $n = 6$, $P < 0.001$; Figure 4.2.7 I).

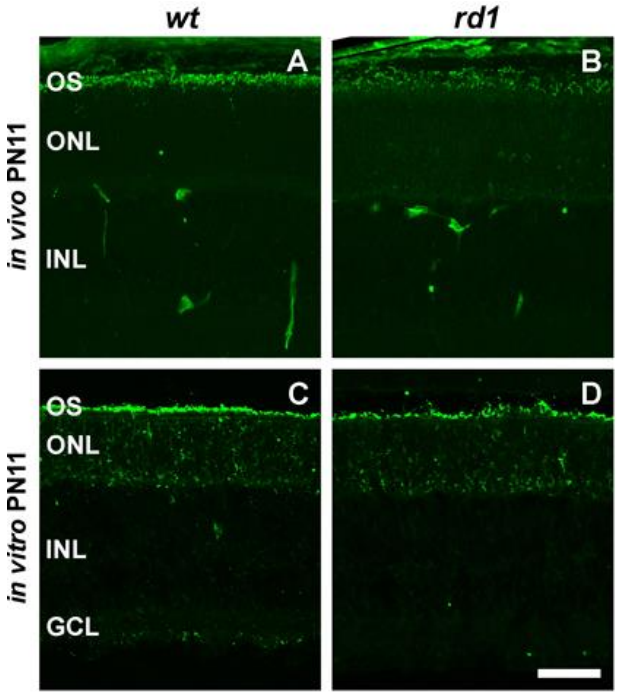

Figure 4.2.10. *Rhodopsin expression in wt and rd1 retina in vivo and in vitro.* In *wt* retina at P11 *in vivo* rhodopsin immunofluorescent staining is restricted to the outer segments of photoreceptors. In *rd1* retina, rhodopsin expression is also observed throughout the cytoplasm of photoreceptors. At P11 *in vitro,* expression of rhodopsin is observed in the cytoplasm of both *wt* and *rd1* photoreceptors. Immunofluorescent signal in the inner retina refers to unspecific mouse IGG staining; pictures shown are representative for images obtained from retinae from at least 3 different animals; Scale bar=50 µM.

Expression of rhodopsin was then analyzed as an indication of rod photoreceptor identity. In *wt* retina, *in vivo* rhodopsin expression is restricted to the outer segments of rod photoreceptors, whereas in *rd1* retina, where outer segments do not develop properly, it is partly mislocalized and also observed throughout the cytoplasm of photoreceptors (Bowes et al., 1988). This phenomenon intensifies under *in vitro* conditions where rhodopsin mislocalization is observed in both *wt* and *rd1* photoreceptors (Figure 4.2.10). In long-term TSA-treated explants, rhodopsin expression was found in most of the surviving *rd1* photoreceptors, whereas in the untreated situation most remaining ONL cells were rhodopsin negative and most likely predominantly cones (Figure 4.2.7 G and H). Significantly, rhodopsin-positive photoreceptor outer segments were observed in TSA-treated specimens, when at the same time in the untreated situation, outer segments were completely absent. This supported the idea that TSA indeed upheld survival of rod photoreceptors and promoted growth of *rd1* outer segments.

All in all, TSA treatment in both short- and long-term retinal culture demonstrated a strong prosurvival effect, whereas NAM had no such protective effects. The experiments therefore suggested a major contribution of HDAC I/II, but not III, to mutation-induced *rd1* photoreceptor death.

HDAC I/II regulate PARP activity

As we had previously found PARP activity to be involved in *rd1* photoreceptor cell death (Paquet-Durand et al., 2007), we wanted to investigate a possible interaction between HDACs and PARP. When immunostainings for acetylated lysines and for poly-ADP-ribose (PAR) – the product of PARP activity – were combined, the merged images revealed PAR-positive photoreceptor nuclei exclusively in cases where acetylation was absent (Figure 4.2.11 A - D). Together with the data on the progression of HDAC activity (Figure 4.2.7 G), this suggested that hypoacetylation and hence HDAC activity was preceding PARP activity.

We then tested whether HDAC I/II inhibition by TSA indirectly also affected PARP activity. With respect to PAR immunostaining, there was a moderate amount of positive photoreceptor nuclei in *wt* retinal explant cultures at P11 (*wt* vehicle: 0.25 % ± 0.1, $n = 3$), and a comparatively much higher number in *rd1* explants (*rd1* vehicle:

0.9 % ± 0.1; Figure 4.2.11 E and G). The presence of PAR-positive photoreceptors in *wt* explants is likely due to the stress that these undergo during culture. In both *wt* and *rd1* explants, the number of PAR-positive cells was reduced by TSA treatment, and this reduction was statistically significant in the *rd1* situation (*rd1* TSA: 0.3 % ± 0.2, $n = 3$, $P < 0.05$; Figure 4.2.11 F and H). These results supported the notion that activation of PARP in *rd1* photoreceptors occurred downstream of HDAC I/II activity.

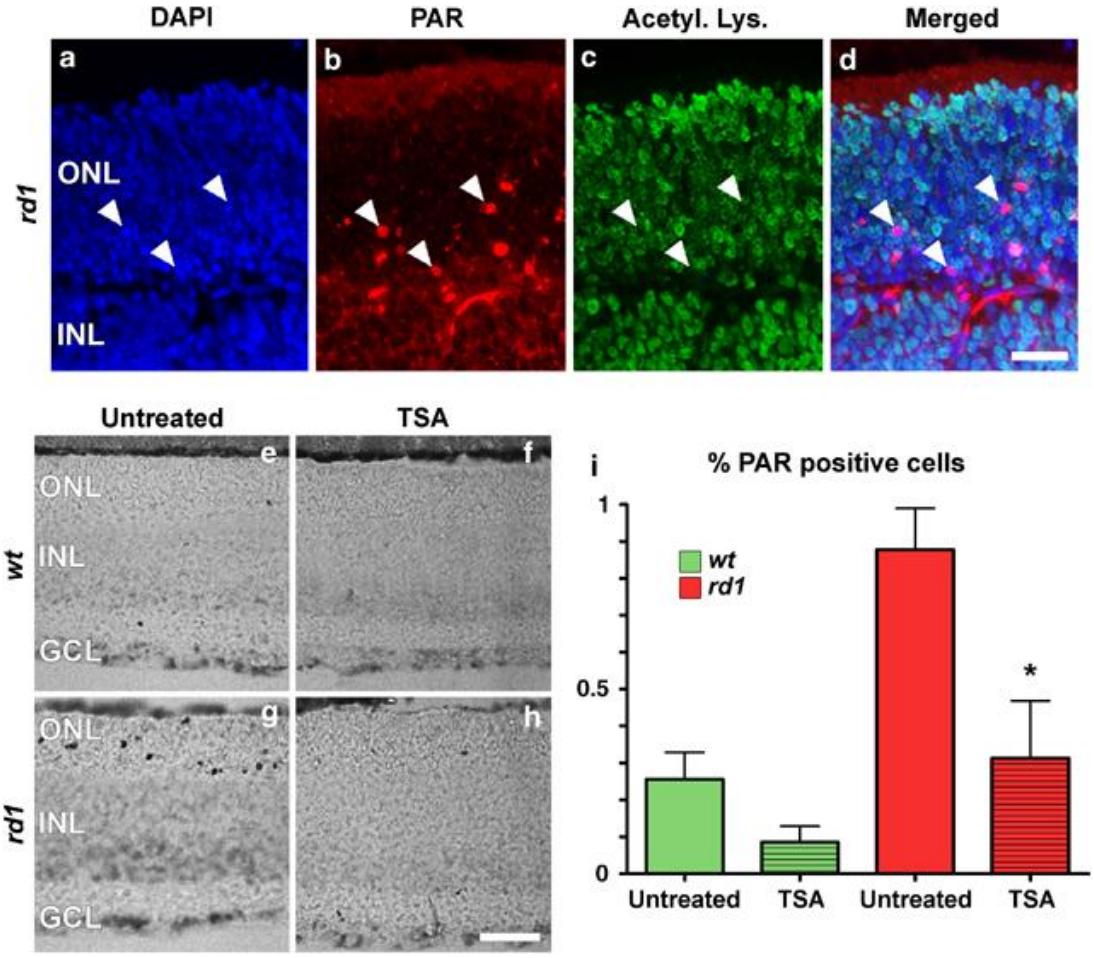

Figure 4.2.8. *HDAC and PARP activities are connected.* In rd1 P11 in vivo specimens, a subset of ONL nuclei showed unusual chromatin condensation as evidenced by DAPI nuclear counterstain (**a**, blue). In most of these cells a strong accumulation of poly-ADP-ribose (PAR) (**b**, red) colocalized with hypoacetylation (**c**, green; merged in **d**; white arrowheads), suggesting a functional connection between acetylation and PARP activity. In short-term retinal explant cultures at P11, photoreceptors showing PAR accumulation were observed in untreated wt (**e**) and rd1 retina (**g**), their number being much higher in the latter case. This number was strongly reduced by TSA treatment in both wt (**f**) and rd1 retina (**h**; quantification in **i**), implying that activation of PARP occurred downstream of HDAC I/II activity. n=3; Scale bar in **d**, **h**=20 μM. Some of the PAR immunostaining between ONL and INL relates to IGG staining in blood vessels

Discussion

The activity of HDACs has previously been connected to a variety of different cellular processes, notably regulation of gene expression, cytoskeletal rearrangements, division, and differentiation (Haberland et al., 2009). Here, we show that HDAC activity was causally related to inherited photoreceptor cell death in the *rd1* mouse and that this detrimental effect was tied to HDACs I/II. HDACs III did not seem to be involved in the degeneration, which corresponds to observations on weakened HDAC III action in degenerating retina (Jaliffa et al., 2009). The strong neuroprotection afforded by HDAC I/II inhibitors in both short- and long-term retinal explant cultures proposes them as novel lead compounds to prevent or delay retinal neurodegeneration.

HDAC and gene regulation

Given the extensive effects of acetylation/deacetylation on gene regulation, the observed HDAC hyperactivation would likely result in significantly altered *rd1* gene transcription, which matches with previous microarray data (Azadi et al., 2006, Hackam et al., 2004, Rohrer et al., 2004). On the other hand, we can at present not exclude the possibility that the observed histone deacetylation was due in part also to a decreased activity of HATs. Our observations that *rd1* gene alterations include downregulation of the transcription factor CREB (Azadi et al., 2006, Paquet-Durand et al., 2006, Pilz and Broderick, 2005) is of particular interest here, as CREB not only appears to confer neuroprotection (Azadi et al., 2006, Paquet-Durand et al., 2006, Pilz and Broderick, 2005) but also has several links to cellular acetylation events. For example, different HDAC I/II isoforms can recruit protein phosphatase-1 to dephosphorylate and inactivate CREB (Gao et al., 2009), which might be related to its downregulation in the *rd1* retina. Moreover, CREB target gene transcription is facilitated by its co-factor CREB-binding protein (CBP), which has HAT activity (Kalkhoven, 2004), and therefore connects CREB activation with histone acetylation. Accordingly, some of the effects on neuronal gene regulation seen when acetylation is increased by HDAC inhibition may be routed through enhanced activity of CREB and CBP (Vecsey et al., 2007). The expression of opsin and other photoreceptor genes is controlled by the photoreceptor-specific transcription factor cone-rod-homeobox (CRX) (Hennig et al., 2008). In conjunction with histone acetylation and CBP, CRX

drives expression of these critical photoreceptor genes in Y79 retinoblastoma cells and in the mouse retina (Palhan et al., 2005, Peng and Chen, 2007).

Cross-talk between HDAC and PARP activity

PARP activity is involved in DNA damage repair and hence often seen as a benign factor, although excessive PARP activity may compromise cellular viability (Schreiber et al., 2006). Increased PARP activity, as seen in *rd1* photoreceptors (Paquet-Durand et al., 2007), consumes NAD+ and generates NAM, which in turn negatively regulates HDAC III activity and thereby favors acetylation of its target proteins (Kruszewski and Szumiel, 2005). As HDAC III-dependent deacetylation of the automodification domain of PARP blocks its activity (Rajamohan et al., 2009), low NAD+ levels could trigger a positive feedback loop accounting for both the high PARP activity and the low HDAC III activity observed in *rd1* photoreceptors. Yet other reports demonstrate that acetylation by p300/CBP promotes the ability of PARP-1 to act as a co-activator in transcription (Hassa et al., 2005), whereas acetylation by histone acetyltransferases PCAF and GCN5L reduces PARP-2 catalytic activity (Haenni et al., 2008, Hassa et al., 2005). The findings highlight a possibility for hyperactive HDAC I/II to intervene with various PARP types, perhaps causing abnormal stimulation of these enzymes. In such a scheme, HDAC I/II activity would be upstream of PARP activation in *rd1* photoreceptor degeneration, which is in accord with our results, where TSA treatment reduced accumulation of PAR. In addition, PARP activity accompanies the event of dying, TUNEL-positive photoreceptors and colocalizes to a large extent with them (Paquet-Durand et al., 2007), whereas in this study, TUNEL colocalization with HDAC activity was only minor. This again implies that HDAC activity was upstream of PARP activation.

HDAC activity in cell death and survival

Experimental evidence suggests that both overactivation of HDACs I/II or their inhibition promotes cell death (Haberland et al., 2009). Similarly, HDAC III activity can have both pro- and antiapoptotic effects depending on cell type and proliferation state (Gan and Mucke, 2008), and the right balance between the activities of different HDAC classes therefore seems to be crucial for maintaining cellular viability (Haberland et al., 2009). In addition, individual members of each HDAC class could

have distinct cell type-specific roles (Chen and Cepko, 2009), perhaps related to their expression levels, which may in part explain the opposing effects of HDAC inhibitors observed in different neurodegeneration paradigms (Morrison et al., 2007). The protective effects of TSA and Scriptaid comply with a number of studies on post-mitotic neurons, where HDAC inhibitors also conferred neuroprotection (Bolger and Yao, 2005, Leng et al., 2008, Morrison et al., 2007), possibly in part due to the prevention of oxidative stress (Ryu et al., 2003) and reactivation of CREB signaling (Biermann et al., 2010, Rouaux et al., 2007). Furthermore, it is conceivable that in the *rd1* situation HDAC inhibition may induce expression or increase the stability of neuroprotective genes and proteins that are not directly related to the pathological mechanism. In this context, the chaperone HSP90, which is a target for HDAC-dependent deacetylation, appears to have a prominent role in neurodegeneration. Acetylation at its K294 residue inhibits HSP90 (Scroggins et al., 2007) and hence HDAC inhibitors indirectly also block HSP90 activity (Kekatpure et al., 2009). Interestingly, HSP90 inhibition induces an upregulation of the neuroprotective chaperone HSP70 and strongly increases neuronal survival (Shen et al., 2005, Wen et al., 2008). Our finding that decreased histone acetylation combines with increased HDAC activity corresponds to very similar observations made in motorneurons in a mouse model for amyotrophic lateral sclerosis, where HDAC inhibition also resulted in neuroprotection (Rouaux et al., 2007). In the *in vivo* retina, HDAC inhibition has been shown to promote survival of ganglion cells after optic nerve crush (Biermann et al., 2010).

Conclusion

The mechanisms governing inherited photoreceptor cell death have remained elusive to date (Sancho-Pelluz et al., 2008). Our discovery that HDAC activity was involved in photoreceptor degeneration may thus help to close a major gap of knowledge between the immediate effects of a single gene mutation (Bowes et al., 1990) and the observed massive changes at the transcriptional level (Azadi et al., 2006). Moreover, increased HDAC activity appeared to be responsible for an activation of PARP in degenerating *rd1* photoreceptors. The exact interplay between PARP and HDAC activity warrants further studies, as it may potentially explain crucial events in the pathological process. This study not only brings up HDAC activity as a ‘missing link,'

uniting several other findings on the mechanisms of photoreceptor cell death, but also highlights HDACs as novel targets for the development of neuroprotective therapies aimed to halt or delay inherited retinal degeneration in humans.

Acknowledgments

We thank H Abdalle, B Klefbohm, K Dengler, and S Kurz-Bernhard for excellent technical assistance and Y Arsenijevic, M-T Perez, and B Wissinger for helpful comments and discussions. This study was supported by grants from the EU (RETNET: MRTN-CT-2003–504003, EVI-GENORET: LSHG-CT-2005–512036, NEUROTRAIN: MEST-CT-2005–020235), Fundación Oftalmológica del Mediterráneo (FOM), KMA, Synfrämjandets Forskningsfond, Stiftelsen för synskadade i f.d. Malmöhus län, Foundation Fighting Blindness (FFB), Swedish Medical Research Council (VRM), Crafoord foundation, Kerstan Foundation, Torsten och Ragnar Söderbergs Foundation, and Deutsche Forschungsgemeinschaft (DFG; PA1751/1–1).

4.3 Degenerating photoreceptors in mouse and rat models of Retinitis pigmentosa display increased DNA methylation

(In finalization for submission)

Farinelli Pietro[1,2], Arango-Gonzalez Blanca[2], Michalakis Stylianos[3], Arshan Perera[3], Biel Martin[3], Mirko Wagner[4], Thomas Carell[4], Zrenner Eberhart[2], Paquet-Durand François[2], Ekström Per A.R.[1]

[1]Division of Ophthalmology, Department of Clinical Sciences, Lund, University of Lund, Lund, 22184 Sweden; [2]Division of Experimental Ophthalmology, Institute for Ophthalmic Research, University of Tübingen, 72076 Tübingen, Germany; [1]Center for Integrated Protein Science Munich (CIPSM) at the Department of Pharmacy - Center for Drug Research, Ludwig-Maximilians-Universität München, 81377 Munich, Munich, Germany;[4]Center for Integrated Protein Science Munich (CIPSM) at the Department of Chemistry, Ludwig-Maximilians-Universität München, 81377 Munich, Munich, Germany

Rationale

It has been reported that different processes affecting gene expression by modification of the histone-tails (performed by histone deacetylases, HDACs, and poly-ADP ribose polymerase, PARP) are increased in the retina of the Retinitis pigmentosa mouse model *rd1* and blockade of their respective pathways results in neuroprotection (Paquet-Durand et al., 2007, Sancho-Pelluz et al., 2010). For a more complete picture, and to open up for yet other therapeutical strategies, the following investigation was focused on the analysis of another epigenetic event, and in this case one that affects exclusively the DNA, namely methylation of cytosines.

Introduction

Retinitis pigmentosa (RP) refers to a heterogeneous group of inherited retinal degenerations that provoke progressive and irreversible loss of photoreceptors, and hence severe vision loss. The early onset of the disease and its prevalence (around

1:4000) makes RP the leading cause of inherited blindness amongst young people (Hartong et al., 2006). Currently, about 43 genes and 160 mutations have been linked to RP (https://sph.uth.tmc.edu/retnet/), but the mechanisms that lead from the mutations to the photoreceptor death are still unresolved, and there is unfortunately also no treatment available. Much would thus be gained if our knowledge of the pathological processes behind this group of diseases could be increased.

Modulation of gene expression is a regular outcome during disease conditions, probably as a consequence of both pro-survival responses and induction of cell death pathways. In an earlier microarray study, the gene expression profile of retinae from the *rd1* mouse, a well-studied animal model for RP, was compared with that of congenic wild-type (wt) retinae at post-natal day (PN) 11, *i.e.* a time point when the photoreceptor degeneration is well under way (Azadi et al., 2006). The study revealed up-regulation of 978 genes, whereas 214 were down-regulated, thus underlining how a disease state can profoundly affect a tissue. Modification of the gene expression may be accomplished through, for instance, epigenetic events, which could be defined as inheritable modifications of the gene expression not primarily due to changes in the DNA sequence (Li, 2002). In this regard, modification of histone tails, the chromatin-associated proteins around which the DNA is tightly wrapped, can compact or relax the structure of the chromatin, repressing or promoting the gene expression, respectively (Munshi et al., 2009). Accordingly, Sancho-Pelluz et al. (Sancho-Pelluz et al., 2010) proved that histone deacetylases (HDACs) class I and II, which among other things are involved in epigenetic modification of gene expression, are over-activated in the *rd1* mouse photoreceptors at PN11. Such an event is likely to induce compaction of the chromatin and may hence have contributed to the observed gene expression changes of the rd1 retina at this time-point.

A different way for epigenetic control of the gene expression is through biochemical modification of the cytosines in the DNA molecule. Methylation of DNA consists of the covalent addition of a methyl group on the carbon 5 of cytosines, that are followed by guanosine (CpG dinucleotides) and is carried out by various DNA methyl transferases (DNMTs) (Goll and Bestor, 2005). They are three catalitically active enzymes (DNMT1, 3A and B (Kinney and Pradhan, 2011)), a trascriptional repressor devoid of methyltransferase activities called DNMT3L (Aapola et al., 2002) and DNMT2, which unlike the other members, seems to be involved in the methylation of

the tRNA (Goll et al., 2006). The methylation occurs mainly in the promoters of the genes, but can also be seen in intergenic non-coding regions and within genes (Jones, 2012). Methylation of the cytosines is generally associated with the repression of the transcription (Jones and Liang, 2009) and may therefore have physiological as well as pathological impacts due to the silencing of imprinted genes. It is hence possible that the photoreceptor degeneration due to RP encompasses alterations not only in acetylation status but also in DNA methylation.

In light of the above we have here used several techniques to investigate the possible involvement of DNA methylation in the photoreceptor degeneration seen in RP models. The investigations have emphasised the *rd1* mouse, which carries a mutation in the β subunit of the rod specific phosphodiesterase 6 gene (PDE6β) (Keeler, 1966). To cover a wider range of RP subtypes we have in addition studied three other rodent mutants: The *rd2* mouse, that carries a mutation in the peripherin-2 gene (Travis et al., 1991), and the S334ter and P23H transgenic rats, which both carry mutations in the rhodopsin gene, but which display different pathological characteristics (Shinde et al., 2012, Oh et al., 2003, Dryja et al., 1990). All of the four models represent mutations that are similar to the ones found in certain cohorts of patients (Bayés et al., 1995, Boon et al., 2008, Kaur et al., 2011).

Our data show an increase in the methylation of the DNA of dying photoreceptors in all analysed animal models for RP, including from two different species. Furthermore, pharmacological inhibition of DNMTs affects the photoreceptor cell death. This fact suggests methylation of the DNA as a common step in the photoreceptor degeneration pathway by different genetic mutations.

Material and methods

Animals

Animals used included C3H rd1/rd1 (*rd1*), C3H rd2/rd2 (*rd2*) and control C3H wild-type (wt) mice (Sanyal and Bal, 1973), all kept in colonies in Lund or, in the case for the mRNA measurements, in Münich. Homozygous P23H and S334ter rhodopsin transgenic rats were originally produced by Chrysalis DNX Transgenic Sciences, Princeton, NJ) of the line Tg(P23H)1Lav and Tg(S334ter)3Lav (P23H and S334ter-3), and were kindly provided by Dr. M. M. LaVail (University of California, San

Francisco, CA) and bred in the Tübingen laboratory animal housing facility. Heterozygous P23H and S334ter rats were obtained by crossing with wild-type, CD rats (CD® IGS Rat; Charles River, Germany) to reflect the genetic background of adRP. CD rats were used as controls. All procedures were performed in accordance with either the Swedish (*rd1* and *rd2*, *wt* mice; permits # M242/07, M220/09, M172/12) and German (S334ter, P23H and CD rats, Anzeige/Mitteilung nach § 4 vom 28.04.08 and 29.04.10) animal care committees. Efforts were made to keep the number of animals used and their suffering to a minimum and the experiments followed the ARVO statement for the use of animals in ophthalmic and visual research. Animals were kept in the animal house under standard white cyclic lighting, with *ad libitum* access to food and water, and were used irrespective of gender.

Loss of retinal tissue due to the degeneration could introduce a bias in the analyses and comparisons between *rd1* and *wt* retinae were therefore typically performed at postnatal day (PN) 11 (although other time-points were included in some experiments). At PN11 degenerating photoreceptors are numerous in the *rd1* retina, but their loss has not yet resulted in any readily measurable thinning of the photoreceptor layer (Hauck et al., 2006, Sancho-Pelluz et al., 2008). For the other models we chose time-points that would, respectively, act toward the same purpose, *i.e.* for *rd2* mice PN19, for *Rho* P23H rats PN15 and for *Rho* S334ter rats PN12.

Organotypic retinal explant culture

Tissue was obtained from, PN5 *rd1* animals were killed by decapitation, and retinae were cultured as previously described (Caffé et al., 2002). In detail, immediately after killing of the animals the eyes were enucleated. To allow preparation of retinal explants for culturing with the retinal pigment epithelium (RPE) still attached, the eyes were incubated in R16 serum-free culture medium (Invitrogen Life Technologies, Paisley, UK; 07490743A), that contained 0.12 % proteinase K (MP Biomedicals, Solon, OH, USA; 193504), at 37 ºC for 15 min. The proteinase K was then inactivated with R16 medium containing 10 % fetal calf serum (Invitrogen Life Technologies; PET10108165), after which the eyes were dissected aseptically in a Petri dish with R16 medium. The retina and RPE were isolated and subsequently transferred to a Millicell culture dish filter insert (Millipore AB, Solna, Sweden; PIHA03050), with the RPE layer facing the culturing membrane and incubated in R16

nutrient medium at 37 ºC. The full volume of nutrient medium, was replaced every second day (with the exception of the one day treatment experiments below) during the culturing period.

PN5 explants were allowed to adjust to culture conditions for 2 days in vitro (DIV). After that, cultures were treated with 5-aza-2'deoxycitydine (decitabine, Sigma, A3656) every second day for four days reaching the equivalent to PN11 (short term: PN5 + 2 DIV + 4 DIV) or to PN19 (long term: PN5 + 2 DIV + 12 DIV). The cultures assigned for treatment were given 0.5, 1.25, 2.5, 5 and 10 μM of decitabine. Quantification of TUNEL positive cells and the counting of the rows of surviving photoreceptors represented the readout for short and long-term cultures respectively. All treatment experiments were done in a paired fashion, and the treated and untreated samples from one and the same animal were subsequently processed together. This meant, for instance, that treated and untreated samples of one and the same pair could readily be stained under the exact same, and hence comparable, conditions.

Fixation, sectioning and microscopy

Mouse and rat eyes and cultured retinas were enucleated, fixed in 4 % PFA in PBS for 2 h and 1h in 4°C respectively. Eyes cryoprotected in Sorensen's sucrose buffer and processed to 12 μm cryosections.

Routine morphological observations were performed on a Zeiss Axiophot (Jena, Germany) microscope equipped with a Zeiss Axiocam digital camera. Fluorescence excitation was provided by a HBO 100W halogen lamp. Images were taken by mean of Zeiss Axiovision 4.2 software; images elaboration and overlays were performed utilizing Adobe Photoshop CS (San Jose, California, USA).

Terminal dUTP nick-end labelling (TUNEL)

TUNEL staining on fixed preparations was performed using an *in situ* cell death detection kit (Roche, Mannheim, Germany) conjugated with TMR red. Controls with this kit and similar preparations have been performed by omitting the terminal deoxynucleotidyl transferase enzyme from the labelling solution (negative control), and by pretreating the sections for 30 min with DNAse I (Roche, 3U/ml) in 50 mM

Tris-HCl, pH 7.5, 1 mg/ml BSA to induce DNA strand breaks (positive control) (Paquet-Durand et al., 2007).

Histological staining / Immunofluorescence

PFA fixed sections were stained for general histological light microscopic analysis with hematoxylin-eosin (HE) according to standard protocols, or underwent immunostaining. For the latter, the sections were washed 3 x 5 minutes each in PBS containing 0.25 % Triton X100 (PTX) plus 1 % BSA. Blocking solution containing PTX and 5 % normal serum from the host animal, from which the secondary antibody was obtained, was applied for 45 minutes. Primary antibodies (see Table I) were diluted in PBS with 1 % BSA and 0.25 % Triton X100, and applied overnight at 4° C. Sections were then washed 3 x 5 min each in PTX and incubated with appropriate secondary antibodies diluted in PTX (see Table I) for 45 minutes. After 3 more washing steps in PBS, the sections were mounted with Vectashield DAPI (Vector, Burlingame, CA, USA). Controls consisted of sections processed in parallel without primary antibody and application of the fluorescence detection system. After three more washing steps in PBS, the sections were mounted with Vectashield DAPI (Vector, Burlingame, CA, USA). Controls consisted of sections processed in parallel without primary antibody and application of the fluorescence detection system. The immunodetection of 5-methylcytosine (5mC) may, conceivably, be influenced by the denaturation state of the DNA, and so we in separate experiments performed pre-treatments, consisting of 3N HCl for 10 min, of the sections before the antibody incubations.

Counting of cells and tissue parameters

The number of TUNEL or 5mC (+) cells was assessed and calculated as reported previously (Paquet-Durand et al., 2006, Paquet-Durand et al., 2009). For each animal at least three sections were quantified to yield an average value, and at least three different animals were analysed for each experimental situation. Values are given as TUNEL (+) cells relative to control ± standard deviation (SD). Statistical significance was tested using both paired and unpaired, two-tailed, Student's t-test or ANOVA test.

For all tests, a p-value < 0.05 was considered to indicate a statistically significant difference.

Western blot

PN11 retinae were isolated in dissecting buffer (10 mM Tris, 1 mM EDTA, 150 mM NaCl, 1 mM Na_3VO_4, 50 nM okadaic acid, pH 7.3) supplemented with protease inhibitor mixture (Complete Mini, Roche) and immediately homogenized in sample buffer [2% sodium dodecyl sulphate (SDS), 10% glycerol, 0.0625 M Tris-HCl, pH 6.8] by use of an electrical pestle. After centrifugation for 10 min at 14,000 x *g*, the supernatant containing proteins was removed and quantified straight after by mean of Bio-Rad DC Protein Assay kit (Hercules, CA, USA). Either 10 or 20 µg of protein from each sample were separated by SDS-PAGE on 12% gels, and blotted onto Immobilon-P polyvinylidene difluoride (PVDF) membranes (Millipore, Billerica, MA, USA). Membranes were incubated for 2h in blocking buffer (5% non-fat dried milk in PBS with 0.1% Tween 20) on gentle rotation and then kept overnight at 4°C with antibodies of interest. The membranes were then washed 3 times for 10 minute, treated for 1h with horseradish peroxidase-conjugated secondary antibodies, followed by another round of washing. Immunoreactions were visualized using the ECL Plus Western Blotting Detection system (Amersham Biosciences, Sunnyvale, CA) and Hyperfilm (Amersham Biosciences).

Methylated DNA immunoprecipitation (MeDIP)

MeDIP has been performed according to the protocol provided from NimbleGen (http://www.nimblegen.com/). In detail: DNA was extracted wt and *rd1* retinae at PN11 with DNeasy kit (Qiagen, Hilden, Germany, 69504) according to manufacturer's instructions. DNA was incubated overnight at 37 °C with *MseI* restriction enzyme (New England Biolabs, Ipswich MA, USA, R0525S) which cuts just unmethylated sequences. The buffer provided by the company needed to be supplemented with 100 ng/µl BSA and the reaction ran over-night at 37 °C. Digested DNA samples were then purified using QIAquick PCR Purification Kit (Qiagen, 28104) according to manufacturer's instructions. 1,25 µl of purified DNA was then diluted in 300 µl of TE buffer (10mM Tris HCl, pH 7,5; 1mM EDTA) and heat denatured at 95 °C for 10 min. 60 µl (250 ng) were then removed and stored as input

control, while to the remaining DNA, 60 µl of 5x IP buffer (100 mM Na-phosphate, pH7,0; 5M NaCl; 10 % Triton X-100; ddH_2O until final volume) were added. Samples were then immunprecipitated using a mouse anti 5-methylcitydine antibody (Abcam, Cambridge, UK, Ab10805) with a 1:1 ratio of antibody/DNA. The incubation DNA/antibody mixture was done on a rotating platform overnight 4 °C at a very low speed to avoid any foaming. Next antibodies conjunction to beads of Protein A-agarose (Invitrogen, Carlsbad CA, USA, 15918-014) was performed for 2h at 4 °C by gentle rolling. After washing the beads in 1x IP buffer, they were centrifuged at 6000 rpm for 2 min at 4 °C and the supernatant was discarded. The washing step was repeated twice again and the beads were resuspended in 250 µl digestion buffer (1M Tris HCl, pH 8,0; 0,5M EDTA; 10 % SDS; ddH_2O until final volume). In order to resuspend the beads, 7 µl (10 mg/ml) of proteinase K (Roche Applied Science, Penzberg, Germany, 03115836011) was added. Microcentrifuge tubes containing the antibody-beads complex and DNA were then sealed with Parafilm and placed in 50 ml Falcon tubes filled with damp paper towel to avoid evaporation and incubated overnight on a rotating platform at 55 °C. In order to purify the samples, 250 µl of phenol (Sigma Aldrich, P-4557) was added. Methylated DNA samples were then vortex for 30 seconds and centrifuged at 14000 rpm for 5 minutes at room temperature. The aqueous supernatant was saved and transferred to a sterile microcentrifuge tube. The former step was then repeated but with the addition of 250 µl of Chloroform:isoamyl alcohol (Sigma Aldrich, C0549). To pellet the DNA purified samples, 1 µl of glycogen (Roche Applied Science, 10901393001), 20 µl of 5M NaCl and 500 µl of ethanol were added and precipitation of the samples occurred after incubation for 30min in -80 °C. The pellets were centrifuged at 14000 rpm for 15 min at 4 °C; the supernatants were carefully removed and the samples washed in 500 µl of cold 70 % ethanol. Centrifugation step was repeated and samples were dried in SpeedVac and resuspended in 30 µl of 10 mM Tris HCl (pH 8,5). We amplified 10 ng of immunoprecipitated and input DNA using GenomePlex Complete Whole Genome Amplification (WGA) kit (Sigma Aldrich, WGA2-50RXN) according to manufacturer's instructions. Finally, each sample was further purified with the Qiagen QIAquick PCR purification Kit (see step 2) according to the manufacture's protocol. Samples were then ready for analysis by microarray (2.1M Deluxe Promoters, NimbleGen) covering over 90 % of the known gene promoters in the mouse DNA.

RNA-Extraction/RT-qPCR

Total RNA extraction was performed using the RNeasy-Mini Kit (Qiagen) according to the manufacturer's protocol. RNA quality was analyzed on an Agilent Bioanalyzer (Agilent Technologies) using the *RNA* 6000 *Series II Nano* kit (Agilent Technologies). Reverse Transcription (RT)-PCR was performed using the ThermoScript RT-PCR System (Invitrogen). qPCR was performed on a LightCycler 480 System (Roche Applied Science) using KAPA SYBR FAST (Peqlab). Three different biological samples were analyzed in duplicates and normalized to the expression of the housekeeping gene aminolevulinic acid synthase (ALAS). Relative quantification was determined by the method described by Pfaffl (2001). The following primers were used (5'→3' orientation):

DNMT1	fw:	CATATCTGCAAGGACATGAG;
DNMT1	rev:	CACATCATGAAAGGTCTACTG;
DNMT3A	fw:	GCACGTTGGAAAGGGAGGCTGA;
DNMT3A	rev:	AGAAGCAGGGTCCGTGGGCT;
DNMT3B	fw:	TGGCACCCTCTTCTTCATTC;
DNMT3B	rev:	ATATACCTTTCCAGACGCGG;
DNMT3L	fw:	AGCTTGCTCCTGCTTCTGA;
DNMT3L	rev:	CGTGGCAGAGACTACCAGAA;
ALAS	fw:	TCGCCGATGCCCATTCTTATC;
ALAS	rev:	GGCCCCAACTTCCATCATCT.

HPLC/MS/MS

After extraction the DNA was enzymatically digested to the nucleosides and subsequently analyzed by LC-ESI-MS.

HPLC-ESI-MS analysis using an Orbitrap XL mass spectrometer: Samples (97 µL injection volume) were chromatographed by a *Dionex* Ultimate 3000 HPLC system with a flow of 0.15 mL/min over an Uptisphere UP3HDO-150/21 column (3 µm, 2.1 mm x 150 mm) from *Interchim*. The column temperature was maintained at 30 °C. The gradient (buffer A: 0.01 % formic acid in H_2O; buffer B: 0.01 % formic

acid in 95 % MeCN / 5 % H_2O) was the following: 0 → 12 min; 0 % → 1 % buffer B; 12 → 20 min; 1 % → 2 % buffer B; 20 → 30 min; 2 % → 10 % buffer B; 30 → 35 min; 10 % → 80 % buffer B; 35 → 41 min; 80 % buffer B; 41 → 51 min; 80 % → 0 % buffer B; 51 → 60 min; 0 % buffer B. Sample elution was monitored at 260 nm (*Dionex* Ultimate 3000 Diode Array Detector). The effluent from the first 5 minutes (total run time of 60 min) was diverted to waste by a *Valco* valve in order to protect the mass spectrometer. The subsequent chromatographic effluent was directly injected into the ion source of a *Thermo Finnigan* LTQ Orbitrap XL without prior splitting. Ions were scanned using a positive polarity mode over a full-scan range of *m/z* 100-500 with a resolution of 30000. The absolute amounts of mC was determined by a stable isotope dilution method and then related to the dG content by UV-detection giving the relative values in percentage. Two technical replicates per sample were performed (Schiesser et al., 2012, Globisch et al., 2010, Münzel et al., 2010).
LC-ESI-MS was carried out on a *Thermo Finnigan* LTQ Orbitrap XL coupled to a *Dionex* Ultimate 3000 HPLC system.

Results

qRT-PCR

The methylation of the DNA is carried out by DNA methyltransferases (DNMTs) (Goll and Bestor, 2005). Currently five members of this enzyme family have been described, but just three of them are catalytically active (DNMT1, DNMT3A and DNMT3B), while the remaining two either represents a co-factor (DNMT3L) or carries out different tasks and is still elusively reported (DNMT2) (Aapola et al., 2002, Goll et al., 2006, Jones, 2012). The view to date is that DNMT3A and 3B establish the somatic pattern of the DNA methylation during embryogenesis, while DNMT1 serves to subsequently maintain this pattern (Goll and Bestor, 2005). Quantitative RT-PCR analysis of different DNMTs in PN11 retinae, revealed no alterations in the gene expression of DNMT1 and 3B (Fig. 4.3.1). However, DNMT3A (3.51 ± 0.91 arbitrary units [a.u.]) and 3L (4.06 ± 0.59) were upregulated in the *rd1* mutants when compared with age-matched wt (1.02 ± 0.24 a.u. and 1.12 ±

0.58 a.u. respectively, $p < 0.5$) (Fig. 4.3.1). This result suggests that DNMT3A and L, but not DNMT1 or 3B, play a role in the DNA methylation at PN11 in the *rd1* animal model.

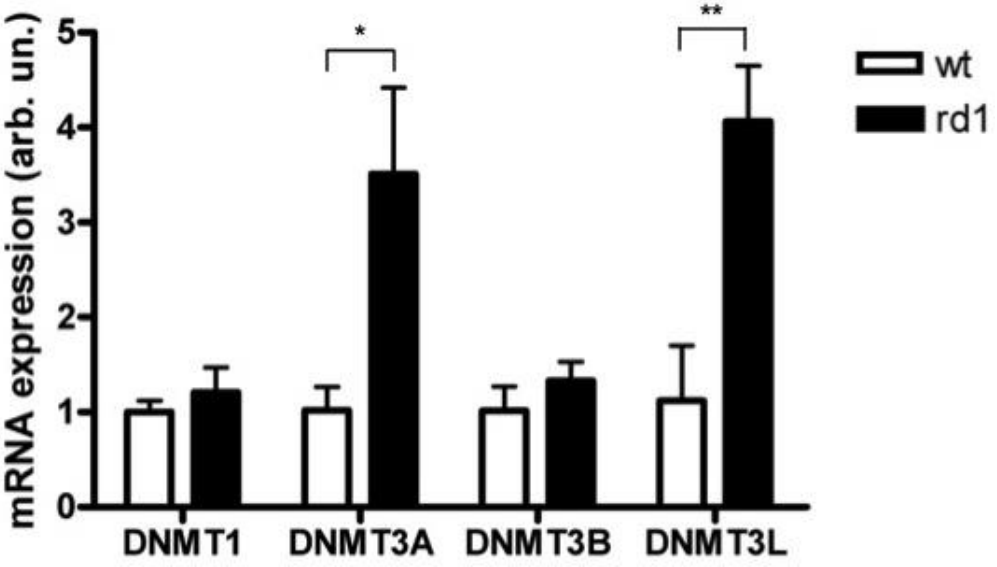

Figure 4.3.1. *DNMT3A and 3L are up-regulated in rd1.* qRT-PCR analysis of different DNA methyl transferases shows no statistical relevant difference in the expression of DNMT1 and 3B. On the other hand DNMT3A and 3L are up-regulated and the difference displays statistical significance. Columns and bars represent mean ± standars deviation (SD) respectively. p-value < 0.05 is considered significant.

DNMT protein expression

The protein expression of the catalytically active DNMTs (DNMT1 and DNMT3A and 3B) was examined by western blot in PN11 *rd1* and wt retinae. The DNMT1, DNMT3A and 3B antibodies all revealed bands at the expected molecular weights, but there were no obvious differences between the control and mutant retina in the expression of any of these proteins (Fig. 4.3.2 G - I).

When the same antibodies were used in immunofluorescence of PN11 material, DNMT1 and DNMT3A were seen to be clearly expressed in the mouse retina, mainly in the ganglion cell layer (GCL) and inner nuclear layer (INL), while the expression in the outer nuclear layer (ONL), where the photoreceptors reside, was faint (Fig. 4.3.2 A, D and B, E). The immunostaining for DNMT3B did not produce high quality images, but the staining was consistent with that of DNMT1 and 3A (Figure 4.3.2 C and F). No major changes on the level or localisation of all of the DNMT proteins

were observed in the inner retina. Preliminary results from DNMT3L immunostaining did not reveal any differences between *rd1* and wt samples (not shown).

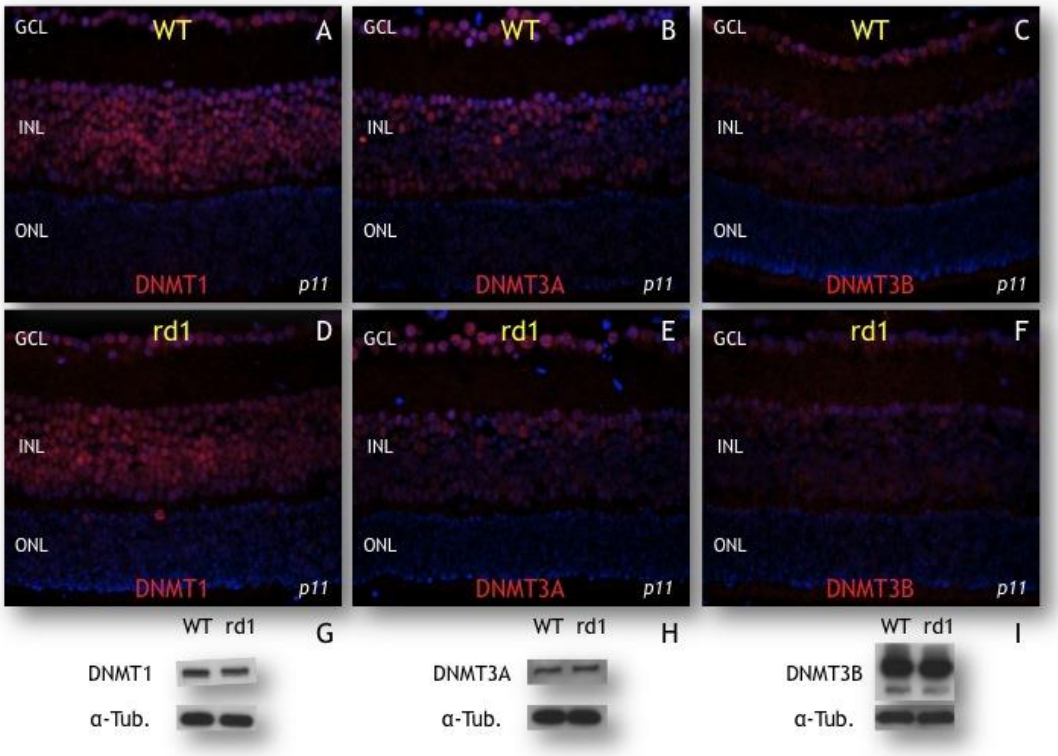

Figure 4.3.2. *Expression and localization analysis for catalytically active DNMTs at PN11*. A) Western blot revealed bands of the expected molecular weigh were found for all of the DNMTs taken into investigation. No clear differences between *rd1* and wt mice stood out. B) Immunofluorescence analysis showed that DNMTs generally localised in the innermost retinal layer, while the expression on the ONL was weak. No obvious difference between wt and *rd1* was detected.

To approach the temporal aspects of DNMT1 and DNMT3A expression in the wt and *rd1* retinae, the analyses included also samples from PN7 (when the degeneration has not yet begun), PN11 (see above) and PN15 (two days after the peak of degeneration, which can be placed at PN13, (Sancho-Pelluz et al., 2008)) (Fig. 4.3.3). For DNMT1 (Fig 4.3.3 A – F) there were neither any distinct qualitative nor quantitative differences between wt or *rd1* within the time frame analysed. By contrast, the DNMT3A expression appeared to undergo some developmentally related changes. At PN7 DNMT3A (Fig. 4.3.3 G and J) was strongly expressed in the GCL and the innermost part of the INL, and this staining was retained in the following time points. At PN7 and PN11 the retinae also showed distinct increased immunoreactions in select cells in the outer part of the INL and considering number, shape and

localisation they may correspond to horizontal cells (Poché and Reese, 2009) and bipolar cells respectively (Fig. 4.3.3 G and K). No clear wt *vs rd1* differences were detected for the DNMT3A protein.

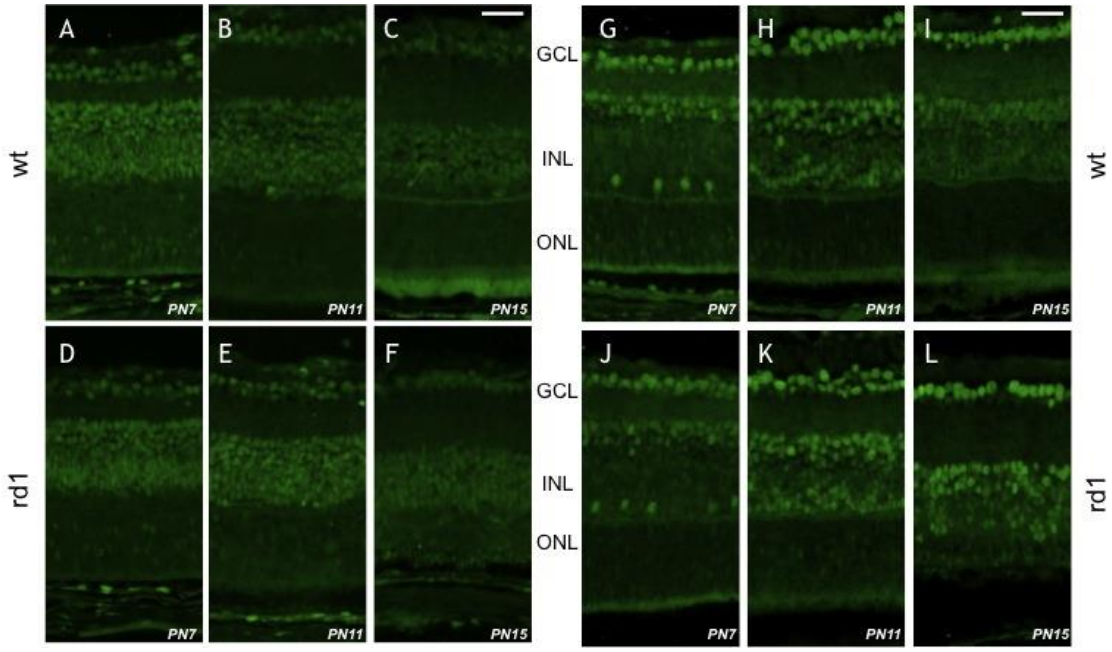

Figure 4.3.3. *Developmental expression of DNMT1 and DNMT3A.* Immunofluorescence analysis in time points between PN7-15 shows that DNMT1 (A - F) expression is generally confined to the inner retina. At later time points DNMT1 expression seems slightly and equally depressed both in wt and in *rd1* compared to early time points. Few dot-like shaped immunoreactivities were detected in the ONL of rd1 mice at PN11. The expression of DNMT3A (G - L) within the INL changes during development. At PN7 horizontal and amacrine cells show stronger immunoreactivities. At PN11 bipolar cells express high level of DNMT3A. GCL = ganglion cell layer; INL = Innel nuclear layer; ONL = Ouetr nucler layer. Scale bar = 20 μm.

DNA methylation; Tissue level

MeDIP. Methylation of the DNA happens generally on the promoters of genes, and this has consequences for the gene expression. We detected variations in the gene expression of DNMT3A, but no difference at protein level. In order to understand whether modifications in the methylation level of the promoters of the genes were present, we performed methylated DNA immunoprecipitation coupled with a microarray analysis of global wt and *rd1* samples, *i.e.* a so called MeDIP analysis. The analysis encompassed two samples of each genotype, with each sample being produced by using 2 retinae. Using such global samples, both genotypes displayed a high number of methylated promoters, but any major quantitative or qualitative

differences between the two analysed groups could not be readily seen (data not shown).

HPLC/MS/MS. A different approach, used high-performance liquid chromatography on global samples, coupled with a double run of mass spectrometry (HPLC/MS/MS). This allowed us to study whether there were modifications of the methylation of the cytosines between *rd1* and wt that affected the total methylation level and not only of the promoters. The readout of this experiment reveals the percentage of methylated cytosines within the samples, and the results suggested that there was no difference between the two types of retinae when studied in this way (wt = 3.27 % ± 0.09; *rd1* = 3.25 % ± 0.04; n = 5 for both types).

DNA methylation; Cellular level

The above two analyses both used global samples, but the *rd1* degeneration affect only a limited number of photoreceptor cells and as observed in the immunostainings, the high number of expressing cells in other layers in the retina might mask any change in the ONL. To circumvent this problem we analysed the level of the DNA methylation in situ with immunofluorescence using an anti-5mC antibody. Methylated DNA was only very rarely found in retinal cells of wt animals and in the inner retinal layers in *rd1* animals (Fig. 4.3.4 A – F). By contrast, a subset of cells in the *rd1* ONL had clearly labelled nuclei, and corresponded numerically to the expected amount of dying photoreceptors at the analysed time point (Fig. 4.3.4 D –F). These results were obtained by the NB-100-744 antibody (see section 2), and confimed by two other antibodies (Ab10805 and Ab51552, data not show). Pre-treatment of sections with 3N HCl (which denatures the DNA) yielded together with the Ab10805 antibody a weak and general nuclear staining of most cells. However, there was still a clear difference between the *rd1* and wt retinae, in that a subset of *rd1* photoreceptor nuclei attained a strong immunostaining, which was not present in the wt situation (Fig. 4.3.5).

In order to determine if this clear up regulation is observed in other animal models for RP, we extended our research to three other mutants: the *rd2* mouse, and the rhodopsin rat mutants S334-ter and P23H Interestingly, in all of these models, and in line with the observations in the *rd1* mouse, a sup-population of photoreceptors showed an increase in the level of nuclear DNA methylation staining at evaluated

time points (Fig. 4.3.4 G – X). This suggests that the increase of methylation of the DNA in dying photoreceptors is mutation independent.

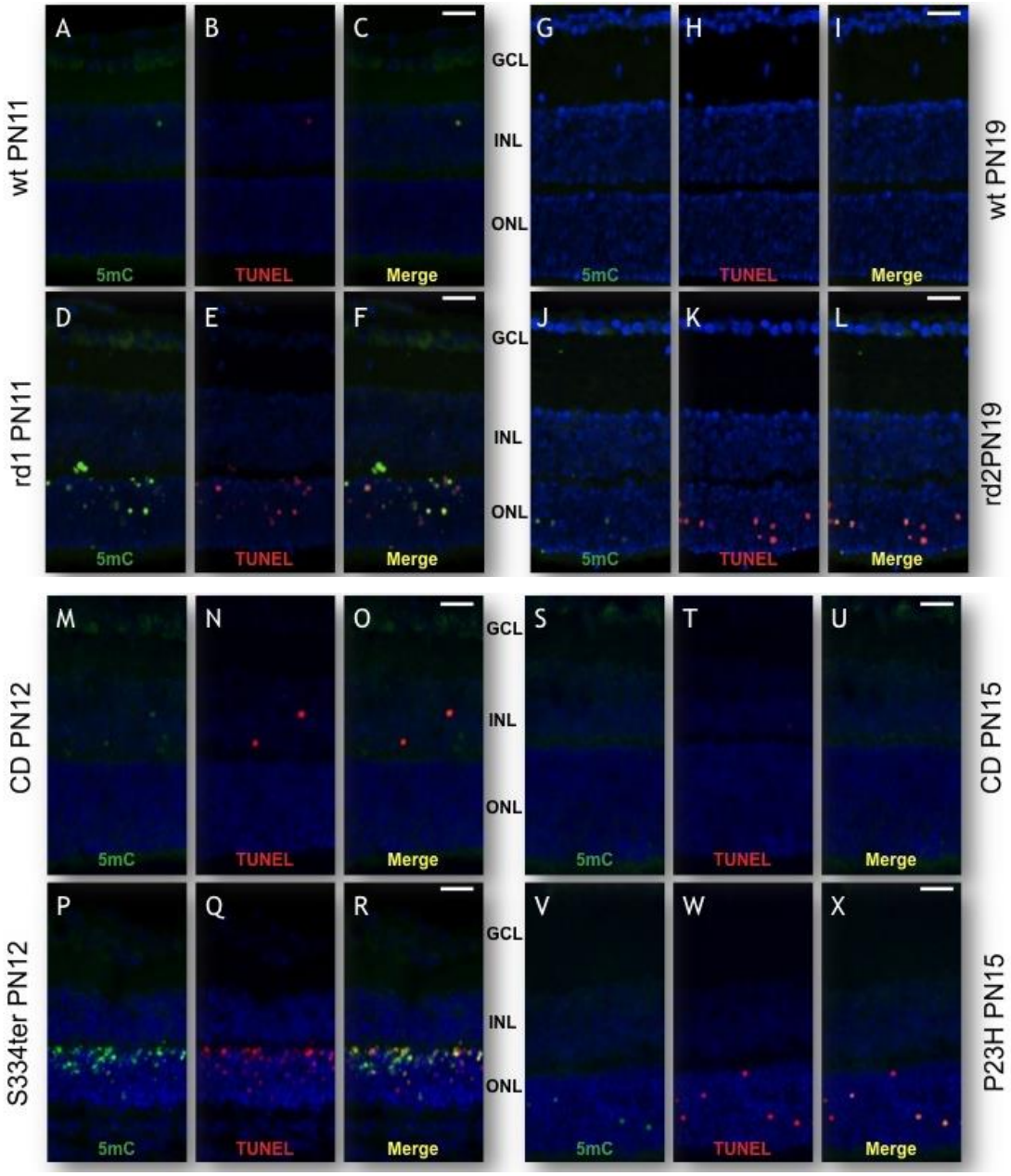

Figure 4.3.4. *5mC is increased and co-labels with TUNEL in models of RP.* (D - E) DNA is hypermethylated in photoreceptors in *rd1* mice at PN11 and increased 5mC co-labeled with TUNEL. At the same time-point in wt mice 5mC is not detected (A – C). Increased 5mC was detected in three additional models of RP, *rd2* (J – L), s334ter (P – R) and P23H (V - X) when compared to relative control retina (G – I, M – O and S – U respectively). GCL = Ganglion cell layer; INL = Innel nuclear layer; ONL = Ouetr nucler layer; 5mC = 5-methylcytosine. Scale bar = 20 μm.

DNA methylation corresponds with TUNEL

In all of the models analysed, TUNEL staining for dying cells co-labelled the same cells to a great extent, suggesting an intimate connection between increased detection of DNA methylation and the degeneration of the photoreceptors (Fig. 4.3.4 F, L, R and X).

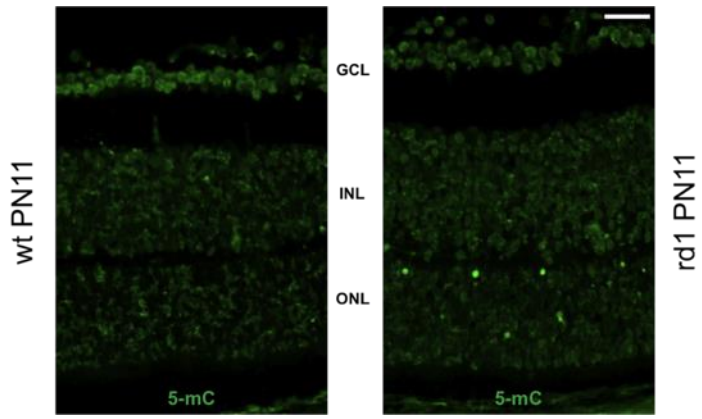

Figure 4.3.5. *Increased detection of 5mC after antigen retrieval treatment.* 3N HCl treatment allowed a change in the detection pattern of 5mC both in *rd1* and wt retinal samples. However, *rd1* retina show also in this case higher number of highly immunopositive photoreceptors. GCL = Ganglion cell layer; INL = Innel nuclear layer; ONL = Outer nucler layer; 5mC = 5-methylcytosine. Scale bar = 20 μm.

Coexistence of epigenetic modificators of the chromatin in RP models

Overactivation of epigenetic regulators of the chromatin including PARP1 (Beneke, 2012, Paquet-Durand et al., 2007) and HDACs class I & II (Sancho-Pelluz et al., 2010), have been reported in dying *rd1* photoreceptors. DNMTs have been shown to cooperate with both these groups of enzymes in the epigenetic modification of the structure of the chromatin and, therefore, in the control of the gene expression (Rountree et al., 2000, Fuks et al., 2001, Aapola et al., 2002). Epigenetic mechanisms like methylation of the DNA and histone acetylation are crucial in a wide range of physiological functions, from memory, to development and cellular reprogramming (Monsey et al., 2011, Han et al., 2010, MacDonald and Roskams, 2009). Figure 4.3.6 indicates that in three different rodent models of RP (*rd1* mouse as well as S334ter and P23H rats), 5mC is detected in cells lacking lysine acetylation. Given that lysine hypoacetylation is a marker for overactivation of HDACs class I and II in the degenerating *rd1* photoreceptors and that PARP1 overactivation is detected in dying cells in a number of different models, *i.e.* such cells that experience overactivation of HDACs (Sancho-Pelluz et al., 2010, Kaur et al., 2011), these data suggest that

multiple epigenetic events simultaneously affect degenerating photoreceptors in various models of RP.

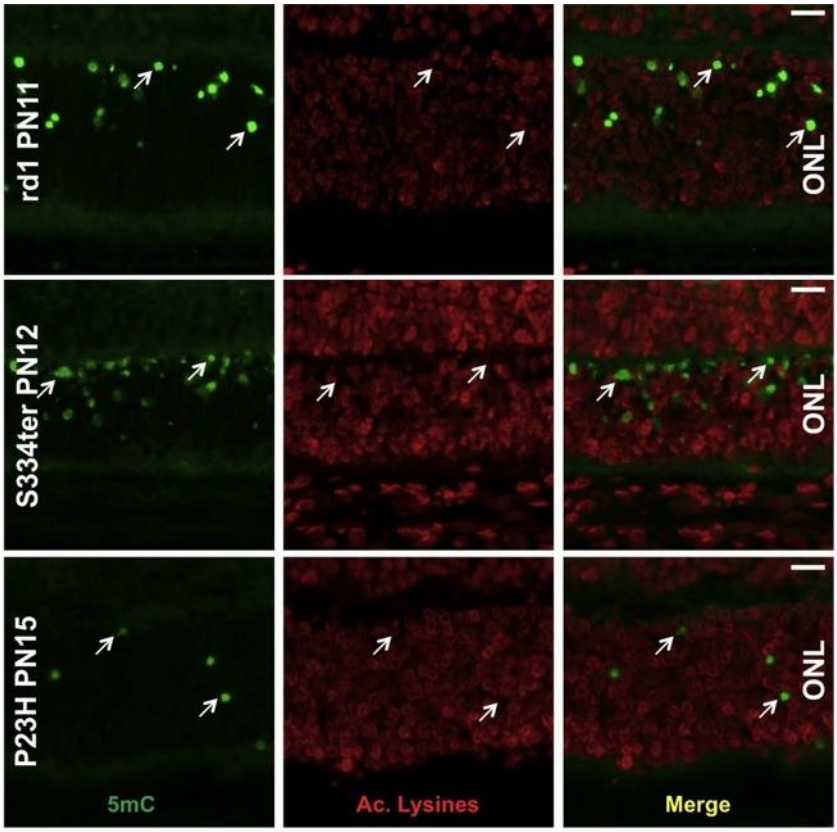

Figure 4.3.6. *Co-existence of overactivation of DNMTs and HDACs*. Lack of acetylation of lysines has been shown to be a marker of HDAC activation (Sancho-Pelluz et al., 2010). In *rd1* mouse, S334ter and P23H rats a number of cells, corresponding to the expected dying cells, displayed both increased methylation of the DNA and reduction of acetylation of lysines. ONL = outer nuclear layer. 5mC = 5-methylcytosine. Scale bar = 20 μm.

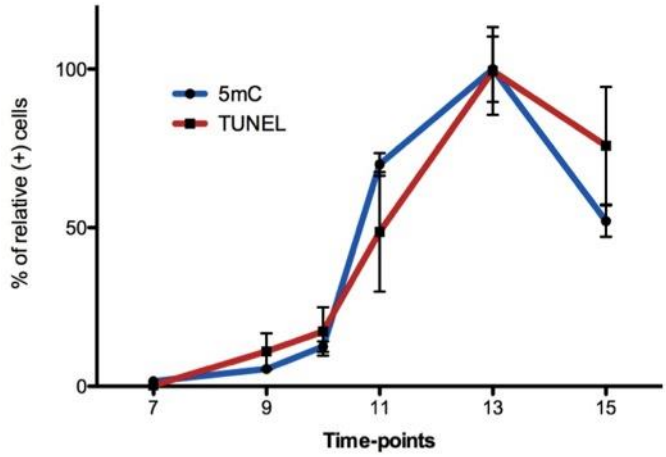

Figure 4.3.7. *Temporal dynamics of 5mC detection in rd1*. Methylated DNA was not or only weakly detected at the earliest time-points. Immunoreactivities greatly increased at PN11 and reached the peak at PN13 and eventually plummeted at PN15. Dots and bars represent percentage of relative positive cells (compared with respective peak value) ± SD.

DNA methylation temporal dynamics

To better understand the dynamics of the DNA methylation, we analysed *rd1* retinal sections from PN7 to PN15 comparing staining for 5mC and TUNEL. Figure 4.3.7 and table 4.3.1 shows, for both markers, the lack of immunoreaction in the *rd1* ONL at PN7. The number of positive cells subsequently rises until PN13 (degeneration peak), followed by a decrease along with the photoreceptor cells decrease. Although both dynamics resemble each other, 5mC staining seems to increase at PN11 and decrease at PN15 more markedly than TUNEL staining. This suggests that the hypermethylation of the DNA is indeed a late event in the phototeceptor cell death but that it happens before DNA fragmentation (TUNEL staining).

	PN7	**PN9**	**PN10**	**PN11**	**PN13**	**PN15**
5mC	0.06 ± 0.01	5.45 ± 1.54	12.57 ± 1.69	70.05 ± 3.56	100 ± 10.29	52.15 ± 4.96
TUNEL	0 ± 0	10.99 ± 5.73	18.42 ± 7.54	48.68 ± 18.81	100 ± 12.92	75.35 ± 19.32

Table 4.3.1. *Tabular representation of temporal dynamics of 5mC and TUNEL staining.* Values express relative percentage of positive cells ± standard deviation. Measuring was performed in the peri-central retina. PN = post-natal day.

In vitro pharmacological inhibition of DNMTs

DNMTs can be pharmacologically inhibited with cytidine-nucleotide analogues (Stresemann and Lyko, 2008). Among those, 5-aza-2'-deoxycytidine (decitabine) has been reported to reduce DNA methylation and restore gene expression changes in human neuronal cell lines (Zschocke et al., 2002), and showed promising results towards curing proliferative diseases (Christman, 2002, Steensma, 2009). Our observations of increased DNA methylation in degenerating photoreceptors is compatible with an increased DNMT activity. We therefore investigated if blockade of DNMT enzymes had any effect on the photoreceptor cell survival using organotypic retina explant cultures of *rd1* retinae. To this end *rd1* retinae were treated with either 0.5, 1.25, 2.5, 5 or 10 µM decitabine (Fig. 4.3.8 A). While all concentrations tested reduced the number of TUNEL positive cells, treatment with decitabine 2.5 µM (Fig. 4.3.8 A and B) displayed the most powerful effect by reducing the number of dying cells by 48 % (control = 4.83 % ± 0.71; 2.5 µM = 2.51 % ± 0.53; $p < 0.05$). In order to evaluate the inhibition of DNA methylation, we

quantified the number of 5mC positive cells. Accordingly, the number of cells with high DNA methylation levels was reduced (Fig. 4.3.7 C and D) by around 41 % compared to untreated controls (control = 2.99 % ± 0.58; treated = 1.76 % ± 0.64; $p < 0.05$).

The short-term treatment by decitabine revealed a protective effect judged by a reduced amount of TUNEL positive cells. It was therefore of interest to analyse whether the DNMT inhibition promotes photoreceptor cell survival in the longer perspective. This was studied by long-term treatment of organotypic cultures (PN5 + 2DIV + 12DIV), treated with decitabine 2.5 µM. In this experiment both groups exhibited the same number of surviving photoreceptor rows at end of culturing (control = 3.36 ± 0.56; treated = 3.37 ± 0.33; n = 6; $p > 0.05$).

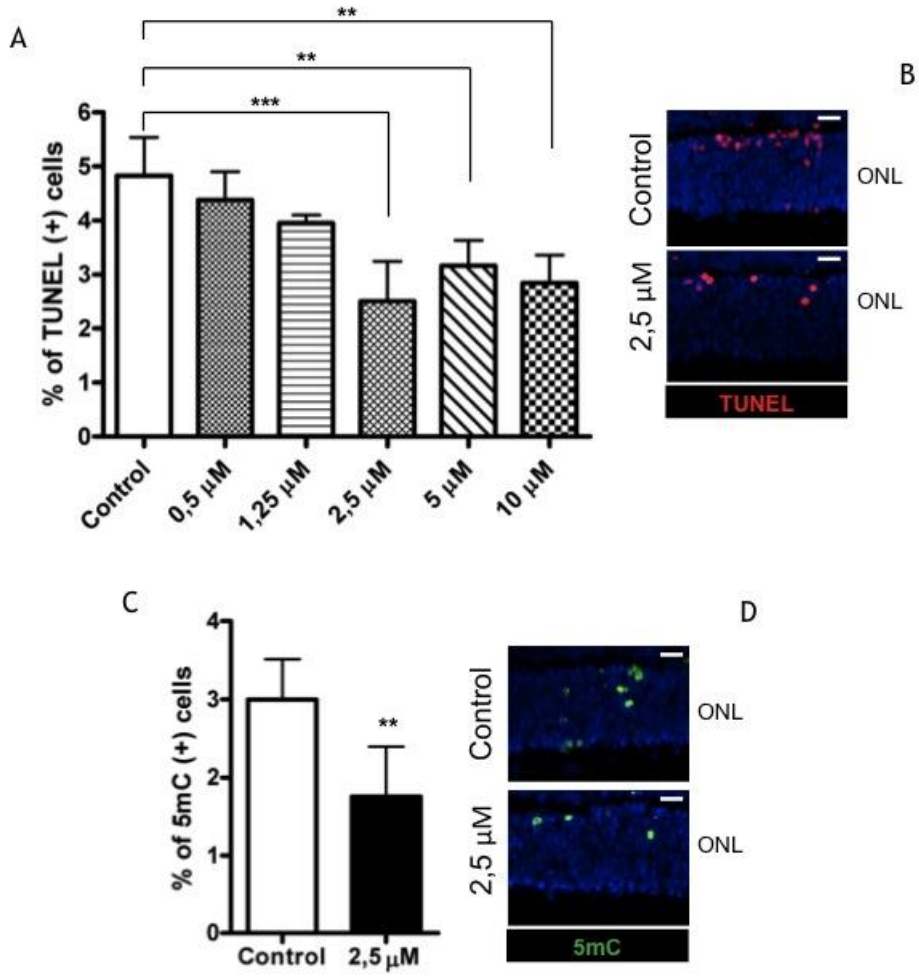

Figure 4.3.8. *Short-term inhibition of DNMTs in organotypic retinal cultures.* A) and B) Administration of a wide range of concentrations of decitabine for 4 days was consistently able to reduce cell death (expressed in % of TUNEL (+) cells) on retinal explants. C) and D) The most positive concentration (2.5 µM) was also able to reduce the number of 5mC (+) cells. Columns and bars represent mean ± SD. ONL = outer nuckear layer. Scale bar = 20 µm.

Discussion

The present investigation revealed hypermethylation of nuclear DNA in the photoreceptors of four different animal models of the hereditary blinding disease Retinitis pigmentosa (RP). The hypermethylation was detected by immunostaining but, when studied in the *rd1* retina, was not seen by MeDIP or HPLC/MS/MS. The MeDIP tool analyses the methylation level of about 90 % of the gene promoters, and involves the isolation of methylated DNA sequences and their analysis on a microarray, whereas the HPLC based analysis aimed at quantifying the methylated cytosines in the whole DNA. Since DNA can be methylated also in intergenic sequences as well as within the genes themselves (Jones, 2012), the increased methylation in the *rd1* retinae may have occurred mainly outside of the promoter regions. In addition, the retina is a complex multilayered tissue with different cell types, and whenever we produce whole retina samples we obtain material from all cells of all types. This has the inherent risk that a signal present in just a fraction of the cells can be lost against the basal signal level of all other cells. Immunostaining, on the other hand, reveals the signal in individual cells, regardless of how many or how few they may be. This acted in our favour here, since without immunostaining the differences in DNA methylation would not have been detected.

The currently five members of the DNMT family are all involved in various aspects of DNA methylation. The expression of several of these was analysed in the present study, which showed that both DNMT3A and 3L were upregulated in the *rd1* retina at the mRNA level. The DNMTs with catalytic activity, *i.e.* DNMT1, DNMT3A and 3B, were also studied at the protein level, where Western blot suggested equal levels in *rd1* and wt retinae. Likewise, immunostaining for DNMT1 and DNMT3A did not imply any upregulation of these proteins. While we for DNMT1 observed a limited number of more intensely stained structures in the *rd1* ONL, we think that these relate to the phase that the photoreceptor nuclei undergo close to their death and which involves condensation, as can also be seen by TUNEL. The remaining DNMT1 in such diminishing nuclei may be more densely packed and therefore yield a stronger immunosignal.

The upregulated DNMT3A mRNA at PN11 was not immediately reflected by an increased translation to the corresponding protein, as studied by Western blot of same

aged samples. It is possible that the higher mRNA level is a consequence of increased mRNA production or stability, and that this has only little or no effect on translational efficiency. Alternatively, the DNMT3A protein levels may be in fact be rising in the *rd1* retina, but without the increase (which may be limited to only some cells) at this point being detectable by western blotting above the already existing amounts in the tissue.

For the DNA methylation assessment, the investigation included the *rd1* mouse and three other RP models: the *rd2* mouse and the S334ter and P23H rats. These models represent mutations of varying kinds and with, most likely, various entry points into the degeneration processes. The *rd1* mouse carries a mutation in the PDE6β gene, giving an intracellular accumulation of cGMP in rod photoreceptors, which triggers molecular mechanisms leading to an early and rapid degeneration of these cells (Paquet-Durand et al., 2009, Sancho-Pelluz et al., 2008). The *rd2* mutation concerns the peripherin-2 gene, encoding a disc membrane-associated glycoprotein expressed in both cone and rod photoreceptors (Travis et al., 1991) and which is essential for photoreceptor morphogenesis and outer segments renewal (Cai et al., 2010). The *rd2* mutants are characterized by the total loss of outer segments and a, relative to *rd1*, slow degeneration (Goldberg, 2006). The S334ter and P23H rats both concern mutations for the photopigment protein rhodopsin: a C-terminal deletion (S334ter) (Shinde et al., 2012), or a single amino acid substitution - proline 23 instead of histidine (P23H) (Dryja et al., 1990). The S334ter mutation affects primarily rhodopsin protein trafficking, whereas the P23H mutation yields an unfolded rhodopsin (Chiang et al., 2012b). In both cases this leads to photoreceptor degeneration, which for the S334ter is very quick, with rods disappearing within 15-20 days, and somewhat slower in the P23H rat (Oh et al., 2003). For both rhodopsin mutants the degeneration processes may involve the unfolded protein response and endoplasmatic reticulum stress (Shinde et al., 2012, Gorbatyuk et al., 2010). Remarkably, and in spite of these variations in genes, functions and degeneration characteristics, all four models presented clearly increased DNA methylation in their degenerating photoreceptors, as judged by immunostaining for 5mC and colocalisation with TUNEL staining for cell death. These results thus suggest that DNA methylation could have a general connection with hereditary photoreceptor degeneration.

DNA methylation is a well-known factor that controls gene expression, including by the fact that methylation of the carbon 5 of the cytosines provokes compaction of the chromatin and thus gene silencing (Jones and Liang, 2009). In addition to DNA methylation, additional epigenetic events have been shown to be affected in models of RP. PARP1 is an enzyme characterised by multiple activities, ranging from DNA repair, post-translational modification and regulation of the transcription (Beneke, 2012), and PARP1 and HDACs class I & II have been reported to be overactivated in the same dying photoreceptors (Paquet-Durand et al., 2007, Sancho-Pelluz et al., 2010). Since we found that 5mC (the possible outcome of DNMTs activation) and lack of lysine acetylation (the result of HDACs activity) coincided, we can indirectly assert that multiple epigenetic reactions happen in the same degenerating photoreceptive cells. This in turn highlights the importance of gene expression regulating pathways in the pathophysiology of the photoreceptors.

To further evaluate the role of the DNA methylation, we utilised organotypic explant cultures of the *rd1* retina in combination with DNMT inhibition. In so called short term experiments (see Materials and methods) we demonstrated that use of the DNMT inhibitor 5-aza-2'-deoxycytidine (decitabine; an azanucleoside) resulted in both a reduced amount of hypermethylated DNA and a decreased number of dying, TUNEL positive photoreceptors. However, when decitabine was used in cultures of longer term, the effect on TUNEL positivity was not translated to an increased number of surviving photoreceptors. A possible explanation for this discrepancy is linked to the mode of action of decitabine, which is thought to rely on its incorporation into newly synthesized DNA, after being metabolized intracellularly to an incorporable cytidine analogue (5-aza-2'-deoxycytidine-5'-triphosphate) (Stresemann and Lyko, 2008). Since this molecule cannot act as a methyl acceptor, the possibility for *de novo* methylation by a DNMT is thus reduced in any new DNA, such as in the daughter cells of proliferating cells. In addition decitabine can promote the degradation of the DNMT that has tried to methylate the cytidine analogue (Stresemann and Lyko, 2008). The retinal photoreceptors are regarded as post-mitotic neurons and are therefore not expected to proliferate in stages outside of their development. However, incorporation of thymidine analogues (to label cells in S-phase of the cell cycle) in photoreceptors has been demonstrated during *rd1* degeneration, but this was suggested to reflect an incorporation due to ongoing DNA

repair in the diseased cells (Menu dit Huart et al., 2004), or a failed attempt to proliferate, rather than proper cell division (Zencak et al., 2013). Regardless of which is true, this fact importantly indicates a possibility for metabolized decitabine to be introduced in the DNA. If our observed DNA methylation in the *rd1* photoreceptors is restricted or concentrated to newly formed DNA, *e.g.* as a result of DNA repair, this would explain how the decitabine treatment reduced the observable DNA methylation. Furthermore, since the incorporated analogue acts as a DNMT trap that promotes DNMT degradation (Stresemann and Lyko, 2008), such a loss of DNMT could lead to an overall reduction in DNA methylation events in these cells. Future investigations will reveal if such a possibility is true and if the neuroprotective capacity of DNMT inhibition can be improved by different treatment regimes, perhaps including combinations with other protective principles.

In summary, we have demonstrated increased DNA methylation in a degeneration related way in four different models of RP, and showed that the DNMT inhibitor decitabine has an intriguing potential for neuroprotection in this context.

4.4 Hsp70 is involved in photoreceptor degeneration in the *rd1* mouse model for *Retinitis pigmentosa*

Manuscript in preparation

Farinelli P[1,2], Arango-Gonzalez B[2], Hans Gottfried Genieser[3], Zrenner E[2], Paquet-Durand F[2], Ekström P[1]

[1]Division of Ophthalmology, Department of Clinical Sciences, Lund, University of Lund, 22184 Lund, Sweden; [2]Division of Experimental Ophthalmology, Institute for Ophthalmic Research, University of Tübingen, 72076 Tübingen, Germany; [3] BIOLOG, Bremen, Germany

Rationale

Nearly every model of RP displays mis-localization of outer segment proteins, which diffuse and accumulate in the cell body affecting the normal cellular activities. In such pathological conditions the proteins struggle to achieve their folding, and this promotes intracellular signals that eventually may lead to cell death. A family of enzymes aid unfolded proteins in finding the correct status and they are collectively called heat shock proteins (Hsps). Surprisingly, Hsps are still poorly investigated in RP. The aim of the following study was to investigate one of the most characterized of the family, Hsp70, in the context of RP.

Introduction

The inherited retinal degenerations constitute a group of heterogeneous genetic diseases, with a worldwide and overall prevalence of 1:2000 (Sohocki et al., 2001), that provoke severe visual impairment. Currently, around 220 mutated loci involved in the development of retinal diseases have been mapped and 170 of those are already identified (*https://sph.uth.edu/retnet/*). Among these disorders, the *Retinitis pigmentosa* (RP) group of diseases stands out as one of the leading causes of loss of vision amongst the working age population, affecting over a million people

worldwide (Hartong et al., 2006). The first symptoms of RP is night blindness and restriction of the visual field (tunnel vision) due to the degeneration of the rod photoreceptors in a mutation dependent fashion, and this is in many cases followed by severe vision loss, or even complete blindness, as a consequence of a secondary and mutation independent cone photoreceptor cell death. Despite decades of research the knowledge of the molecular pathways underlying RP is still sketchy, which inevitably has contributed to the existing lack of suitable treatments.

Native polypeptides must be correctly folded in order to be able to carry out physiological functions, and this is assisted by molecular chaperone proteins (Ellis, 2006), which also promote the reduction of protein aggregates (Dobson, 2004), thereby providing cytoprotection. The heat shock protein (Hsp) sub-family of the chaperones is probably the most characterized of this kind of molecules. The Hsps are highly conserved in all living organisms and were originally shown to respond to heat treatment (Lindquist, 1986), but it has been subsequently demonstrated that they can respond to a wide range of stressors (Bergeron et al., 1996, Nissim et al., 1992, Wagner et al., 1999, Wallen et al., 1997). The 70 kDa member of this family (Hsp70) is ubiquitously expressed and involved in protein folding/unfolding, organelle and membrane transport of secretory proteins and control of regulatory pathways (Hartl and Hayer-Hartl, 2002, Neupert and Brunner, 2002, Pratt and Toft, 2003, Ryan and Pfanner, 2001). In addition, Hsp70 has the ability to suppress apoptosis, including in neurons (Antonoff et al., 2010), and this may involve preventing pro-caspase 9 from binding to Apaf-1 (apoptotic protease activating factor 1) and forming the apoptosome (Beere et al., 2000).

Proper folding of proteins is necessary for normal cellular functions, and from a pathobiological viewpoint it is interesting that unfolded and mis-localized proteins have been detected in several animal models of RP (Gao et al., 2002, Grossman et al., 2011, Ishiguro et al., 1987, Price et al., 2011, Shinde et al., 2012, Saliba et al., 2002). In this context, mutations in the rhodopsin gene can activate the unfolded protein response (UPR) (Berson, 1996), a cellular stress response that involves accumulation of proteins in the endoplasmic reticulum (ER) and subsequent ER stress, which is pro-apoptotic (Stefani et al., 2012). Indeed, mutant P23H rhodopsin gets trapped within the ER of photoreceptors and fails to translocate to the outer segments, which results in cytotoxicity (Kroeger et al., 2012). This has a direct connection with Hsp70

proteins, since these have been reported to play a role in the UPR (Endo et al., 2007, Gupta et al., 2010), and in particular since the AAV delivery of an Hsp70 homologue reduced cell death rate and improved vision in transgenic P23H rats (Gorbatyuk et al., 2010).

The *rd1* mouse, carrying a mutation in the gene for the β subunit of rod specific phosphodiesterase 6 (PDE6β) (Keeler, 1966), is the perhaps most characterized RP animal model. The defect in the PDE6 leads to an accumulation of cGMP within the photoreceptors, which starts the degenerative events likely via activation of cGMP protein kinase (PKG) (Paquet-Durand et al., 2009). However, the *rd1* photoreceptors also show signs of rhodopsin mislocalization (Ishiguro et al., 1987) and it is possible that this aggravates the situation for the cells. In the present study we therefore investigated whether the *rd1* degeneration engages Hsp70 in any way. For comparison we studied Hsp70 in the context of yet other RP genes, such as the *rd2* mouse, which carries a mutation in the peripherin-2 gene, as well as S334ter and P23H rat rhodopsin mutants. Our results suggest that Hsp70 plays an integral part in the cellular responses in several forms of retinal degenerations.

Material and methods

Animals

Animals used included C3H rd1/rd1 (*rd1*), rd2/rd2 (*rd2*) and control C3H wild-type (*wt*) mice (Sanyal S, 1973) and all were kept in colonies in Lund. Homozygous P23H and S334ter rhodopsin transgenic rats (originally produced by Chrysalis DNX Transgenic Sciences, Princeton, NJ) of the line Tg(P23H)1Lav and Tg(S334ter)3Lav (P23H and S334ter-3), were kindly provided by Dr. M. M. LaVail (University of California, San Francisco, CA). To obtain heterozygous P23H and S334ter rats, homozygous such were crossed with wt, CD rats (CD® IGS Rat; Charles River, Germany) to reflect the genetic background of autosomal dominant RP. CD rats were used as controls. All procedures were performed in accordance with either the Swedish National Animal Care and Ethics Committee (*rd1* and *wt* mice; permits # M242/07, M220/09, M172/12), or the Tübingen University committee on animal protection (S334ter, P23H and CD rats), and protocols compliant with § 4 paragraph 3 of the German law on animal protection were reviewed and approved by the

"Einrichtung für Tierschutz, Tierärztlichen Dienst und Labortierkunde" (Anzeige/Mitteilung nach § 4 vom 28.04.08 and 29.04.10). All efforts were made to minimize the number of animals used and their suffering and the experiments conformed to the ARVO statement for the use of animals in ophthalmic and visual research. Animals were kept in their respective animal houses under standard white cyclic lighting, with free access to food and water, and were used irrespective of gender.

To minimize any bias from loss of retinal tissue due to the degeneration, comparisons of *rd1* and healthy wt retinae were typically performed at postnatal day (PN) 11 (although other time-points were included in some experiments). At PN11 degenerating photoreceptors are frequent in the *rd1* retina, but their demise has not yet resulted in any considerable thinning of the photoreceptor layer (Hauck et al., 2006, Sancho-Pelluz et al., 2008). For the other models other time points were chosen according to the same principle.

Organotypic retinal explant culture

To initiate retinal explant cultures, retinal tissue was dissected from enucleated eyes of PN5 *rd1* animals immediately after killing by decapitation, and the procedures in principle followed previous descriptions (Caffé et al., 2002). Briefly, the eyes were incubated in R16 serum-free culture medium (Invitrogen Life Technologies, Paisley, UK; 07490743A) containing 0.12 % proteinase K (MP Biomedicals, Solon, OH, USA; 193504), at 37 ºC for 15 min, which allowed removal of the sclera but leaving the retinal pigment epithelium (RPE) still attached to the retina. After this incubation, the activity of proteinase K was blocked with R16 medium containing 10 % fetal calf serum (Invitrogen Life Technologies; PET10108165), and the eyes dissected aseptically in a Petri dish with R16 medium. The microscopy assisted dissection procedure involved careful removal of the anterior segment, lens, vitreous, sclera, the choroid, and the vessels that could be reached, after which the retinal preparation was subjected to four cuts perpendicular to its rim, giving rise to an explant resembling a four leaf clover. The latter was placed in a Millicell culture dish filter insert (Millipore AB, Solna, Sweden; PIHA03050), with the RPE layer down, facing the culturing membrane. Each insert was then placed in a separate well of a six-well culture plate and incubated in R16 nutrient medium at 37 ºC. Each well was given 1.5 ml medium, which usually was replaced every second day during the culturing period.

Prior to a 4 day treatment with or without addition of 10 µM geranylgeranylacetone (GGA), a Hsp70 inducer (Sigma-Aldrich, place, G5048), the PN5 explants were allowed to adjust to normal, control culture conditions for 2 days *in vitro* (DIV). The end point of the culturing experiments (PN5 + 2 DIV + 4 DIV with treatment) thus by extrapolation corresponds to *in vivo* age PN11, a time-point suitable for retinal analyses.

In a separate experiment we used 50 µM of a cGMP analogue exerting PKG inhibitory properties, DF001, for the 4 days treatment. In each of the above experiments the preparations were eventually fixed and sectioned, as described below.

Fixation and sectioning and microscopy

Mouse eyes (or explanted retinae still attached to the culturing filters) were fixed in 4 % paraformaldehyde (PFA) in phosphate buffered saline (PBS) for 2 h. Rat tissues were fixed in PFA in PBS for 5 min in room temperature (RT) and 55 min in 4°C. This was followed by thorough rinses with PBS, after which the preparations were placed in sucrose containing PBS to prepare for cryosectioning, which yielded 8-12 µm frozen sections, used as indicated.

Microscopy

Morphological observations and routine fluorescent microscopy were performed on a Zeiss Axiophot microscope equipped with a Zeiss Axiocam digital camera. Fluorescence excitation was provided by a HBO 100W halogen lamp. Images were captured using Zeiss Axiovision 4.2 software; image overlays and contrast enhancement were done utilizing Adobe Photoshop CS. Confocal microscopy was performed with a Leica TCS SP2 (Solms, Germany).

Terminal dUTP nick-end labelling (TUNEL)

Sections of PFA fixed preparations were washed three times in PBS. TUNEL staining was performed using an *in situ* cell death detection kit (Roche, Mannheim, Germany) conjugated with TMR red. Controls with this kit and similar preparations have been performed earlier (Paquet-Durand et al., 2007), by means of excluding the terminal deoxynucleotidyl transferase enzyme from the labelling solution (negative control),

and by pretreating the sections for 30 min with DNAse I (Roche, 3U/ml) in 50 mM Tris-HCl, pH 7.5, 1 mg/ml BSA to induce DNA strand breaks (positive control). The negative control gave no staining at all, while the positive control resulted in general staining of all nuclei in all layers of the retina.

Histological staining / Immunofluorescence

Sections were washed 3 x 5 minutes each in PBS containing 0.25 % Triton X100 (PTX) plus 1 % BSA. Blocking solution containing PTX and 5 % normal serum from the host animal, from which the secondary antibody was obtained, was applied for 45 minutes. Primary antibodies (see Table I) were diluted in PBS with 1 % BSA and 0.25 % Triton X100, and applied overnight at 4° C. Sections were then washed 3 x 5 min each in PTX and incubated with appropriate secondary antibodies diluted in PTX (see Table I) for 45 minutes. After 3 more washing steps in PBS, the sections were mounted with Vectashield DAPI (Vector, Burlingame, CA, USA). Controls consisted of sections processed in parallel without primary antibody and application of the fluorescence detection system.

Counting of positive cells

For Hsp70 and TUNEL temporal dynamics *in vivo*, as well as for analysis of the effect on TUNEL positivity of GGA treatment *in vitro*, counting of positive (+) cells with the nuclear stain DAPI as counterstaining was performed as follows: three non-contiguous sections were analysed from at least three independent samples of each kind (mutant and control in the case of drug administration, just mutant in the case of temporal investigation) of the *in vivo* preparations, or from five paired treated/untreated specimens from the treatment experiments. Pictures were taken throughout the whole retina from each section to be analysed and the pictures were then assessed by the AxioVision software. Data were collected as the retinal area analysed expressed in square pixels (p^2) and number of detected (+) cells. The percentage of positive cells (% (+) cells) was then calculated as follows:

$$A_c = A_o / C_{DAPI}$$

$$\downarrow$$

$$C_t = A_t / A_c$$

$$\downarrow$$

$$\% (+) \text{ Cells} = (+) \text{ cells} / C_t$$

In this formula (+) cells represents the total number of the positively labelled cells, while C_t is the overall number of cells taken into account, A_t is the total area analyzed, A_c is the average area of a cell, A_o is the random area expressed in pixel^2 and C_{DAPI} represents the total DAPI positive cells in A_o. Values are given as TUNEL or Hsp70 (+) cells ± standard deviation (SD). Statistical significance was tested using both paired and unpaired, two-tailed, Student's t-test or ANOVA test using GraphPad Prism. For all tests, a p-value < 0.05 was considered to indicate a statistically significant difference.

Mathematical modelling

The data points were interpolated by means of the computer software Mathematica and its Interpolation function. In Mathematica this function is called Hermite interpolation (http://reference.wolfram.com/mathematica/ref/Interpolation.html), which returns a piecewise polynomial, in the present case of degree three. This goes through all the given data points and constructs an approximate function that interpolates the collected data. If the thus interpolated function is regular the Hermite interpolation gives a good approximation inside the interval of data points. The derivative of the function with $f(x) = 0$ reveals the peak.

qRT-PCR

The retinal samples were dissected and stored at -80 °C in RNAlater (Ambion) until further use. The RNA extraction from stored samples was performed with RNeasy micro kit (Qiagen), as per the manufacturer's instruction. The RNA was quantified using Nanodrop (Thermo Scientific) and 0.5 µl of RNA was used for cDNA preparation. cDNA was prepared with iScript Advanced cDNA synthesis kit (Biorad) according to the manufacturer's instruction. The cDNA was diluted 10-fold and 2 µl of diluted cDNA was used for quantitative PCR experiments. RT negative control without the reverse transcriptase was used as internal control for cDNA preparation

and to check for genomic DNA contamination. Taqman probes (Life Technologies) were used (Table 4.4.1) and PCR was run on iQ5 real time cycler (Biorad). The *wt* and *rd1* samples were run in quadruplicates for each of the probes. The data was $\log_2$ transformed and fold changes were calculated by ΔC_T method.

Gene	Amplicon length	Assay design	Catalogue No.
Hsp40	57	Probe spans exons	Mm01351377_m1
Hsp70	62	Probe spans exons	Mm00434069_s1
Hsp90	128	Probe spans exons	Mm00658568_gH
β-Actin	115	Both primers and probe map within a single exon	Mm00607939_s1

Table 4.4.1. *Taqman probes used in the qRT-PCR.*

Results

Expression and temporal appearance of Hsp70 protein

The cellular expression and localization of Hsp70 in degenerating retinae from *rd1* or corresponding control retinae was investigated. As fig. 4.4.1 A shows, Hsp70 was not detected in PN11 *wt* mouse retina, while a sub-population of photoreceptors was clearly labelled in same aged *rd1* tissue. Confocal microscopy confirmed Hsp70 PN11 expression in inner segments, cell bodies and nuclei of *rd1* photoreceptors (Fig. 4.4.3 C).

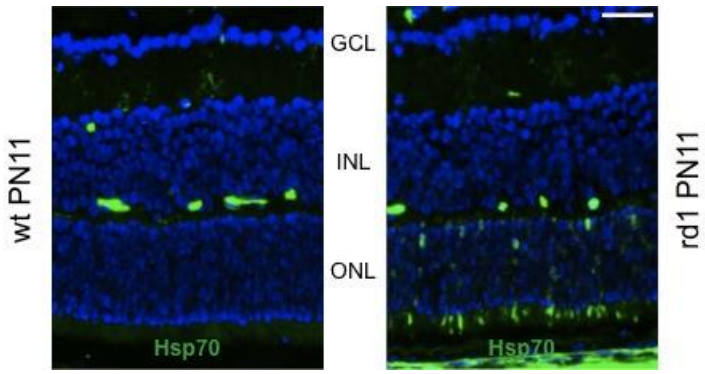

Figure 4.4.1. *Expression of Hsp70 in rd1 mice*. Immunostaining for Hsp70 (green) and DAPI (blue) show extremely low level in wt PN11, but a group of photoreceptors are labelled in *rd1* mutants. GCL = ganglion cell layer; INL = inner nuclear layer; ONL = outer nuclear layer. Bar = 50 μm.

In order to understand whether the increased Hsp70 expression is an early or late event in the degeneration process of a given *rd1* rod photoreceptor, we co-labelled for Hsp70 plus cell death (TUNEL) (Fig. 4.4.2 A, C and E), or for Hsp70 plus avidin staining (Fig. 4.4.2 B, D and F) for oxidatively damaged DNA (Sanz et al., 2007). TUNEL positivity is a late event in the death of an *rd1* rod (Sahaboglu et al., 2013), and in the *rd1* retina it often coincides with avidin staining (Sanz et al., 2007). At PN13, which is close to the peak of *rd1* rod cell death, Hsp70 positive cells did not co-localize with TUNEL nor with avidin staining (Fig. 4.4.2 A, C and E). Moreover, Hsp70 and TUNEL staining were not detected together in any studied time-point between PN7 to 15 (data not shown). The lack of co-labelling of Hsp70 with these markers thus suggests that the Hsp70 upregulation occurs relatively early in the rod photoreceptor degeneration process. Alternatively, however, the Hsp70 staining could be related to cones (or other cells) rather than rods, but given that the cone

degeneration at the degeneration time points studied here is far from its peak (Sancho-Pelluz et al., 2008), this seems less likely. Moreover, co-labelling for Hsp70 and cone arrestin or F4/80, which are markers for cones and microglial cells (the only other cell types present in the photoreceptor layer), respectively, did not suggest any co-localization (Fig. 4.4.2 G, I and K, and H, K and L respectively), which strengthens the notion that the Hsp70 positive cells are rods.

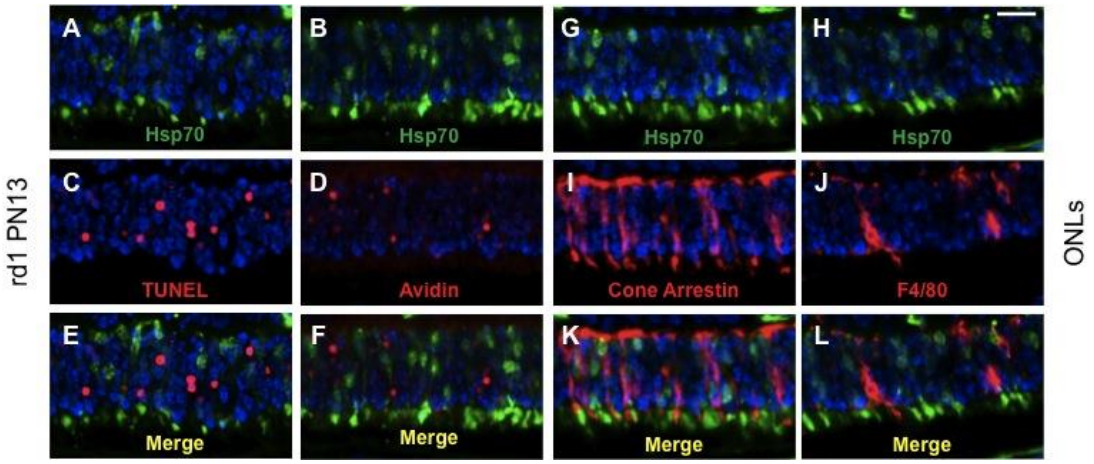

Figure 4.4.2. *Hsp70 does not co-localize with stress or cone and microglial cells markers.* Hsp70 (green) is extensively expressed in the ONL of PN13 *rd1* retina, but fails to co-localize with TUNEL (A, C and E), avidin (B, D and F), Cone arrestin (G, I and K) and F4/80 (H, J and L), all in red. Bars = 30 μm.

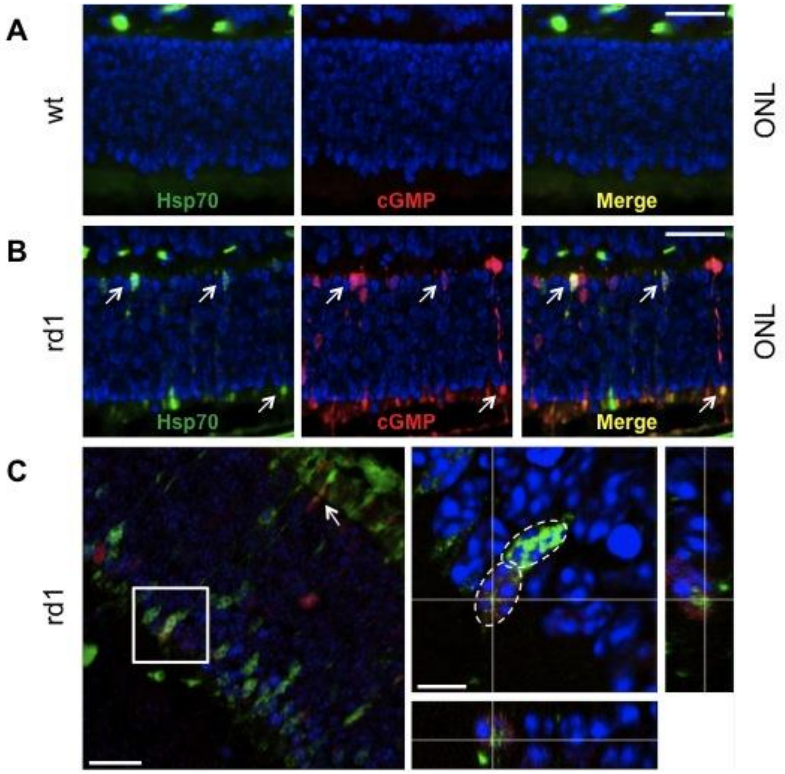

Figure 4.4.3. *Hsp70 and cGMP co-localize in rd1 photoreceptors*. In PN11 wt retina (A), neither Hsp70 (green) nor cGMP (red) are detectable. In the *rd1* mutant (B), the first relevant biological event provoked by the mutation within the PDE6 gene is the accumulation of cGMP. A subset of photoreceptors with high level of cGMP, shows concomitant high level of Hsp70 (highlighted with white arrows). Co-localisation between Hsp70 and cGMP is confirmed with confocal microscopy (C). ONL = outer nuclear layer. Bar = 20 μm and 5 μm (bottom right).

To address the question of temporal order of expression even further, we co-labelled for Hsp70 and cGMP, which can be considered as the first real sign of the pathology in PDE6β mutants (Paquet-Durand et al., 2009), and also a marker of photoreceptor degeneration in other RP models (Trifunović et al., 2010). Retinae from PN11 *wt* material displayed neither Hsp70 expression nor cGMP accumulation, while both were readily seen in *rd1* specimens (Fig. 4.4.3 A and B). There was also an overlap between Hsp70 and cGMP stainings (Fig. 4.4.3 B and C), including in the photoreceptor inner segments, cell bodies and nuclei. We therefore concluded that the increased Hsp70 expression occurred early on in the degeneration of an *rd1* rod photoreceptor, but it was still not obvious whether cGMP comes before Hsp70 or *vice versa*. In an attempt to clarify this, we used the retinal explant system to study the effects of an inhibitor of cGMP-activated protein kinase (PKG). The degeneration in *rd1* photoreceptors has its origin in the accumulation of cGMP, and we have previously shown that the detrimental effects of cGMP is to a major extent due to the subsequent overactivation of PKG (Paquet-Durand et al., 2009), for example since PKG inhibitors promote rescue of *rd1* photoreceptors. PKG has furthermore been suggested as a potential contributor to the expression of Hsp70 by phosphorylating HSF1, the transcription factor that governs the expression of the heat shock proteins (Ohnishi et al., 1999). We therefore administered DF001, an analogue of cGMP that inhibits PKG to cultured *rd1* retinae and the treated specimens and their untreated controls were then stained for Hsp70. We found a reduction of the expression of Hsp70 in treated samples (Control: 10.7 % ± 1.3, n = 3; treated: 8.4 % ± 0.6, n = 2), indicating the involvement of PKG signalling in the expression of Hsp70.

We finally performed co-labelling for Hsp70 plus acetyl-lysine (Fig. 4.4.4). Acetylated lysines are substrates for histone deacetylases (HDACs), which are overactivated in *rd1* degenerating photoreceptors (Sancho-Pelluz et al., 2010). This results, for instance, in a staining pattern of the *rd1* ONL that includes many “gaps” or staining void nuclei. The expression of HDACs and Hsps has been reported to be

reciprocally regulated and modification of the general acetylation level has been shown to be able to affect the expression of Hsps (Kee et al., 2008, Chen et al., 2002, Hageman et al., 2010). In the *rd1* mouse we found that Hsp70 often localizes to gaps of acetyl lysine staining (Fig. 4.4.4). Given that the overactivation of HDACs partially co-labels TUNEL staining (Sancho-Pelluz et al., 2010), unlike what Hsp70 staining does, our results suggest that the early chain of events leading to photoreceptor degeneration is chronologically composed by accumulation of cGMP, activation of PKG, overexpression of Hsp70 and overactivation of HDACs.

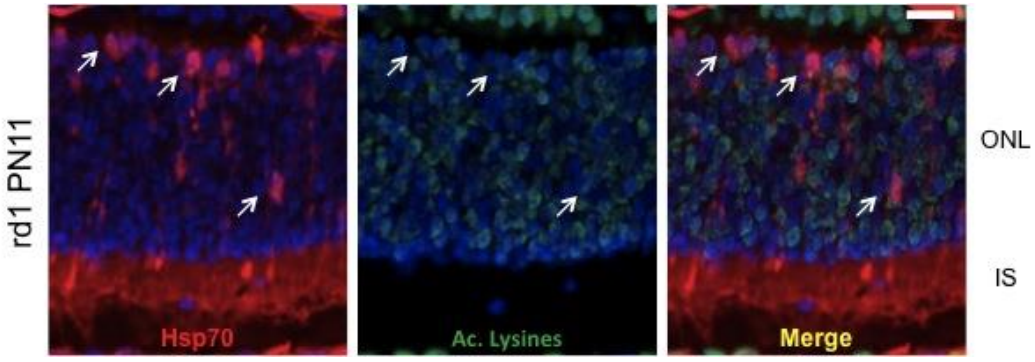

Figure 4.4.4. *Hsp70 is expressed in nuclei lacking of acetylated lysines.* In *rd1* retinae, anti-Hsp70 antibody labels segments, cell bodies and nuclei of cells with reduced levels of lysines acetylation, showing that accumulation of Hsp70 anticipated HDACs activation. ONL = nuclear layer; IS = inner segments. Bar = 20 μm

Time dependent dynamics of HSP70 expression

The number of Hsp70 expressing rods was assessed at multiple time-points, to determine the peak of Hsp70 expression in comparison to the temporal dynamics of TUNEL. Hsp70 was never detected in the ONL of *wt* animals in any given time-point, although there was some signal in the photoreceptor segments in the older ages (data not shown). The analyses encompassed *rd1* retinae from PN7 to PN21 (at the latter time-point nearly all rods have disappeared) (Fig. 4.4.5 A and B). Hsp70 was expressed in only few photoreceptor cells the at the earliest time point of detection, PN9, after which it increased both at PN10 and PN11 and even more sharply so at PN13, just like other markers in retinal degeneration such as TUNEL (Sancho-Pelluz et al., 2010). But unlike TUNEL (Fig. 4.4.5 C), which had a clear peak at around PN13 (6,0 % ± 1,1 (+) cells) after which it decreased to PN17 where it then plateaued, the Hsp70 expression increased further at PN15 (12,4 % ± 1,4), and was at a high

level even at PN17, after which it decreased gradually to low levels at PN21. Using a mathematical approach, the peaks of the Hsp70 and TUNEL curves were determined. The Hermite interpolation is a method of interpolating data points as a polynomial function. The limit of the functions obtained provided estimated peaks that were present at PN 14 + 5 hours for Hsp70 (12.7 % of (+) cells estimated) and at PN 13 + 16 hours for TUNEL (6,2 %).

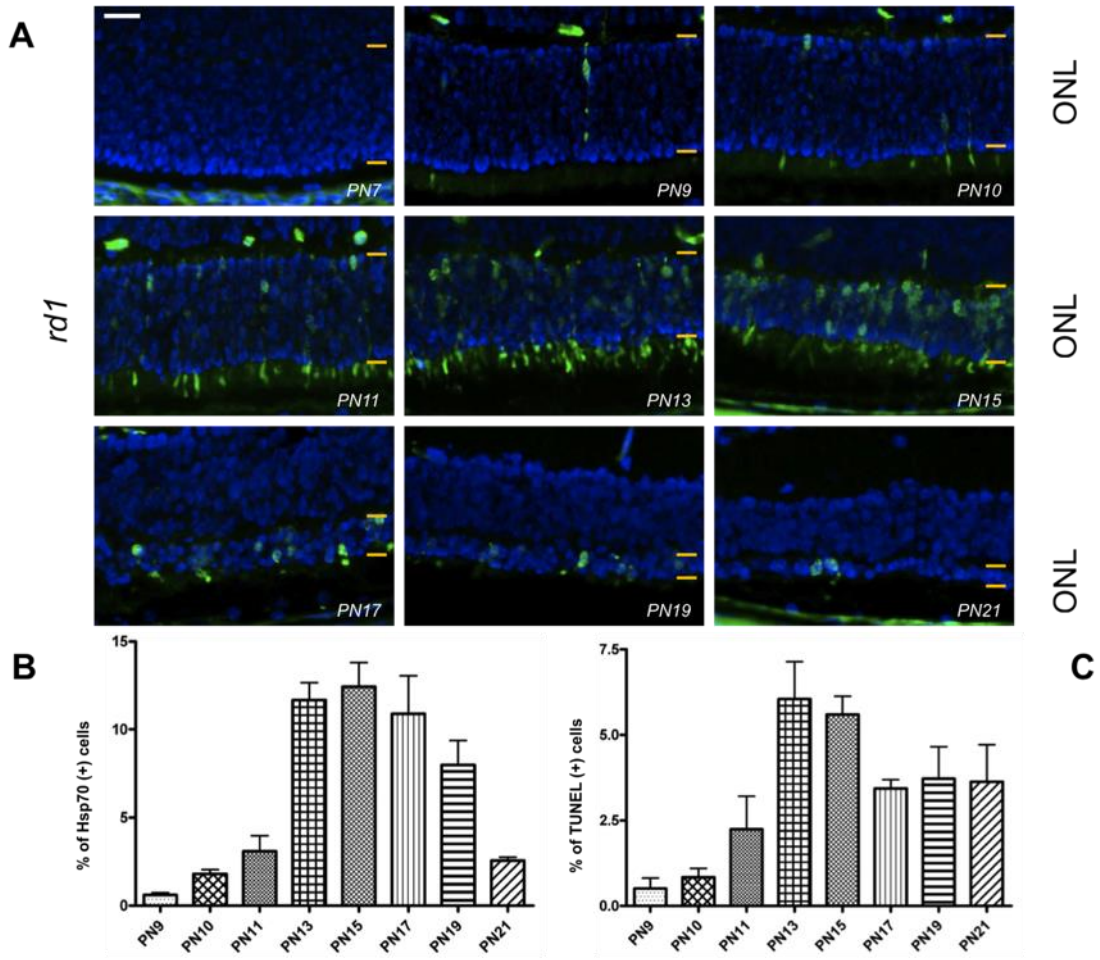

Figure 4.4.5. *Temporal expression of Hsp70 and TUNEL.* A) Outer retina of *rd1* mice are labeled for Hsp70 (green) and DAPI (blue). The yellow dashes show the size of the outer nuclear layers (ONL) in different time points. Hsp70 has been investigated between PN 7-21. Bar = 20 μm. B) and C), bar graphs expressing average plus standard deviation (SD) show the quantification of the Hsp70 and TUNEL positive (+) cells respectively. TUNEL has been quantified within time points comprised between PN 9-21.

To ascertain whether there was any contribution of cones at the latest time point analysed (PN21), we carried out immunostaining for cone-arrestin together with Hsp70 and TUNEL (Fig. 4.4.6), but the latter very rarely co-localized with cone staining. Therefore, at the time points under investigation here Hsp70 was almost exclusively expressed in rods.

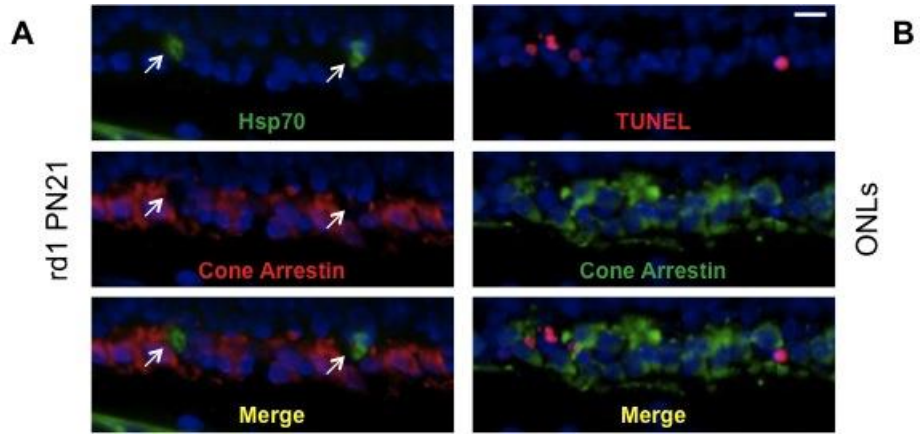

Figure 4.4.6. *Cones response to Hsp70 and TUNEL at PN21.* A) At PN21 cones (red labeling) of *rd1* mice normally don't express Hsp70 (white arrows) and B) few of them (green) are dying at this time point. ONLs = outer nuclear layers. Bar = 20 μm.

Pharmacological modulation of HSP70

Several reports indicate that pharmacological induction of Hsp70 expression promotes cytoprotective effects. Interestingly, geranylgeranyl-acetone (GGA), an inducer of Hsp70, was recently proven to be neuroprotective for photoreceptor cells in a rat model of retinal detachment (Kayama et al., 2011) after systemic administration. In order to see if a similar protective effect could be achieved on *rd1* photoreceptors, we performed organotypic retinal cultures with *rd1* retina explanted at PN5 with 2 DIV in normal medium, followed by 4 days with the administration of 10 μM GGA (PN5 + 2DIV + 4 DIV). The end point of the treatment thus represented approximately PN11, after which the samples were analysed for TUNEL and Hsp70 positivity. GGA at 10 μM provoked a reduction of the numerical average of TUNEL (+) cells (treated 4,0 % ± 1,1 (+) cells of all cells, control 4,4 % ± 0,7), and an increase in the percentage of Hsp70 (+) cells (treated 6,9 % ± 0,9, control 6,0 % ± 1,2). However, these differences were not statistically significant. The differences between the absolute numbers of Hsp70 (+) cells in the GGA experiment and the PKG inhibitor experiment above can likely be attributed to intrinsic differences in the preparations. According to the time dependent dynamics data we collected (see above), the Hsp70 expression shoot up rapidly between PN11-13, and therefore differences of few hours between different preparations at this time point may provoke sizeable differences in the final counting.

Retinal expression of HSF1 protein and of Hsp40, -70, -90 mRNA

A class of transcription factors called heat shock factors (HSFs) promote the expression of various Hsps (Pirkkala et al., 2001, Tam et al., 2010), and the prototypical member of this family is HSF1. In an unstressed situation, the HSF1 transcription factor is sequestered in a complex constituted of Hsp40, -70 and -90 proteins (Tam et al., 2010). As soon as stress occurs, the inhibitory binding of the multichaperone complex is released and HSF1 is free to undergo phosphorylation and form trimers (Anckar and Sistonen, 2011). Once activated and bound to a heat shock sequence in the DNA, HSF1 exerts its transcription factor function, which includes promotion of Hsp40, -70 and -90 mRNA expression (Tam et al., 2010). In order to determine possible connections between HSF1 and Hsp70 we performed immunostaining for HSF1 on PN11 tissues. HSF1 protein in *wt* was seen in all retinal layers and in both cytoplasmic and nuclear compartments (Fig. 4.4.7) and the picture was very similar in the *rd1* case, although a subset of photoreceptor nuclei in the *rd1* retinae appeared to have more condensed staining. This suggests that the generally low Hsp70 expression in all of the retinal layers of *wt* and *rd1* retinae is not a result of low expression of the HSF1 transcription factor as such.

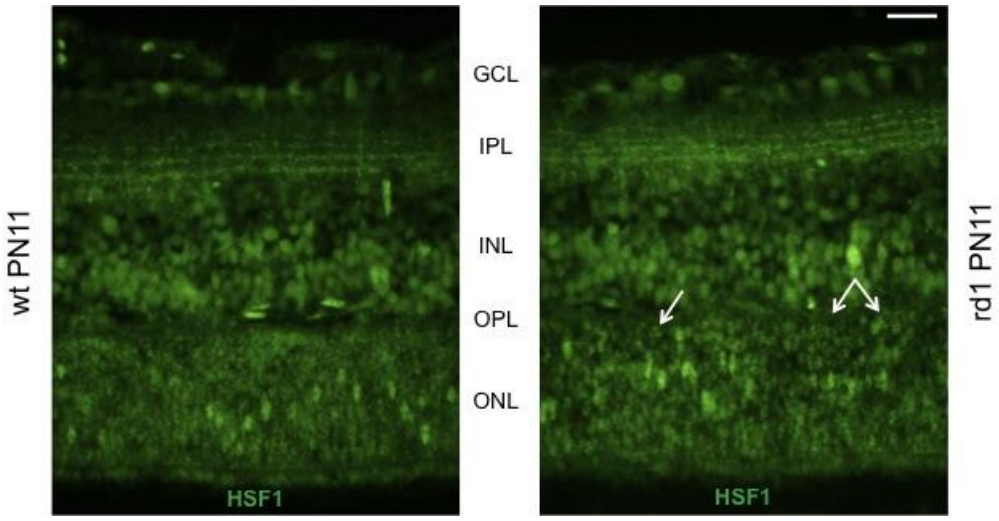

Figure 4.4.7. *HSF1 expression in wt and rd1 retina.* Total HSF1 is expressed throughout the retina both in wt and mutant. No difference in the expression level is detectable; however in *rd1* a group of cells within the photoreceptors layer, indicated with the white arrows, display slightly more condensed staining. GCL = ganglion cell layer; IPL = inner plexiform layer; INL = inner nuclear layer; OPL = outer plexiform layer; ONL = outer nuclear layer. Bar = 20 μm.

In the context of genotype comparisons we also used qRT-PCR to quantify the expression of the HSF1 governed Hsp40, Hsp70 and Hsp90 genes, but in none of the cases did we find a significant difference between the *rd1* and wt retinae (Fig. 4.4.8). This is in line with the equal general staining of HSF1 in the two genotypes and underlines that there are no gross alterations in Hsp expression in the degenerating *rd1* retina. However, there is still the possibility that individual photoreceptor cells display increased mRNA for one or several of the Hsps, but that these changes are masked in the global sample. Alternatively, the high levels of Hsp70 protein in some *rd1* photoreceptors may have different causes, such as increased protein stability, which would give the same outcome.

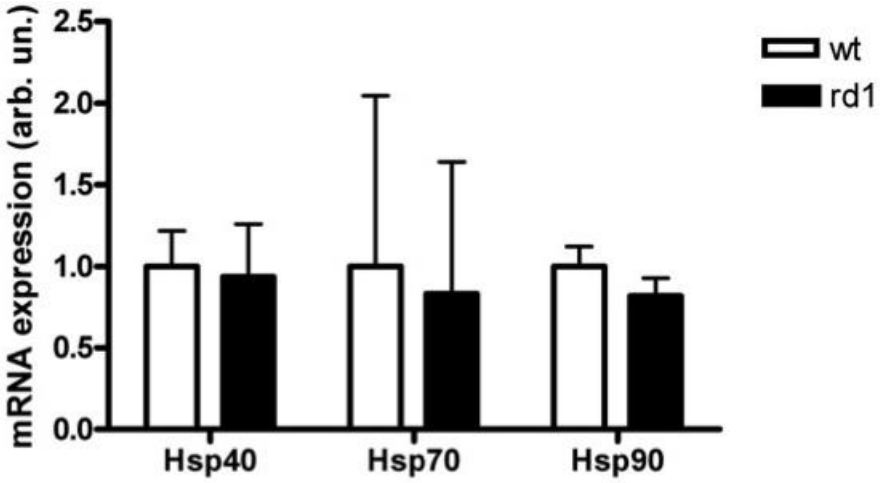

Figure 4.4.8. *Expression of HSF1 induced gene in wt and rd1 retinae.* qRT-PCR analysis of different Hsps shows no statistical relevant difference in the expression of Hsp40, 70 and 90 between mutant and control. Columns and bars represent mean ± standars deviation (SD) respectively.

Expression of Hsp70 in other models of RP

The clear upregulation of Hsp70 protein in the *rd1* photoreceptors prompted us to study this aspect in also other RP models. The degeneration in the *rd2* mouse concerns a different RP gene and starts later and progresses slower than in the *rd1* case. Instead of the PN11 assessment used in the *rd1* situation we hence for this model made comparisons using PN19 preparations. While the PN11 *rd1* retina displayed increased Hsp70 expression in selected photoreceptors, including in their outer segments, compared to wt, the PN19 *rd2* samples did not reveal any increased photoreceptor staining (Fig. 4.4.9 A and D).

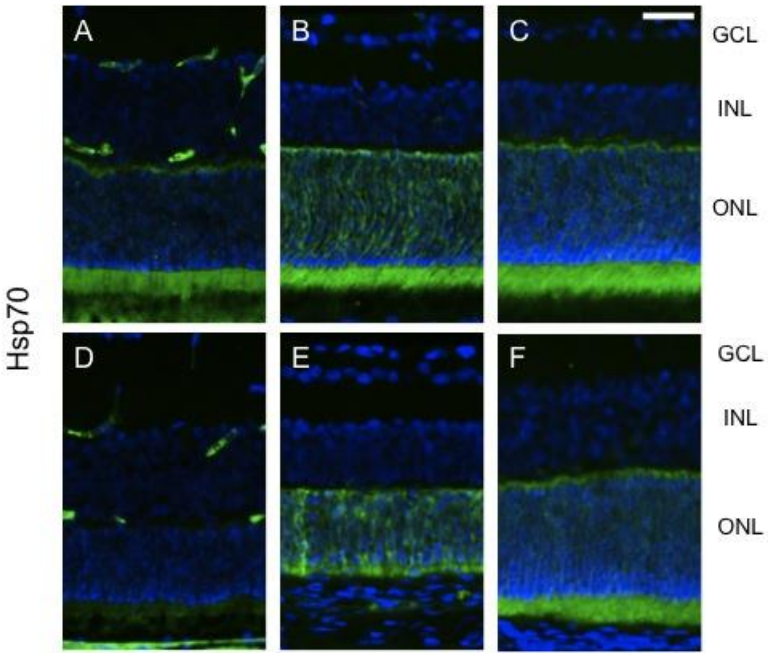

Figure 4.4.9. *Expression of Hsp70 in rd2 mice and rat rhodopsin mutants.* Comparison between *rd2* and control (A and D) shows reduction of the expression in mutants, with more emphasis on segments and synaptic terminations. Hsp70 in rat is detected mainly in the cytoplasm of cells within the ONL and segments. In mutants, Hsp70 is differentially distributed both in S334ter (B and E), while in P23H no differences were clearly visible (C and F). No staining was detected into the inner retinal layers. Pictures were taken close to the insertion of the optic nerve. GCL = ganglion cell layer; INL = inner nuclear layer; ONL = outer nuclear layer. Bar = 50 μm.

The *S334ter* and *P23H* rat models represent two variants of yet another RP gene mutation and also another species. Both models are known to suffer from defective protein trafficking and folding (Liu et al., 1996, Green et al., 2000), making them relevant to study in the Hsp70 context. Comparisons were made between mutants and *wt* material, using time-points where the individual mutants are known to show considerable levels of degeneration, respectively. As fig. 4.4.9 B and C show, *wt* retinae at PN12 and 15 express Hsp70 in the cytoplasm, synaptic terminals and segments of the photoreceptors, whereas other retinal layers are in principle devoid of staining. The *S334ter* mutation gives a harsh degeneration phenotype with strong effects on the photoreceptor cells, such that these at PN12 fail to develop outer segments (Martinez-Navarrete et al., 2011). There were in the *S334ter* samples thus only very little Hsp70 staining at the level of the photoreceptor segments and we also noted a decrease in staining intensity at the *S334ter* synaptic terminals. Importantly, we observed a clear tendency for increased cytoplasmatic immunoreactivity in a number of the PN12 *S334ter* photoreceptors (Fig. 4.4.9 E). The *P23H* model displays

a more protracted degeneration than the *S334ter* rat, so hence we here matched PN15 age *P23H* and *wt* retinae. By contrast to the *S334ter* situation, there were no indications for differential Hsp70 staining in the degenerating *P23H* retina when compared with its wt counterpart (Fig. 4.4.9 C and F).

Discussion

The present report describes increased levels of Hsp70 protein in the degenerating photoreceptor cells of a well-known animal model for RP, the *rd1* mouse. Comparisons with three other RP models, one mouse and two rat models, showed that while the Hsp70 response was not detected in all situations of photoreceptor degeneration, an increase was seen in the retinae which display the most aggressive forms of degeneration, *i.e.* in those from the *rd1* mouse and the *S334ter* rat. In normal conditions Hsp70 performs basal activities such as controlling protein folding, but its expression can dramatically increase in response of different stressors (Wagner et al., 1999), and the level of Hsp70 response in degenerating retinae may thus depend on the magnitude of the degeneration related stress. In the *rd1* mouse and the *S334ter* rat the photoreceptor degeneration is particularly early and rapid, and the retinae of both of these models experience a high percentage of dying cells during their respective degeneration period. This may have resulted in a situation of overall more pronounced retinal stress, including in the individual photoreceptors.

The Hsp70 expression in the *rd1* model lacked co-localization with cone markers, which showed that the affected cells were indeed rod photoreceptors. Neither did Hsp70 co-localize with oxidatively damaged DNA and TUNEL, which are both late events in the death of the *rd1* rods (Sanz et al., 2007, Sahaboglu et al., 2013). By contrast, some photoreceptor cells displayed an overlap between Hsp70 and cGMP. In the *rd1* retina the accumulation of cGMP and subsequent PKG activation are early and triggering events for the photoreceptor degeneration (Paquet-Durand et al., 2009), and together with the current findings this suggests that the Hsp70 upregulation happens at the initial stages of the degeneration of a given cell. We also noted a reduction of Hsp70 expression in cultured retinal explants after treatment with a PKG inhibitor. This indicates that the photoreceptor protective effect by PKG inhibition (Paquet-Durand et al., 2009) relieves the stress and thus the need for Hsp70, and it

furthermore implies that while Hsp70 upregulation is early, it occurs only after PKG activation. However, the transcription factor HSF1, which regulates the expression of several Hsps including Hsp70 (Pirkkala et al., 2001), can be phosphorylated by PKG (Ohnishi et al., 1999), and one may thus argue that the degeneration dependent activation of PKG in itself contributes to Hsp70 upregulation via HSF1 phosphorylation. We do not think this has played a major role in the present case, though. A previous investigation showed that the degeneration in the *rd2* model, which has a different genetic cause than *rd1*, is likewise accompanied by increased cGMP and can be protected by PKG inhibition (Paquet-Durand et al., 2009). Yet there were no signs of Hsp70 upregulation in the *rd2* photoreceptors in the present study, as would have been expected if the PKG activation as such contributed significantly to the Hsp70 regulation.

We have recently reported that the increase in cGMP of *rd1* photoreceptors starts at about PN8, to reach a peak at around PN13 (Sahaboglu et al., 2013). In the same study the start of TUNEL positivity was delayed by 2-3 days compared to cGMP, whereas both peaked at PN13, after which the number of cGMP positive cells remained higher than that of the TUNEL positive ones (Sahaboglu et al., 2013). The latter suggested that cellular cGMP positivity in a given cell lasted longer than TUNEL positivity, since the cellular lifetime of a marker will directly influence its detection probability. Indeed, various calculations based on these and other results showed that cGMP positivity in a given cell lasts for about 36 h, and is followed by a transition phase of about 5-6 h, to be concluded by the TUNEL phase of another 6-7 h and then cell death (Sahaboglu et al., 2013). The results presented in the current study reveals Hsp70 detection at PN9 with a calculated peak at about PN14, and with the number of Hsp70 positive cells remaining higher that the TUNEL cells after this peak. This yields a situation similar to the cGMP-TUNEL relation in Sahaboglu et al. (2013), but also exposes a slight delay between the peak time-points for Hsp70 and cGMP, which goes very well with the partial overlap of cGMP and Hsp70 (Fig. 4.4.3). Together this again suggests that cGMP in a given photoreceptor comes before the Hsp70 upregulation of the same cell, which, given the properties of Hsp70 (Antonoff et al., 2010, Beere et al., 2000), could represent an endogenous attempt towards cellular protection. Indeed, such a situation – a massive cGMP increase triggering an endogenous (but futile) survival mechanism before eventual cell death – is convincing

and fully compatible with the temporal aspects of cell death in the *rd1* retina, as established by mathematical considerations of the kinetics of cGMP and TUNEL and other parameters (Sahaboglu et al., 2013). Besides, the reported cytoprotective properties of Hsp70 (Kayama et al., 2011, Young, 2010) together with the lack of co-labeling with TUNEL may suggest that, as long as Hsp70 is expressed, the photoreceptors are kept away from the cell death pathways.

Experimentally increased Hsp70 has a beneficial effect on the retinal degeneration in *P23H* rats (Gorbatyuk et al., 2010), which fits with the proposed neuroprotective actions of Hsp70 (Antonoff et al., 2010, Kayama et al., 2011) as well as with the upregulated Hsp70 in the *rd1* rods seen here. The neuroprotective actions could rely on the ability of Hsp70 to reduce insoluble protein aggregation, or to block apoptotic pathways by inhibiting the formation of the apoptosome (Beere et al., 2000), but also its capacity to activate the pro-survival kinase Akt, as was shown after pharmacologic, and advantageous, induction of Hsp70 in a rat model for detached retina (Kayama et al., 2011). In our experiments with the Hsp70 inducer GGA, however, we saw no significant change in the number of TUNEL or Hsp70 positive cells in treated *rd1* retinal explants (although there was a tendency for reduction and increase, respectively). While we cannot rule out that there could have been a transient increase of Hsp70 after each medium change, the TUNEL results suggest that this did not translate into a protective effect. Since the Akt kinase has been reported to be overactivated in the *rd1* mouse photoreceptors (Johnson et al., 2005), both players in such a possible Hsp70-Akt protective route may already be engaged close to their full extent in the *rd1* retina, precluding further improvement by GGA treatment. Alternatively, the lack of neuroprotection with GGA could be the result of that Hsp70 is an ATP-consuming protein (Young, 2010). The degenerating photoreceptors of the *rd1* retina are known to suffer from an overactivation of another energy consuming protein, poly (ADP-ribose) polymerase PARP (Paquet-Durand et al., 2007, Sahaboglu et al., 2010). This is a burden for the photoreceptors, because both PARP inhibition and the crossing of *rd1* animals with PARP1 knock-out mice lead to a milder retinal degeneration (Paquet-Durand et al., 2007, Sahaboglu et al., 2010). A particularly interesting future possibility would therefore be to induce Hsp70 concomitant with preservation of energy by PARP inhibition in *rd1* retinae. It is furthermore possible that experimental Hsp70 induction might have better chances for success when

applied in situations where it is not already in play to the same extent as in the *rd1* retina, such as in the *rd2* or *P23H* models also described in the present study.

In conclusion, we have here demonstrated the clear upregulation of Hsp70 protein in the degenerating rod photoreceptors of the *rd1* model for the blinding disease RP. The Hsp70 upregulation may reflect an endogenous survival response of the affected photoreceptors, but due to unknown circumstances this is not sufficient for cellular protection. Our results furthermore suggest that the Hsp70 response differs when it comes to the exact disease causing mutation. Therefore, given the success of Tam et al. (2010) in achieving protection in a model for autosomal dominant RP with an Hsp expression paradigm, the challenge with Hsp70 may be to find the right conditions for promoting photoreceptor survival. This could include simultaneous manipulations of more than one pathway or letting any Hsp70 based therapy focus on those mutations, which on their own do not seem to involve the upregulation of this protein.

Acknowledgements

Torsten och Ragnar Söderbergs Stiftelser, KMA, Stiftelsen Olle Engkvist Byggmästare, VRM, Stiftelsen för Synskadade i f.d. Malmöhus län, Ögonfonden Charlotte and Tistou Kerstan Foundation, Deutsche Forschungsgemeinschaft (DFG; PA1751/1-1) and the EU project DRUGSFORD (HEALTH-F2-2012-304963). We like to extend our thanks to Birgitta Klefbohm and Hodan Abdshill for expert technical assistance regarding retinal explant experiments as well as Emanuela Monni for valuable contribution and expertise in confocal microscopy and Karthikeyan Devaraju for assistance and critical analysis of qRT-PCR data.

5. Discussion

Overall contributions of the thesis to the RP field and future directions

Four different entities, Klotho, HDACs, DNA methylation and Hsp70, whose functions in the degenerating retina were previously either virtually unknown or not well described, have been studied in this thesis. The information gathered during the work provides experimental and novel evidence of the association of these four factors with neurodegeneration or neuroprotection in the context of RP. The gained knowledge increases the understanding of the pathomechanisms behind the disease and could aid in the development of pharmacological or other neuroprotective approaches to slow down the RP related loss of vision in humans. As such, the results also forward novel biomarkers for RP. A brief recapitulation of the findings follows.

α-Klotho. The presented work in paper we provided the first experimental evidence of degeneration related Klotho expression in the retina. Using four different RP models from two different species we found over-expression of α-Klotho in the subset of photoreceptors that are in the process of neurodegeneration. As separately studied in the *rd1* model there was also an increased expression of β-Klotho, another Klotho family member, in the degenerating photoreceptors. We were furthermore able to demonstrate that administration of ectopic α-Klotho ectodomain severely affected the retinal organization in otherwise healthy retinae. The exact role of Klotho in the degeneration process remains to be determined, as discussed in the report, and here follows some additional aspects on the Klotho involvement in retinal physiology and pathology.

α-Klotho carries out multiple tasks, both within a cell and as a circulating hormone. One function of α-Klotho is to form complexes with fibroblast growth factor receptors (FGFRs), which then allows the binding and signalling of the growth factors FGF15 and 23 (Wu et al., 2007, Kurosu et al., 2006). This is potentially very relevant here, since a) we observed FGF15 to have a lower expression in the *rd1* mouse retina and b) FGF19 (the human orthologue of mouse FGF15) supports survival in primary adult pig photoreceptor cultures (Siffroi-Fernandez et al., 2008). The increased Klotho expression may thus be a response to the reduced FGF15 in the degenerating retinae in order to save the photoreceptors. If such compensation has already happened in the

rd1 retina, this could explain why further, exogenous addition of α-Klotho did not improve the survival of these photoreceptors. In the *wt* explant situation, the addition of Klotho occurred in a situation of low basal levels of Klotho and normal levels of FGF15 and gave increased disorganization of the retina. Given the proposed involvement of FGF15 in mouse brain cell proliferation and differentiation (Fischer et al., 2011), it is possible that the addition of α-Klotho has disturbed any regular action of FGF15 in the retinal differentiation and layering that occurs over the time studied.

As a circulating hormone, α-Klotho can activate insulin signaling (Kuro-o, 2009). Insulin signaling is present also in the retina (Reiter et al., 2003), and its inhibition may lead to detrimental effects while its induction may promote survival (Wu et al., 2004, Barber et al., 2001). Interestingly, in the *rd1* photoreceptors Akt, a downstream kinase in the insulin dependent pathways, is over-activated (Johnson et al., 2005), and it is possible that the increased Klotho has played a part in this cellular attempt to survive. Again this could indicate why further Klotho treatment does not promote protection. Further work will be needed to determine the exact role of α-Klotho in retina and its contribution in RP.

Epigenetic factors. Chapter 4.2 suggests that the HDAC enzymes class I & II are overactivated in the *rd1* retina compared to *wt* animals and contribute to photoreceptor cell death. HDACs are a group of enzymes that remove acetyl groups from acetyl lysines in a wide range of substrates (not just histones as the name would indicate). Lysine acetylation is a protein post-translational modification that plays a pivotal role in the regulation of gene expression (Choudhary et al., 2009), since acetylation of the histone tails allows the relaxation of the chromatin structure, promoting transcription. HDACs overactivation has been suggested to be an early-to-medium late event in the photoreceptor degeneration, considering its limited overlapping with TUNEL. Moreover, blockade of HDACs class I & II with trichostatin A (TSA) showed neuroprotective properties after short-term treatment and promoted survival after long-term treatment. Last, overactivation of PARP1, another epigenetic factors (Beneke, 2012), have been already reported in *rd1* (Paquet-Durand et al., 2007). In chapter 4.2 we showed that PARP1 and HDACs overactivations happen simultaneously.

The previous work thus paved the way for chapter 4.3, and this study provides evidence for an increase in DNA methylation in dying photoreceptors of several

models of RP. This, together with data collected in the manuscript described in chapter 4.2, in turn suggests the existence of multiple and concomitant increases of the activities of various epigenetic modifiers of chromatin. There are at this point thus a number of reasons to propose that a degenerating photoreceptor undergoes several and profound alterations related to its chromatin. Just as for the Klotho proteins, the observed increase of 5mC may be considered as a late event in RP.

Our experiments suggest that under certain conditions the inhibition of the DNA-methylation responsible DNMTs via decitabine (a non-methylatable cytosine analogue) reduces the number of dying cells. It will therefore be of interest to in future studies combine decitabine administration with other drugs known to affect the status of the chromatin and that are also known to promote survival, like inhibitors of HDAC class I & II and of PARP1 (Paquet-Durand et al., 2007, Sancho-Pelluz et al., 2010).

Hsp70. Manuscript in chapter 4.4 describes that the molecular chaperone Hsp70 is differentially expressed in models of RP characterized by quick degeneration (*rd1* mouse and *S334ter* rat) compared to relative controls. In slower degenerating models (*rd2* mouse and *P23H* rat) the Hsp70 expression substantially replicates the *wt* scenario and no increased expression is observed. This suggests a mutation specific involvement of Hsp70 that mirrors the harshness of the degeneration. In situations with a rapid degeneration, Hsp70 could serve as a very early, albeit insufficient, neuroprotective response that may be elicited by the stress from many photoreceptors dying over a given time period. In more protracted degenerations, the Hsp70 response may be limited, which by consequence makes the detection difficult due to lower absolute expression levels or fewer positive cells at any given moment. It is possible that the slower degeneration types are the ones most susceptible for protection by experimental Hsp70 stimulation.

Links between the projects

The studies have recognized four separate factors that correlate with the degeneration of photoreceptors. However, it is fully possible that some or all of these are in some way(s) linked together, and this is of major interest to establish. Indeed, literature data are compatible with a linkage between some of the factors studied (see below) and I

therefore devote this section to an overview of the possible interconnections between the presented observations.

Gene expression and α-Klotho. The regulation of gene expression is one of the main tasks performed by several of the proteins I have studied for this thesis, notably DNA methyl transferases (DNMTs) (chapter 4.3), histone deacetylases (HDACs) and poly (ADP-ribose) polymerases (PARPs) (chapter 4.2). The control of gene expression of α-Klotho is poorly investigated. However, a recent report showed that the age-related decline of α-Klotho expression in the rhesus monkey is provoked by hypermethylation of its promoter (King et al., 2011). Additionally, hypermethylation of the promoter of α-Klotho has been reported in human cervical carcinoma (Lee et al., 2010) where they propose epigenetically targeting the α-Klotho promoter to tackle carcinoma. In the *rd1* mouse we found both hypermethylation of DNA in dying photoreceptors and an increased expression of α-Klotho, suggesting that its expression might not necessarily be primarily regulated by methylation of the promoter. However, a thorough investigation on the methylation level of the α-Klotho gene promoter has yet to be done.

Pharmacological restoration of pathologically altered gene expression is a neuroprotective strategy that has provided encouraging results in various disease models (Yi et al., 2012, Kaminskyy et al., 2011, Nishioka et al., 2011, Jia et al., 2012). This can be achieved *e.g.* via the manipulation of enzymes that alter the condensation of the chromatin. For instance, chapter 4.3 showed that short-term treatment with decitabine 2,5 μM (a DNMT inhibitor) decreased both the number of TUNEL and 5mC (+) cells. This treatment could thus be used to assess whether decitabine is able to provoke demethylation on target genes, like α-Klotho. Interestingly, in colorectal cancer α-Klotho is down-regulated and decitabine can restore its expression, but not the HDAC inhibitor trichostatin A (TSA) (Pan et al., 2011), which has a similar ability as decitabine to restore gene expression and which has been showed to promote neuroprotection in the *rd1* retina (Sancho-Pelluz et al., 2010). Future studies may be able to determine whether those drugs can affect the expression of α-Klotho in the retina.

α-Klotho and Hsp70. Possible links between expression and function of α-Klotho and Hsp70 have not been sufficiently studied. Intriguingly, though, in the only paper currently published, α-Klotho has been reported to provide protection in a model of

ischaemic acute kidney injury through the expression of Hsp70 (Sugiura et al., 2010). In the *rd1* mouse retina we found different subsets of photoreceptors that express high levels of α-Klotho or Hsp70, but we could in separate experiments not observe any co-localization (Fig. 5.1). In the paper we suggested that Hsp70 has early neuroprotective functions while α-Klotho expression is likely to be a much later (and potentially even detrimental, although this remains to be determined) event, which is substantiated by this lack of co-expression. Thus, it is not likely that the phenotype in *rd1* mouse is consequence of any interplay between α-Klotho and Hsp70, at least not in that specific order. Moreover, all the studied models displayed increased levels of α-Klotho but the Hsp70 increase was limited to two of these.

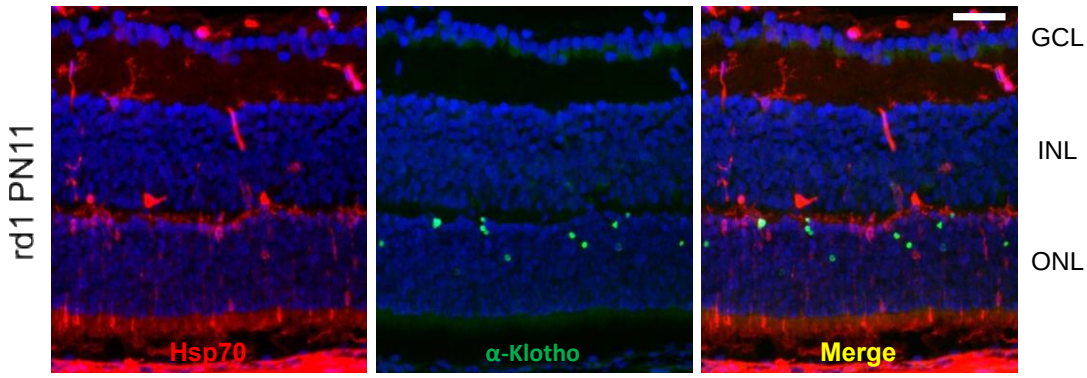

Figure 5.1. *Hsp70 overexpressing cells do not display overlay with increased α-Klotho.* Hsp70 overexpression is and early neuroprotective response, whereas α-Klotho is a late, maybe neurotoxic, factor in *rd1* retinae. The merged picture clearly shows lack of co-localisation at PN11. GCL = ganglion cell layer; INL = inner nuclear layer; ONL = outer nuclear layer. Bar = 50 μm.

Interplay between HDAC, PARPs and Hsp70. Literature data indicates that the expression of HDACs and Hsps is mutually regulated and modification of the acetylation level is able to affect the expression of Hsps (Kee et al., 2008, Chen et al., 2002, Hageman et al., 2010). We found Hsp70 expressed in cells lacking acetyl lysine staining, meaning that they experience overactivation of HDACs. Pharmacological inhibition of HDACs has been proved to promote cytoprotective effect in several different investigative set-ups (Wang et al., 2007, Marinova et al., 2009, Marinova et al., 2011), including in the *rd1* retina (Sancho-Pelluz et al., 2010). It would thus be interesting to test whether TSA has the ability to modulate Hsp70 expression in the *rd1* model.

The PARP enzyme family uses NAD as a co-factor to build-up homo-polymers of poly (ADP-ribose) (PAR) on acceptor proteins, which modifies their activities. The consumption of NAD may act to promote the energetic collapse that in the *rd1* mouse could be a critical point in the cell death pathway (Paquet-Durand et al., 2007). Accumulation of PAR was found in *rd1* photoreceptor cells that had reduced staining for acetyl lysine, *i.e.* increased HDAC activity coincides with PARP activity (Fig. 5.2).

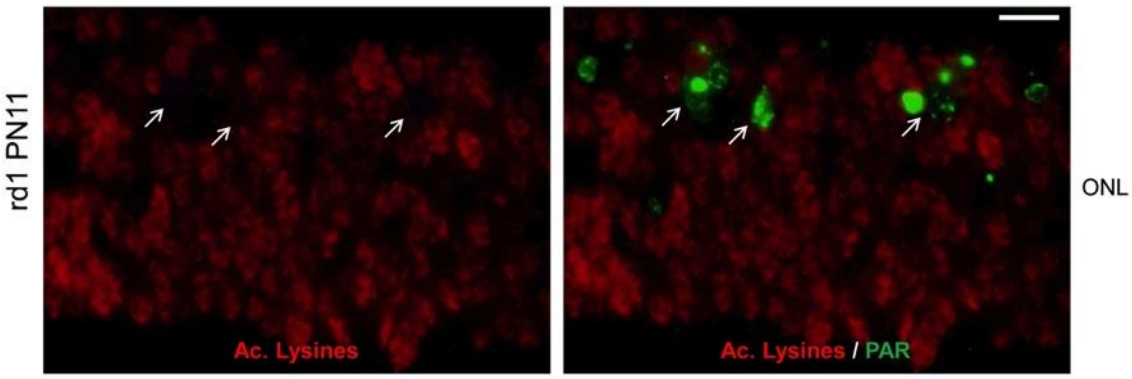

Figure 5.2. *HDACs and PARP enzymes overactivation coincide in dying photoreceptors.* Accumulation of poly (ADP-ribose) (green) and gaps of lysine acetylation (red) are detected in the same dying cells (Paquet-Durand et al., 2007, Sancho-Pelluz et al., 2010) in *rd1* retinae at PN11. ONL = outer nuclear layer. Bar = 20 µm.

The possibility of HDAC activation as a consequence of PARP1 activation has not been studied. However, inhibition of class I and II HDACs reduced the accumulation of PAR polymers (Sancho-Pelluz et al., 2010), and therefore very likely inhibited PARP1, which together suggested that HDACs are activated prior to PARP1.

The group I have worked with already reported that in the *rd1* photoreceptors, PARP1 is over-activated and that inhibition of this enzyme promote survival (Paquet-Durand et al., 2007). With relation to the Hsp70 study, it is interesting to note that when the transcription factor HSF1 binds heat shock elements (HSE) on the DNA sequence it is able, at least in part, to activate PARP1 (Anckar and Sistonen, 2011, Beneke, 2012), in order to unwind the chromatin and allow transcription of HSF1 target genes. But data in this regard are contrasting: Fossati and collaborators reported that the activation of PARP1 impairs the transcriptional activity of HSF1 in murine fibroblasts (Fossati et al., 2006). However, these data may not exclude each other, but rather indicate a reciprocal control of the activities between HSF1 and PARP1. As a general model, it is tempting to speculate that in response to stress HSF1 can mildly activate

PARP1 to loosen up the chromatin. On top of this the heavily damaged DNA, like in *rd1* mice, could increase the activation of PARP1 to extents that are detrimental to the photoreceptors. The accumulation of poly (ADP-ribose) (PAR) may furthermore depress the binding of HSF1 on the DNA, and hence the transcription of Hsp70, efficiently shutting down its expression prematurely. Accordingly, accumulations of PAR are not supposed to co-localize with Hsp70, but for technical reasons (both primary antibodies are of mouse origin) this experiment has not been performed for this thesis.

The link between PARP activation and Hsp70 expression may be even wider. Hsp70 is an ATP consuming protein, whereas PARP activation indirectly decreases the cellular energy content by the consumption of NAD, suggesting that there may be a PARP1- Hsp70 competition over energy. In fact, Hsp70 expression was facilitated in PARP1 -/- mice (Fossati et al., 2006) and altogether these data are compatible with PARP1 activation contributing to repress Hsp70 expression in *rd1* photoreceptors and thus playing as a forerunner for the cell death pathways. Finally, also different patterns of promoter methylation play a role in the silencing of the expression of Hsps in murine cell lines (Gorzowski et al., 1995, Drujan and De Maio, 1999) and we thus cannot exclude the existence of a complex interplay between different epigenetic modulators in the expression of Hsp70.

DNMTs/HDACs system. The most straightforward and studied interplay between the factors I have studied in this thesis, is represented by the connections between HDACs and DNMTs. In fact, different isotypes of HDACs and DNMTs cooperate in the epigenetic modification of the gene expression (Rountree et al., 2000, Fuks et al., 2001, Aapola et al., 2002). Epigenetic mechanisms like methylation of the DNA and histone acetylation are critical in many physiological functions, ranging from memory, to development and cellular reprogramming (Monsey et al., 2011, Han et al., 2010, MacDonald and Roskams, 2009). In different rodent models of RP, we suggest that both HDACs and DNMTs are overactivated and the outcome of their activities overlap.

In order to tackle photoreceptor degeneration, combined administration of the HDAC class I & II inhibitor TSA and decitabine might be an intriguing strategy. Both of these drugs displayed, to different extents, neuroprotective properties (Sancho-Pelluz

et al., 2010). However, we must undertake this path with caution because it would not be surprising if excessive blockade of regulative pathways turned out to be damaging.

Final Remarks

The goal of studies aimed at paving the way for neuroprotective strategies is to identify disease markers and to evaluate suitable molecular targets. In figure 5.3 is shown a possible – but likely incomplete – sequence of events that can be suggested to contribute, directly or indirectly, to cell death in *rd1* rods. The highlights point at the entities discovered and discussed in the present thesis.

Intracellular accumulation of cGMP is probably the first event (Paquet-Durand et al., 2009), which in turn activates membrane CNG cation channels (influx of calcium) and cGMP-activated kinase PKG, but one should keep in mind that the latter is 100-fold more sensitive to cGMP than the channels (Trifunović et al., 2010). Increase of cGMP triggers pro-cell death pathways, but maybe also the assumed endogenous neuroprotective actions of Hsp70. We showed here that as long as Hsp70 is expressed, photoreceptors seem able to resist the stress induced by the mutation. Detrimental overactivation of HDACs class I and II (Sancho-Pelluz et al., 2010) is likely to follow, as is activation of the calcium activated protease calpain (Paquet-Durand et al., 2006) and PARP1, with accumulation of probably neurotoxic poly (ADP-ribose) polymers (Paquet-Durand et al., 2007). Towards the late stages, perhaps close to cell death, we found increase of methylation of the DNA and up-regulation of α-Klotho.

Choosing the perfect target is a difficult issue. If we pharmacologically approach early events, like the accumulation of the second messenger cGMP, we have good possibilities to block the neurotoxic pathways, but this may also have serious repercussions on downstream processes needed for the normal cellular physiology. Blockade of targets that appear later may thus minimize the possibility that indispensable pathways are affected; although for some such targets the cell death machinery has already crossed the point of no return. One interesting, but so far little - if at all - tried approach, would be to arrange for simultaneous but limited inhibition of both earlier and later events.

The thesis work detected and studied two late events (α-Klotho expression and DNA methylation) as well as two earlier events (Hsp70 and HDACs), according to co-localisation with TUNEL staining. Administration of α-Klotho did not display any neuroprotection, but the use of the aza-nucleoside decitabine, which inhibits DNMTs, and the HDACs class I & II inhibitor TSA in both cases reduced the number of TUNEL positive cells after short-term treatments. The TSA treatment also promoted survival after long-term treatment.

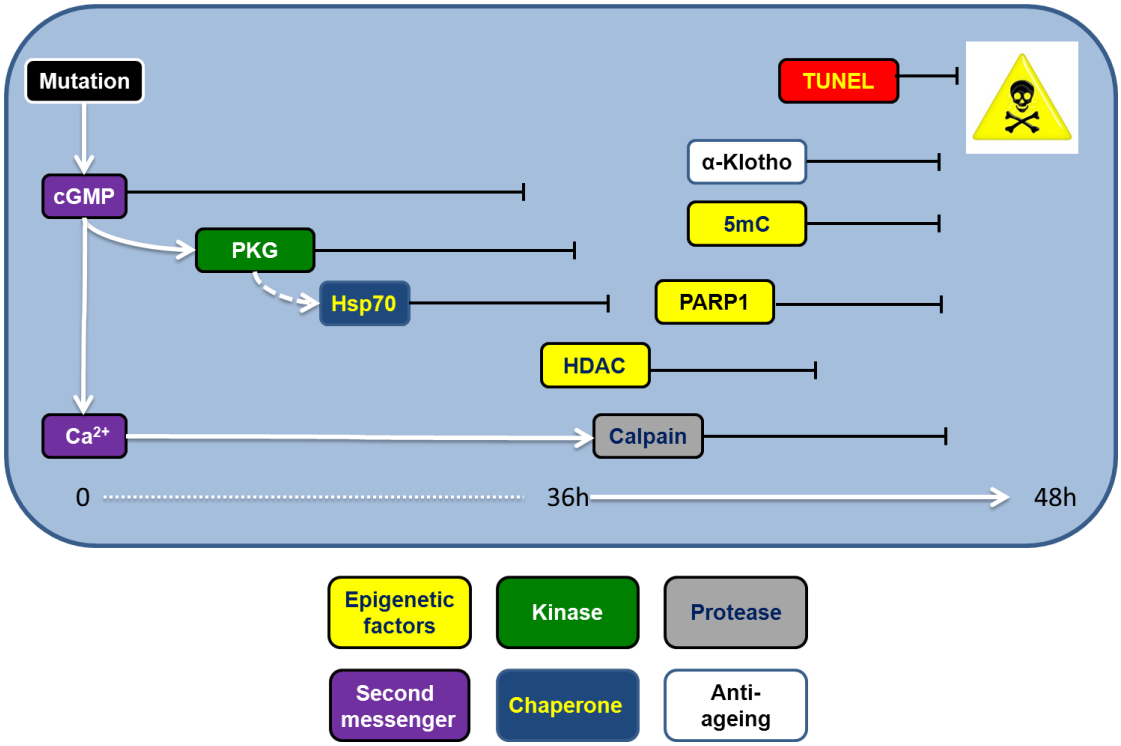

Figure 5.3. *Possible sequence of event leading to photoreceptors degeneration in rodent models of Retinitis pigmentosa.* In *rd1* mouse, mutation in the PDE6β gene provokes primarily an increase of intracellular cGMP and calcium (Bowes et al., 1990, Farber and Lolley, 1974). The first activate PKG (Paquet-Durand et al., 2009), which in turn may have (indicated by the dashed white arrow) influence on Hsp70 expression. After that we suggested the activation of HDACs which in this thesis have been shown to play a role in the control of the activation of PARP enzymes. On the other hand, high level of intracellular calcium can activate calpain proteases (Paquet-Durand et al., 2006). As late events we found DNA hypermethylation abd increased expession of α-Klotho. All of these factors are shared with r*d2* mouse as well as S334ter and P23H, with the exception of the overexpression of Hsp70, which is not affected in slow degenerating models. The black bars suggest the possible slot in which every factor is detectable and superimposition of bars and box indicates co-labeling. Indeed, HDAC, calpain (Paquet-Durand et al., 2006), PARP activation, as well as increased DNA methylation and α-Klotho co-label with TUNEL.

One of the most intriguing and potentially promising pharmacological target could be represented by Hsp70, and the opportunity of inducing an early and presumably endogenous neuroprotective factor with geranylgeranylacetone (GGA) in more slowly

degenerating models than *rd1*, where Hsp70 is already in action, is indeed attractive. However, the overexpression of Hsp70 may increase the ATP consumption, which could counteract its other effects, particularly in a model like the *rd1* mouse that already appears to suffer from energy depletion. Combinatory approaches, which in this case would consist of blockade of neurotoxic enzymes and induction of protective factors, might in theory produce synergistic effects even with reduced concentrations of the drugs, limiting in turn side effects.

In conclusion, the work has established several novel factors in relation to inherited photoreceptor degeneration. This knowledge platform could serve as an incitement for further work, including such that focuses on exact treatment paradigms in order to obtain neuroprotection. Drug concentrations and treatment times used in other systems may very well be suboptimal when applied to the degenerating retina. To this end, one could elaborate on several aspects, ranging from treatment length to the number and frequency of the administrations. Furthermore, targeted combined treatments, as discussed previously, might allow selective blockade of multiple molecular targets at relatively low drug concentration. Information on the best conditions for the current disease setting may thus with time become available, and this is likely what a potentially neuroprotective drug needs.

6. Summary

Retinitis pigmentosa (RP) groups a family of hereditary neurodegenerative diseases of the retina characterized by progressive loss of photoreceptors and for which treatment is still lacking. The aim of this thesis was to find and investigate novel markers of retinal degeneration in order to aid the understanding of the disease and the development of neuroprotective treatments. In this work four different rodent models for RP were used (*rd1* and *rd2* mice; S334ter and P23H rats), allowing the identification of several new players in inherited retinal degeneration. In order to do that, a wide range of techniques, including biochemistry and molecular biology, as well as microscopy and organotypic culturing methodologies were used. The main results achieved in this dissertation may be summarised as follows:

1. Increased expression of α-Klotho was seen in dying photoreceptors of all four models of RP. Addition of α-Klotho ectodomain on organotypic retinal cultures impaired retinal organization. In addition, fibroblast growth factor 15 (FGF15) was down-regulated in *rd1* and *rd2* mice, indicating an imbalance of the α-Klotho/FGF15 axis.

2. Histone deacetylases (HDAC) class I and II were over-activated and played a critical role in the cell death pathways of the *rd1* mouse retina. Blockade of class I and II of this family of enzymes with trichostatin A (TSA) protected photoreceptors *in vitro*.

3. Increased methylation of DNA occurred in dying photoreceptors of all four rodent RP models. Moreover, short-term treatment with decitabine, a specific inhibitor of DNA methyltransferases (DNMTs) rescued photoreceptors.

4. Differential expression of photoreceptor Hsp70 was detected in *rd1* mice and S334ter rat retina and could represent an early endogenous neuroprotective event. Hsp70 did not co-label with late stress markers such as TUNEL, suggesting that Hsp70 protected photoreceptors as long as it was expressed. Hsp70 induction may therefore have neuroprotective potential.

In conclusion, the studies report on four different and novel molecular players in retinal degeneration - Klotho, HDACs, DNMTs, and Hsp70 - that are all either overexpressed or overactivated in different models of RP. This provides us with 1) a new understanding of the complexity of the degeneration process as such, 2) support

for the idea that despite the varying mutations there are common pathways leading to photoreceptor degeneration in RP, and 3) ideas for how new neuroprotective strategies, aiming not only at one mutation, can be developed.

7. References

AAPOLA, U., LIIV, I. & PETERSON, P. 2002. Imprinting regulator DNMT3L is a transcriptional repressor associated with histone deacetylase activity. *Nucleic Acids Research,* 30**,** 3602-3608.

AHNELT & KOLB 1994. Horizontal cells and cone photoreceptors in primate retina: a Golgi-light microscopic study of spectral connectivity. *J Comp Neurol,* May 15**,** 387-405.

ALFINITO & TOWNES-ANDERSON 2002. Activation of mislocalized opsin kills rod cells: a novel mechanism for rod cell death in retinal disease. *Proc Natl Acad Sci U S A,* Apr 16**,** 5655-60.

ANCKAR, J. & SISTONEN, L. 2011. Regulation of HSF1 Function in the Heat Stress Response: Implications in Aging and Disease. *Annual Review of Biochemistry,* 80**,** 1089-1115.

ANTONOFF, M. B., CHUGH, R., SKUBE, S. J., DUDEJA, V., BORJA-CACHO, D., CLAWSON, K. A., VICKERS, S. M. & SALUJA, A. K. 2010. Role of Hsp-70 in Triptolide-Mediated Cell Death of Neuroblastoma. *The Journal of surgical research,* 163**,** 72-78.

ARSHAVSKY, V. Y. & BURNS, M. E. 2012. Photoreceptor Signaling: Supporting Vision across a Wide Range of Light Intensities. *Journal of Biological Chemistry,* 287**,** 1620-1626.

ARSHAVSKY, V. Y., LAMB, T. D. & PUGH, E. N. 2002. G PROTEINS AND PHOTOTRANSDUCTION. *Annual Review of Physiology,* 64**,** 153-187.

AZADI, S., PAQUET-DURAND, F., MEDSTRAND, P., VAN VEEN, T. & EKSTRÖM, P. A. R. 2006. Up-regulation and increased phosphorylation of protein kinase C (PKC) δ, μ and θ in the degenerating rd1 mouse retina. *Mol Cell Neurosci,* 31**,** 759-773.

BARBER, A. J., NAKAMURA, M., WOLPERT, E. B., REITER, C. E. N., SEIGEL, G. M., ANTONETTI, D. A. & GARDNER, T. W. 2001. Insulin Rescues Retinal Neurons from Apoptosis by a Phosphatidylinositol 3-Kinase/Akt-mediated Mechanism That Reduces the Activation of Caspase-3. *Journal of Biological Chemistry,* 276**,** 32814-32821.

BAYÉS, M., GIORDANO, M., BALCELLS, S., GRINBERG, D., VILAGELIU, L., MARTÍNEZ, I., AYUSO, C., BENÍTEZ, J., RAMOS-ARROYO, M., CHIVELET, P., SOLANS, T., VALVERDE, D., AMSELEM, S., GOOSSENS, M., BAIGET, M., GONZÀLEZ-DUARTE, R. & BESMOND, C. 1995. Homozygous tandem duplication within the gene encoding the β-subunit of

rod phosphodiesterase as a cause for autosomal recessive retinitis pigmentosa. *Hum Mutat,* 5**,** 228-234.

BEERE, H., WOLF, B., CAIN, K., MOSSER, D., MAHBOUBI, A., KUWANA, T., TAILOR, P., MORIMOTO, R., COHEN, G. & GREEN, D. 2000. Heat-shock protein 70 inhibits apoptosis by preventing recruitment of procaspase-9 to the Apaf-1 apoptosome. *Nat Cell Biol,* Aug**,** 469-75.

BELTRAN, W. A., CIDECIYAN, A. V., LEWIN, A. S., IWABE, S., KHANNA, H., SUMAROKA, A., CHIODO, V. A., FAJARDO, D. S., ROMÁN, A. J., DENG, W.-T., SWIDER, M., ALEMÁN, T. S., BOYE, S. L., GENINI, S., SWAROOP, A., HAUSWIRTH, W. W., JACOBSON, S. G. & AGUIRRE, G. D. 2012. Gene therapy rescues photoreceptor blindness in dogs and paves the way for treating human X-linked retinitis pigmentosa. *Proceedings of the National Academy of Sciences,* 109**,** 2132-2137.

BENEKE, S. 2012. Regulation of chromatin structure by poly(ADP-ribosyl)ation. *Frontiers in Genetics,* 3.

BERGERON, M., MIVECHI, N., GIACCIA, A. & GIFFARD, R. 1996. Mechanism of heat shock protein 72 induction in primary cultured astrocytes after oxygen-glucose deprivation. *Neurol Res,* Feb**,** 64-72.

BERSON, E. L. 1996. Retinitis pigmentosa: unfolding its mystery. *Proceedings of the National Academy of Sciences,* 93**,** 4526-4528.

BHANDAWAT, V., REISERT, J. & YAU, K.-W. 2005. Elementary Response of Olfactory Receptor Neurons to Odorants. *Science,* 308**,** 1931-1934.

BIERMANN, J., GRIESHABER, P., GOEBEL, U., MARTIN, G., THANOS, S., GIOVANNI, S. D. & LAGRÈZE, W. A. 2010. Valproic Acid–Mediated Neuroprotection and Regeneration in Injured Retinal Ganglion Cells. *Investigative Ophthalmology & Visual Science,* 51**,** 526-534.

BITTERMAN, K. J., ANDERSON, R. M., COHEN, H. Y., LATORRE-ESTEVES, M. & SINCLAIR, D. A. 2002. Inhibition of Silencing and Accelerated Aging by Nicotinamide, a Putative Negative Regulator of Yeast Sir2 and Human SIRT1. *Journal of Biological Chemistry,* 277**,** 45099-45107.

BLAZYNSKI, C. & PEREZ, M.-T. R. 1991. Adenosine in vertebrate retina: Localization, receptor characterization, and function. *Cellular and Molecular Neurobiology,* 11**,** 463-484.

BOLGER, T. A. & YAO, T.-P. 2005. Intracellular Trafficking of Histone Deacetylase 4 Regulates Neuronal Cell Death. *The Journal of Neuroscience,* 25**,** 9544-9553.

BOON, C. J. F., DEN HOLLANDER, A. I., HOYNG, C. B., CREMERS, F. P. M., KLEVERING, B. J. & KEUNEN, J. E. E. 2008. The spectrum of retinal dystrophies caused by mutations in the peripherin/RDS gene. *Progress in Retinal and Eye Research,* 27**,** 213-235.

BOWES, C., LI, T., DANCIGER, M., BAXTER, L., APPLEBURY, M. & FARBER, D. 1990. Retinal degeneration in the rd mouse is caused by a defect in the beta subunit of rod cGMP-phosphodiesterase. *Nature,* Oct 18**,** 677-80.

BOWES, C., VAN VEEN, T. & FARBER, D. 1988. Opsin, G-protein and 48-kDa protein in normal and rd mouse retinas: developmental expression of mRNAs and proteins and light/dark cycling of mRNAs. *Exp Eye Res,* Sep**,** 369-90.

BÜLOW 1968. Light scattering by pigment epithelium granules in the human retina. *Acta Ophthalmol (Copenh),* 46**,** 1048-53.

BUSSKAMP, V. & ROSKA, B. 2011. Optogenetic approaches to restoring visual function in retinitis pigmentosa. *Curr Opin Neurobiol,* Dec**,** 942-946.

CAFFÉ, A. R., AHUJA, P., HOLMQVIST, B., AZADI, S., FORSELL, J., HOLMQVIST, I., SÖDERPALM, A. K. & VAN VEEN, T. 2002. Mouse retina explants after long-term culture in serum free medium. *J Chem Neuroanat,* 22**,** 263-273.

CAI, X., CONLEY, S. M. & NAASH, M. I. 2010. Gene Therapy in the <i>Retinal Degeneration Slow Model of Retinitis Pigmentosa
Retinal Degenerative Diseases. *In:* ANDERSON, R. E., HOLLYFIELD, J. G., LAVAIL, M. M. & MANDAL, M. N. A. (eds.). Springer New York.

CALDWELL, R. B., MCLAUGHLIN, R. J. & BOYKINS, L. G. 1982. Intramembrane changes in retinal pigment epithelial cell junctions of the dystrophic rat retina. *Investigative Ophthalmology & Visual Science,* 23**,** 305-18.

CARTER-DAWSON, L. D. & LAVAIL, M. M. 1979. Rods and cones in the mouse retina. II. Autoradiographic analysis of cell generation using tritiated thymidine. *The Journal of Comparative Neurology,* 188**,** 263-272.

CHEN, B. & CEPKO, C. 2007. Requirement of histone deacetylase activity for the expression of critical photoreceptor genes. *BMC Developmental Biology,* 7**,** 78.

CHEN, B. & CEPKO, C. L. 2009. HDAC4 Regulates Neuronal Survival in Normal and Diseased Retinas. *Science,* 323**,** 256-259.

CHEN, C.-K., INGLESE, J., LEFKOWITZ, R. J. & HURLEY, J. B. 1995. Ca-dependent Interaction of Recoverin with Rhodopsin Kinase. *Journal of Biological Chemistry,* 270**,** 18060-18066.

CHEN, T., SUN, H., LU, J., ZHAO, Y., TAO, D., LI, X. & HUANG, B. 2002. Histone acetylation is involved in hsp70 gene transcription regulation in Drosophila melanogaster. *Archives of Biochemistry and Biophysics,* 408**,** 171-176.

CHIANG, W.-C., HIRAMATSU, N., MESSAH, C., KROEGER, H. & LIN, J. H. 2012a. Selective activation of ATF6 and PERK endoplasmic reticulum stress signaling pathways prevent mutant rhodopsin accumulation. *Investigative Ophthalmology & Visual Science*.

CHIANG, W.-C., MESSAH, C. & LIN, J. H. 2012b. IRE1 directs proteasomal and lysosomal degradation of misfolded rhodopsin. *Molecular Biology of the Cell,* 23**,** 758-770.

CHOUDHARY, C., KUMAR, C., GNAD, F., NIELSEN, M., REHMAN, M., WALTHER, T., OLSEN, J. & MANN, M. 2009. Lysine acetylation targets protein complexes and co-regulates major cellular functions. *Science,* Aug 14**,** 834-40.

CHRISTMAN, J. 2002. 5-Azacytidine and 5-aza-2'-deoxycytidine as inhibitors of DNA methylation: mechanistic studies and their implications for cancer therapy. *Oncogene***,** 5483-5495.

COLANTONIO, D. A., DUNKINSON, C., BOVENKAMP, D. E. & VAN EYK, J. E. 2005. Effective removal of albumin from serum. *PROTEOMICS,* 5**,** 3831-3835.

DERETIC, D., HUBER, L. A., RANSOM, N., MANCINI, M., SIMONS, K. & PAPERMASTER, D. S. 1995. rab8 in retinal photoreceptors may participate in rhodopsin transport and in rod outer segment disk morphogenesis. *Journal of Cell Science,* 108**,** 215-224.

DJAMGOZ, M. B. A. & WAGNER, H. J. 1992. Localization and function of dopamine in the adult vertebrate retina. *Neurochemistry International,* 20**,** 139-191.

DOBSON, C. M. 2004. Principles of protein folding, misfolding and aggregation. *Seminars in Cell & Developmental Biology,* 15**,** 3-16.

DRUJAN, D. & DE MAIO, A. 1999. Expression of HSP70 is impaired at the transcriptional level in stressed murine neuroblastoma cells. *Shock,* Dec**,** 443-8.

DRYJA, T., MCGEE, T., REICHEL, E., HAHN, L., COWLEY, G., YANDELL, D., SANDBERG, M. & BERSON, E. 1990. A point mutation of the rhodopsin gene in one form of retinitis pigmentosa. *Nature,* Jan 25**,** 364-6.

EGGER, G., LIANG, G., APARICIO, A. & JONES, P. 2004. Epigenetics in human disease and prospects for epigenetic therapy. *Nature,* May 27**,** 457-63.

EHINGER 1983. Functional role of dopamine in the retina. *1983,* 2**,** 213-232.

ELLIS, R. J. 2006. Molecular chaperones: assisting assembly in addition to folding. *Trends in Biochemical Sciences,* 31**,** 395-401.

ENDO, S., HIRAMATSU, N., HAYAKAWA, K., OKAMURA, M., KASAI, A., TAGAWA, Y., SAWADA, N., YAO, J. & KITAMURA, M. 2007. Geranylgeranylacetone, an Inducer of the 70-kDa Heat Shock Protein (HSP70), Elicits Unfolded Protein Response and Coordinates Cellular Fate Independently of HSP70. *Molecular Pharmacology,* 72**,** 1337-1348.

FAMIGLIETTI JR, E. V. 1983. 'Starburst' amacrine cells and cholinergic neurons: mirror-symmetric ON and OFF amacrine cells of rabbit retina. *Brain Research,* 261**,** 138-144.

FAN, Y., LUDEWIG, R. & SCRIBA, G. K. E. 2009. 9-Fluorenylmethoxycarbonyl-labeled peptides as substrates in a capillary electrophoresis-based assay for sirtuin enzymes. *Analytical Biochemistry,* 387**,** 243-248.

FARBER, D. B. & LOLLEY, R. N. 1974. Cyclic Guanosine Monophosphate: Elevation in Degenerating Photoreceptor Cells of the C3H Mouse Retina. *Science,* 186**,** 449-451.

FISCHER, T., FAUS-KESSLER, T., WELZL, G., SIMEONE, A., WURST, W. & PRAKASH, N. 2011. Fgf15-mediated control of neurogenic and proneural gene expression regulates dorsal midbrain neurogenesis. *Dev Biol,* Feb 15**,** 496-510.

FOSSATI, S., FORMENTINI, L., WANG, Z.-Q., MORONI, F. & CHIARUGI, A. 2006. Poly(ADP-ribosyl)ation regulates heat shock factor-1 activity and the heat shock response in murine fibroblasts. *Biochemistry and Cell Biology,* 84**,** 703-712.

FRANZE, K., GROSCHE, J., SKATCHKOV, S. N., SCHINKINGER, S., FOJA, C., SCHILD, D., UCKERMANN, O., TRAVIS, K., REICHENBACH, A. & GUCK, J. 2007. Müller cells are living optical fibers in the vertebrate retina. *Proceedings of the National Academy of Sciences,* 104**,** 8287-8292.

FRASSON, M., SAHEL, J., FABRE, M., SIMONUTTI, M., DREYFUS, H. & PICAUD, S. 1999. Retinitis pigmentosa: rod photoreceptor rescue by a calcium-channel blocker in the rd mouse. *Nat Med,* Oct**,** 1183-7.

FUKS, F., BURGERS, W. A., GODIN, N., KASAI, M. & KOUZARIDES, T. 2001. Dnmt3a binds deacetylases and is recruited by a sequence-specific repressor to silence transcription. *EMBO J,* 20**,** 2536-2544.

GAN, L. & MUCKE, L. 2008. Paths of Convergence: Sirtuins in Aging and Neurodegeneration. *Neuron,* 58**,** 10-14.

GAO, J., CHEON, K., NUSINOWITZ, S., LIU, Q., BEI, D., ATKINS, K., AZIMI, A., DAIGER, S. P., FARBER, D. B., HECKENLIVELY, J. R., PIERCE, E. A., SULLIVAN, L. S. & ZUO, J. 2002. Progressive photoreceptor degeneration, outer segment dysplasia, and rhodopsin mislocalization in mice with targeted disruption of the retinitis pigmentosa-1 (Rp1) gene. *Proceedings of the National Academy of Sciences,* 99**,** 5698-5703.

GAO, J., SIDDOWAY, B., HUANG, Q. & XIA, H. 2009. Inactivation of CREB mediated gene transcription by HDAC8 bound protein phosphatase. *Biochemical and Biophysical Research Communications,* 379**,** 1-5.

GLOBISCH, D., MÜNZEL, M., MÜLLER, M., MICHALAKIS, S., WAGNER, M., KOCH, S., BRÜCKL, T., BIEL, M. & CARELL, T. 2010. Tissue Distribution

of 5-Hydroxymethylcytosine and Search for Active Demethylation Intermediates. *PLoS ONE,* 5**,** e15367.

GOLDBERG, A. F. X. 2006. Role of Peripherin/rds in Vertebrate Photoreceptor Architecture and Inherited Retinal Degenerations. *In:* KWANG, W. J. (ed.) *Int Rev Cytol.* Academic Press.

GOLL, M. G. & BESTOR, T. H. 2005. Eukaryotic Cytosine Methyltransferases. *Annual Review of Biochemistry,* 74**,** 481-514.

GOLL, M. G., KIRPEKAR, F., MAGGERT, K. A., YODER, J. A., HSIEH, C.-L., ZHANG, X., GOLIC, K. G., JACOBSEN, S. E. & BESTOR, T. H. 2006. Methylation of tRNAAsp by the DNA Methyltransferase Homolog Dnmt2. *Science,* 311**,** 395-398.

GORBATYUK, M. S., KNOX, T., LAVAIL, M. M., GORBATYUK, O. S., NOORWEZ, S. M., HAUSWIRTH, W. W., LIN, J. H., MUZYCZKA, N. & LEWIN, A. S. 2010. Restoration of visual function in P23H rhodopsin transgenic rats by gene delivery of BiP/Grp78. *Proceedings of the National Academy of Sciences,* 107**,** 5961-5966.

GORZOWSKI, J. J., ECKERLEY, C. A., HALGREN, R. G., MANGURTEN, A. B. & PHILLIPS, B. 1995. Methylation-associated Transcriptional Silencing of the Major Histocompatibility Complex-linked hsp70 Genes in Mouse Cell Lines. *Journal of Biological Chemistry,* 270**,** 26940-26949.

GREEN, E., RENDAHL, K., ZHOU, S., LADNER, M., COYNE, M., SRIVASTAVA, R., MANNING, W. & FLANNERY, J. 2001. Two animal models of retinal degeneration are rescued by recombinant adeno-associated virus-mediated production of FGF-5 and FGF-1. *Mol Ther,* Apr 8**,** 507-515.

GREEN, E. S., MENZ, M. D., LAVAIL, M. M. & FLANNERY, J. G. 2000. Characterization of Rhodopsin Mis-sorting and Constitutive Activation in a Transgenic Rat Model of Retinitis Pigmentosa. *Invest Ophthalmol Vis Sci,* 41**,** 1546-1553.

GROSSMAN, G. H., WATSON, R. F., PAUER, G. J. T., BOLLINGER, K. & HAGSTROM, S. A. 2011. Immunocytochemical evidence of Tulp1-dependent outer segment protein transport pathways in photoreceptor cells. *Experimental Eye Research,* 93**,** 658-668.

GUILLONNEAU, X., BRYCKAERT, M., LAUNAY-LONGO, C., COURTOIS, Y. & MASCARELLI, F. 1998a. Endogenous FGF1-induced Activation and Synthesis of Extracellular Signal-regulated Kinase 2 Reduce Cell Apoptosis in Retinal-pigmented Epithelial Cells. *Journal of Biological Chemistry,* 273**,** 22367-22373.

GUILLONNEAU, X., RÉGNIER-RICARD, F., LAPLACE, O., JONET, L., BRYCKAERT, M., COURTOIS, Y. & MASCARELLI, F. 1998b. Fibroblast Growth Factor (FGF) Soluble Receptor 1 Acts as a Natural Inhibitor of FGF2

Neurotrophic Activity during Retinal Degeneration. *Molecular Biology of the Cell,* 9**,** 2785-2802.

GUPTA, S., DEEPTI, A., DEEGAN, S., LISBONA, F., HETZ, C. & SAMALI, A. 2010. HSP72 Protects Cells from ER Stress-induced Apoptosis via Enhancement of IRE1α-XBP1 Signaling through a Physical Interaction. *PLoS Biol,* 8**,** e1000410.

HABERLAND, M., MONTGOMERY, R. & OLSON, E. 2009. The many roles of histone deacetylases in development and physiology: implications for disease and therapy. *Nat Rev Genet,* Jan**,** 32-42.

HACKAM, A. S., STROM, R., LIU, D., QIAN, J., WANG, C., OTTESON, D., GUNATILAKA, T., FARKAS, R. H., CHOWERS, I., KAGEYAMA, M., LEVEILLARD, T., SAHEL, J.-A., CAMPOCHIARO, P. A., PARMIGIANI, G. & ZACK, D. J. 2004. Identification of Gene Expression Changes Associated with the Progression of Retinal Degeneration in the rd1 Mouse. *Investigative Ophthalmology & Visual Science,* 45**,** 2929-2942.

HAENNI, S. S., HASSA, P. O., ALTMEYER, M., FEY, M., IMHOF, R. & HOTTIGER, M. O. 2008. Identification of lysines 36 and 37 of PARP-2 as targets for acetylation and auto-ADP-ribosylation. *The International Journal of Biochemistry & Cell Biology,* 40**,** 2274-2283.

HAGEMAN, J., RUJANO, M. A., VAN WAARDE, M. A. W. H., KAKKAR, V., DIRKS, R. P., GOVORUKHINA, N., OOSTERVELD-HUT, H. M. J., LUBSEN, N. H. & KAMPINGA, H. H. 2010. A DNAJB Chaperone Subfamily with HDAC-Dependent Activities Suppresses Toxic Protein Aggregation. *Molecular Cell,* 37**,** 355-369.

HAMEL, C. 2006. Retinitis pigmentosa. *Orphanet Journal of Rare Diseases,* 1**,** 40.

HAN, J., SACHDEV, P. S. & SIDHU, K. S. 2010. A Combined Epigenetic and Non-Genetic Approach for Reprogramming Human Somatic Cells. *PLoS ONE,* 5**,** e12297.

HARTL, F. U. & HAYER-HARTL, M. 2002. Molecular Chaperones in the Cytosol: from Nascent Chain to Folded Protein. *Science,* 295**,** 1852-1858.

HARTONG, D. T., BERSON, E. L. & DRYJA, T. P. 2006. Retinitis pigmentosa. *The Lancet,* 368**,** 1795-1809.

HASSA, P. O., HAENNI, S. S., BUERKI, C., MEIER, N. I., LANE, W. S., OWEN, H., GERSBACH, M., IMHOF, R. & HOTTIGER, M. O. 2005. Acetylation of Poly(ADP-ribose) Polymerase-1 by p300/CREB-binding Protein Regulates Coactivation of NF-κB-dependent Transcription. *Journal of Biological Chemistry,* 280**,** 40450-40464.

HAUCK, S. M., EKSTRÖM, P. A. R., AHUJA-JENSEN, P., SUPPMANN, S., PAQUET-DURAND, F., VAN VEEN, T. & UEFFING, M. 2006. Differential Modification of Phosducin Protein in Degenerating rd1 Retina Is Associated

with Constitutively Active Ca2+/Calmodulin Kinase II in Rod Outer Segments. *Mol Cell Proteomics,* 5**,** 324-336.

HAWKINS, R. K., JANSEN, H. G. & SANYAL, S. 1985. Development and degeneration of retina in rds mutant mice: Photoreceptor abnormalities in the heterozygotes. *Experimental Eye Research,* 41**,** 701-720.

HECK, M. & HOFMANN, K. P. 2001. Maximal Rate and Nucleotide Dependence of Rhodopsin-catalyzed Transducin Activation. *Journal of Biological Chemistry,* 276**,** 10000-10009.

HENNIG, A. K., PENG, G.-H. & CHEN, S. 2008. Regulation of photoreceptor gene expression by Crx-associated transcription factor network. *Brain Research,* 1192**,** 114-133.

ISHIGURO, S., FUKUDA, K., KANNO, C. & MIZUNO, K. 1987. Accumulation of immunoreactive opsin on plasma membranes in degenerating rod cells of rd/rd mutant mice. *Cell Struct Funct,* Apr**,** 141-55.

JALIFFA, C., AMEQRANE, I., DANSAULT, A., LEEMPUT, J., VIEIRA, V., LACASSAGNE, E., PROVOST, A., BIGOT, K., MASSON, C., MENASCHE, M. & ABITBOL, M. 2009. Sirt1 Involvement in rd10 Mouse Retinal Degeneration. *Investigative Ophthalmology & Visual Science,* 50**,** 3562-3572.

JEON, C.-J., STRETTOI, E. & MASLAND, R. H. 1998. The Major Cell Populations of the Mouse Retina. *The Journal of Neuroscience,* 18**,** 8936-8946.

JIA, H., PALLOS, J., JACQUES, V., LAU, A., TANG, B., COOPER, A., SYED, A., PURCELL, J., CHEN, Y., SHARMA, S., SANGREY, G., DARNELL, S., PLASTERER, H., SADRI-VAKILI, G., GOTTESFELD, J., THOMPSON, L., RUSCHE, J., MARSH, J. & THOMAS, E. 2012. Histone deacetylase (HDAC) inhibitors targeting HDAC3 and HDAC1 ameliorate polyglutamine-elicited phenotypes in model systems of Huntington's disease. *Neurobiol Dis,* May**,** 351-61.

JOHNSON, L., VEEN, T. & EKSTRÖM, P. R. 2005. Differential Akt activation in the photoreceptors of normal and rd1 mice. *Cell and Tissue Research,* 320**,** 213-222.

JONES, P. 2012. Functions of DNA methylation: islands, start sites, gene bodies and beyond. *Nat Rev Genet,* May 29**,** 484-92.

JONES, P. & LIANG, G. 2009. Rethinking how DNA methylation patterns are maintained. *Nat Rev Genet,* Nov**,** 805-11.

KALKHOVEN, E. 2004. CBP and p300: HATs for different occasions. *Biochemical Pharmacology,* 68**,** 1145-1155.

KAMINSKYY, V. O., SUROVA, O. V., VACULOVA, A. & ZHIVOTOVSKY, B. 2011. Combined inhibition of DNA methyltransferase and histone deacetylase

restores caspase-8 expression and sensitizes SCLC cells to TRAIL. *Carcinogenesis,* 32**,** 1450-1458.

KARLSTETTER, M., EBERT, S. & LANGMANN, T. 2010. Microglia in the healthy and degenerating retina: Insights from novel mouse models. *Immunobiology,* 215**,** 685-691.

KAUR, C., HAO, A.-J., WU, C.-H. & LING, E.-A. 2001. Origin of microglia. *Microscopy Research and Technique,* 54**,** 2-9.

KAUR, J., MENCL, S., SAHABOGLU, A., FARINELLI, P., VAN VEEN, T., ZRENNER, E., EKSTRÖM, P., PAQUET-DURAND, F. & ARANGO-GONZALEZ, B. 2011. Calpain and PARP Activation during Photoreceptor Cell Death in P23H and S334ter Rhodopsin Mutant Rats. *PLoS ONE,* 6**,** e22181.

KAYAMA, M., NAKAZAWA, T., THANOS, A., MORIZANE, Y., MURAKAMI, Y., THEODOROPOULOU, S., ABE, T., VAVVAS, D. & MILLER, J. W. 2011. Heat Shock Protein 70 (HSP70) Is Critical for the Photoreceptor Stress Response after Retinal Detachment via Modulating Anti-Apoptotic Akt Kinase. *The American Journal of Pathology,* 178**,** 1080-1091.

KEE, H. J., EOM, G. H., JOUNG, H., SHIN, S., KIM, J.-R., CHO, Y. K., CHOE, N., SIM, B.-W., JO, D., JEONG, M. H., KIM, K. K., SEO, J.-S. & KOOK, H. 2008. Activation of Histone Deacetylase 2 by Inducible Heat Shock Protein 70 in Cardiac Hypertrophy. *Circulation Research,* 103**,** 1259-1269.

KEELER 1966. Retinal Degeneration in the Mouse Is Rodless Retina. *Journal of Heredity,* 57**,** 47-50.

KEKATPURE, V. D., DANNENBERG, A. J. & SUBBARAMAIAH, K. 2009. HDAC6 Modulates Hsp90 Chaperone Activity and Regulates Activation of Aryl Hydrocarbon Receptor Signaling. *Journal of Biological Chemistry,* 284**,** 7436-7445.

KING, G., ROSENE, D. & ABRAHAM, C. 2011. Promoter methylation and age-related downregulation of Klotho in rhesus monkey. *AGE***,** 1-15.

KINNEY, S. & PRADHAN, S. 2011. Regulation of expression and activity of DNA (cytosine-5) methyltransferases in mammalian cells. *Prog Mol Biol Transl Sci,* 101**,** 311-33.

KISER, P. D., GOLCZAK, M., MAEDA, A. & PALCZEWSKI, K. 2012. Key enzymes of the retinoid (visual) cycle in vertebrate retina. *Biochimica et Biophysica Acta (BBA) - Molecular and Cell Biology of Lipids,* 1821**,** 137-151.

KOCH, S., SOTHILINGAM, V., GARCIA GARRIDO, M., TANIMOTO, N., BECIROVIC, E., KOCH, F., SEIDE, C., BECK, S. C., SEELIGER, M. W., BIEL, M., MÜHLFRIEDEL, R. & MICHALAKIS, S. 2012. Gene therapy restores vision and delays degeneration in the CNGB1−/− mouse model of retinitis pigmentosa. *Human Molecular Genetics,* 21**,** 4486-4496.

KOMEIMA, K., ROGERS, B. S., LU, L. & CAMPOCHIARO, P. A. 2006. Antioxidants reduce cone cell death in a model of retinitis pigmentosa. *Proceedings of the National Academy of Sciences,* 103**,** 11300-11305.

KROEGER, H., CHIANG, W.-C. & LIN, J. 2012. Endoplasmic Reticulum-Associated Degradation (ERAD) of Misfolded Glycoproteins and Mutant P23H Rhodopsin in Photoreceptor Cells. *In:* LAVAIL, M. M., ASH, J. D., ANDERSON, R. E., HOLLYFIELD, J. G. & GRIMM, C. (eds.) *Retinal Degenerative Diseases.* Springer US.

KRUSZEWSKI, M. & SZUMIEL, I. 2005. Sirtuins (histone deacetylases III) in the cellular response to DNA damage--facts and hypotheses. *DNA Repair (Amst),* Nov 21**,** 1306-13.

KUHNE 1879. Chemische Vorgange in der Netzhaut
In: . *Handb. der Physiol.,* Leipzig 3 (1).

KURO-O, M. 2009. Klotho and aging. *Biochimica et Biophysica Acta (BBA) - General Subjects,* 1790**,** 1049-1058.

KURO-O, M., MATSUMURA, Y., AIZAWA, H., KAWAGUCHI, H., SUGA, T., UTSUGI, T., OHYAMA, Y., KURABAYASHI, M., KANAME, T., KUME, E., IWASAKI, H., IIDA, A., SHIRAKI-IIDA, T., NISHIKAWA, S., NAGAI, R. & NABESHIMA, Y. 1997. Mutation of the mouse klotho gene leads to a syndrome resembling ageing. *Nature,* Nov 6**,** 45-51.

KUROSU, H., OGAWA, Y., MIYOSHI, M., YAMAMOTO, M., NANDI, A., ROSENBLATT, K. P., BAUM, M. G., SCHIAVI, S., HU, M.-C., MOE, O. W. & KURO-O, M. 2006. Regulation of Fibroblast Growth Factor-23 Signaling by Klotho. *J Biol Chem,* 281**,** 6120-6123.

KUROSU, H., YAMAMOTO, M., CLARK, J. D., PASTOR, J. V., NANDI, A., GURNANI, P., MCGUINNESS, O. P., CHIKUDA, H., YAMAGUCHI, M., KAWAGUCHI, H., SHIMOMURA, I., TAKAYAMA, Y., HERZ, J., KAHN, C. R., ROSENBLATT, K. P. & KURO-O, M. 2005. Suppression of Aging in Mice by the Hormone Klotho. *Science,* 309**,** 1829-1833.

LANGMANN, T. 2007. Microglia activation in retinal degeneration. *Journal of Leukocyte Biology,* 81**,** 1345-1351.

LAU, D., MCGEE, L. H., ZHOU, S., RENDAHL, K. G., MANNING, W. C., ESCOBEDO, J. A. & FLANNERY, J. G. 2000. Retinal Degeneration Is Slowed in Transgenic Rats by AAV-Mediated Delivery of FGF-2. *Investigative Ophthalmology & Visual Science,* 41**,** 3622-3633.

LAVAIL, M. M., MATTHES, M. T., YASUMURA, D. & STEINBERG, R. H. 1997. Variability in Rate of Cone Degeneration in the Retinal Degeneration (rd/rd) Mouse. *Experimental Eye Research,* 65**,** 45-50.

LEE, J., JEONG, D.-J., KIM, J., LEE, S., PARK, J.-H., CHANG, B., JUNG, S.-I., YI, L., HAN, Y., YANG, Y., KIM, K., LIM, J.-S., YANG, I., JEON, S., BAE, D., KIM, C.-J. & LEE, M.-S. 2010. The anti-aging gene KLOTHO is a novel

target for epigenetic silencing in human cervical carcinoma. *Molecular Cancer,* 9**,** 109.

LENG, Y., LIANG, M.-H., REN, M., MARINOVA, Z., LEEDS, P. & CHUANG, D.-M. 2008. Synergistic Neuroprotective Effects of Lithium and Valproic Acid or Other Histone Deacetylase Inhibitors in Neurons: Roles of Glycogen Synthase Kinase-3 Inhibition. *The Journal of Neuroscience,* 28**,** 2576-2588.

LESKOV, I. B., KLENCHIN, V. A., HANDY, J. W., WHITLOCK, G. G., GOVARDOVSKII, V. I., BOWNDS, M. D., LAMB, T. D., PUGH JR, E. N. & ARSHAVSKY, V. Y. 2000. The Gain of Rod Phototransduction: Reconciliation of Biochemical and Electrophysiological Measurements. *Neuron,* 27**,** 525-537.

LEVEILLARD, T., MOHAND-SAID, S., LORENTZ, O., HICKS, D., FINTZ, A.-C., CLERIN, E., SIMONUTTI, M., FORSTER, V., CAVUSOGLU, N., CHALMEL, F., DOLLE, P., POCH, O., LAMBROU, G. & SAHEL, J.-A. 2004. Identification and characterization of rod-derived cone viability factor. *Nat Genet,* 36**,** 755-759.

LI, E. 2002. Chromatin modification and epigenetic reprogramming in mammalian development. *Nat Rev Genet,* 3**,** 662-673.

LI, Y., TSAI, Y., HSU, C., EROL, D., YANG, J., WU, W., DAVIS, R., EGLI, D. & TSANG, S. 2012. Long-term safety and efficacy of human-induced pluripotent stem cell (iPS) grafts in a preclinical model of retinitis pigmentosa. *Mol Med,* Dec 6**,** 1312-9.

LINDQUIST, S. 1986. The Heat-Shock Response. *Annual Review of Biochemistry,* 55**,** 1151-1191.

LIU, C., LI, Y., PENG, M., LATIES, A. M. & WEN, R. 1999. Activation of Caspase-3 in the Retina of Transgenic Rats with the Rhodopsin Mutation S334ter during Photoreceptor Degeneration. *J Neurosci,* 19**,** 4778-4785.

LIU, X., GARRIGA, P. & KHORANA, H. G. 1996. Structure and function in rhodopsin: correct folding and misfolding in two point mutants in the intradiscal domain of rhodopsin identified in retinitis pigmentosa. *Proceedings of the National Academy of Sciences,* 93**,** 4554-4559.

MACDONALD, J. L. & ROSKAMS, A. J. 2009. Epigenetic regulation of nervous system development by DNA methylation and histone deacetylation. *Progress in Neurobiology,* 88**,** 170-183.

MARC, R., MURRY, R. & BASINGER, S. 1995. Pattern recognition of amino acid signatures in retinal neurons. *The Journal of Neuroscience,* 15**,** 5106-5129.

MARINOVA, Z., LENG, Y., LEEDS, P. & CHUANG, D.-M. 2011. Histone deacetylase inhibition alters histone methylation associated with heat shock protein 70 promoter modifications in astrocytes and neurons. *Neuropharmacology,* 60**,** 1109-1115.

MARINOVA, Z., REN, M., WENDLAND, J. R., LENG, Y., LIANG, M.-H., YASUDA, S., LEEDS, P. & CHUANG, D.-M. 2009. Valproic acid induces functional heat-shock protein 70 via Class I histone deacetylase inhibition in cortical neurons: a potential role of Sp1 acetylation. *Journal of Neurochemistry,* 111**,** 976-987.

MARSHAK, D. W. 1989. Peptidergic neurons of the macaque monkey retina. *Neuroscience Research Supplements,* 10**,** S117-S130.

MARTINEZ-NAVARRETE, G., SEILER, M., ARAMANT, R., FERNANDEZ-SANCHEZ, L., PINILLA, I. & CUENCA, N. 2011. Retinal degeneration in two lines of transgenic S334ter rats. *Exp Eye Res,* Mar**,** 227-37.

MASLAND, R. H. 2001. The fundamental plan of the retina. *Nat Neurosci,* 4**,** 877-886.

MASSEY, S. C. & REDBURN, D. A. 1987. Transmitter circuits in the vertebrate retina. *Progress in Neurobiology,* 28**,** 55-96.

MENDES, H. F., VAN DER SPUY, J., CHAPPLE, J. P. & CHEETHAM, M. E. 2005. Mechanisms of cell death in rhodopsin retinitis pigmentosa: implications for therapy. *Trends in molecular medicine,* 11**,** 177-185.

MENU DIT HUART, L., LORENTZ, O., GOUREAU, O., LÉVEILLARD, T. & SAHEL, J. A. 2004. DNA repair in the degenerating mouse retina. *Molecular and Cellular Neuroscience,* 26**,** 441-449.

MILLER, R. F. 2008. Cell Communication Mechanisms in the Vertebrate Retina The Proctor Lecture. *Investigative Ophthalmology & Visual Science,* 49**,** 5184-5198.

MOCKEL, A., PERDOMO, Y., STUTZMANN, F., LETSCH, J., MARION, V. & DOLLFUS, H. 2011. Retinal dystrophy in Bardet–Biedl syndrome and related syndromic ciliopathies. *Progress in Retinal and Eye Research,* 30**,** 258-274.

MOHAND-SAID, S., DEUDON-COMBE, A., HICKS, D., SIMONUTTI, M., FORSTER, V., FINTZ, A.-C., LÉVEILLARD, T., DREYFUS, H. & SAHEL, J.-A. 1998. Normal retina releases a diffusible factor stimulating cone survival in the retinal degeneration mouse. *Proceedings of the National Academy of Sciences,* 95**,** 8357-8362.

MOLDAY, R. S., HICKS, D. & MOLDAY, L. 1987. Peripherin. A rim-specific membrane protein of rod outer segment discs. *Investigative Ophthalmology & Visual Science,* 28**,** 50-61.

MONSEY, M. S., OTA, K. T., AKINGBADE, I. F., HONG, E. S. & SCHAFE, G. E. 2011. Epigenetic Alterations Are Critical for Fear Memory Consolidation and Synaptic Plasticity in the Lateral Amygdala. *PLoS ONE,* 6**,** e19958.

MORRISON, B. E., MAJDZADEH, N. & D'MELLO, S. R. 2007. Histone deacetylases: Focus on the nervous system. *Cellular and Molecular Life Sciences,* 64**,** 2258-2269.

MUCHOWSKI, P. J. 2002. Protein Misfolding, Amyloid Formation, and Neurodegeneration: A Critical Role for Molecular Chaperones? *Neuron,* 35**,** 9-12.

MUNSHI, A., SHAFI, G., ALIYA, N. & JYOTHY, A. 2009. Histone modifications dictate specific biological readouts. *Journal of Genetics and Genomics,* 36**,** 75-88.

MÜNZEL, M., GLOBISCH, D., BRÜCKL, T., WAGNER, M., WELZMILLER, V., MICHALAKIS, S., MÜLLER, M., BIEL, M. & CARELL, T. 2010. Quantification of the Sixth DNA Base Hydroxymethylcytosine in the Brain. *Angewandte Chemie International Edition,* 49**,** 5375-5377.

MUSTAFI, D., ENGEL, A. H. & PALCZEWSKI, K. 2009. Structure of cone photoreceptors. *Progress in Retinal and Eye Research,* 28**,** 289-302.

NAWY, S. & JAHR, C. E. 1990. Suppression by glutamate of cGMP-activated conductance in retinal bipolar cells. *Nature,* 346**,** 269-271.

NAWY, S. & JAHR, C. E. 1991. cGMP-gated conductance in retinal bipolar cells is suppressed by the photoreceptor transmitter. *Neuron,* 7**,** 677-683.

NEUPERT , W. & BRUNNER, M. 2002. The protein import motor of mitochondria. *Nat Rev Mol Cell Biol,* Aug**,** 555-65.

NEWMAN, E. & REICHENBACH, A. 1996. The Müller cell: a functional element of the retina. *Trends in Neurosciences,* 19**,** 307-312.

NISHIOKA, C., IKEZOE, T., YANG, J., UDAKA, K. & YOKOYAMA, A. 2011. Simultaneous inhibition of DNA methyltransferase and histone deacetylase induces p53-independent apoptosis via down-regulation of Mcl-1 in acute myelogenous leukemia cells. *Leukemia research,* 35**,** 932-939.

NISSIM, I., HARDY, M., PLEASURE, J., NISSIM, I. & STATES, B. 1992. A mechanism of glycine and alanine cytoprotective action: stimulation of stress-induced HSP70 mRNA. *Kidney Int,* Sep**,** 775-82.

OH, K. T., LONGMUIR, R., OH, D. M., STONE, E. M., KOPP, K., BROWN, J., FISHMAN, G. A., SONKIN, P., GEHRS, K. M. & WELEBER, R. G. 2003. Comparison of the clinical expression of retinitis pigmentosa associated with rhodopsin mutations at codon 347 and codon 23. *American journal of ophthalmology,* 136**,** 306-313.

OHNISHI, K., WANG, X., TAKAHASHI, A., MATSUMOTO, H. & OHNISHI, T. 1999. The protein kinase inhibitor, H-7, suppresses heat induced activation of heat shock transcription factor 1. *Mol Cell Biochem,* Jul**,** 129-35.

PALCZEWSKI, K., SUBBARAYA, I., GORCZYCA, W. A., HELEKAR, B. S., RUIZ, C. C., OHGURO, H., HUANG, J., ZHAO, X., CRABB, J. W., JOHNSON, R. S., WALSH, K. A., GRAY-KELLER, M. P., DETWILER, P. B. & BAEHR, W. 1994. Molecular cloning and characterization of retinal photoreceptor guanylyl cyclase-activating protein. *Neuron,* 13**,** 395-404.

PALHAN, V. B., CHEN, S., PENG, G.-H., TJERNBERG, A., GAMPER, A. M., FAN, Y., CHAIT, B. T., LA SPADA, A. R. & ROEDER, R. G. 2005. Polyglutamine-expanded ataxin-7 inhibits STAGA histone acetyltransferase activity to produce retinal degeneration. *Proceedings of the National Academy of Sciences of the United States of America,* 102**,** 8472-8477.

PAN, J., ZHONG, J., GAN, L., CHEN, S., JIN, H., WANG, X. & WANG, L. 2011. Klotho, an anti-senescence related gene, is frequently inactivated through promoter hypermethylation in colorectal cancer. *Tumor Biology,* 32**,** 729-735.

PAQUET-DURAND, F., AZADI, S., HAUCK, S. M., UEFFING, M., VAN VEEN, T. & EKSTRÖM, P. 2006. Calpain is activated in degenerating photoreceptors in the rd1 mouse. *J Neurochem,* 96**,** 802-814.

PAQUET-DURAND, F., HAUCK, S. M., VAN VEEN, T., UEFFING, M. & EKSTRÖM, P. 2009. PKG activity causes photoreceptor cell death in two retinitis pigmentosa models. *J Neurochem,* 108**,** 796-810.

PAQUET-DURAND, F., SILVA, J., TALUKDAR, T., JOHNSON, L. E., AZADI, S., VAN VEEN, T., UEFFING, M., HAUCK, S. M. & EKSTRÖM, P. A. R. 2007. Excessive Activation of Poly(ADP-Ribose) Polymerase Contributes to Inherited Photoreceptor Degeneration in the Retinal Degeneration 1 Mouse. *J Neurosci,* 27**,** 10311-10319.

PENG, G.-H. & CHEN, S. 2007. Crx activates opsin transcription by recruiting HAT-containing co-activators and promoting histone acetylation. *Human Molecular Genetics,* 16**,** 2433-2452.

PFAFFL, M. 2001. A new mathematical model for relative quantification in real-time RT-PCR. *Nucleic Acids Research,* May 1**,** e45.

PIERCE, E. A. 2001. Pathways to photoreceptor cell death in inherited retinal degenerations. *BioEssays,* 23**,** 605-618.

PILZ, R. & BRODERICK, K. 2005. Role of cyclic GMP in gene regulation. *Front Biosci,* May 1**,** 1239-68.

PIRKKALA, L., NYKANEN, P. & SISTONEN, L. 2001. Roles of the heat shock transcription factors in regulation of the heat shock response and beyond. *The FASEB Journal,* 15**,** 1118-1131.

POCHÉ, R. A. & REESE, B. E. 2009. Retinal horizontal cells: challenging paradigms of neural development and cancer biology. *Development,* 136**,** 2141-2151.

PRATT, W. B. & TOFT, D. O. 2003. Regulation of Signaling Protein Function and Trafficking by the hsp90/hsp70-Based Chaperone Machinery. *Experimental Biology and Medicine,* 228**,** 111-133.

PRICE, B. A., SANDOVAL, I. M., CHAN, F., SIMONS, D. L., WU, S. M., WENSEL, T. G. & WILSON, J. H. 2011. Mislocalization and Degradation of Human P23H-Rhodopsin-GFP in a Knockin Mouse Model of Retinitis Pigmentosa. *Invest Ophthalmol Vis Sci,* 52**,** 9728-9736.

RAJAMOHAN, S. B., PILLAI, V. B., GUPTA, M., SUNDARESAN, N. R., BIRUKOV, K. G., SAMANT, S., HOTTIGER, M. O. & GUPTA, M. P. 2009. SIRT1 Promotes Cell Survival under Stress by Deacetylation-Dependent Deactivation of Poly(ADP-Ribose) Polymerase 1. *Molecular and Cellular Biology,* 29**,** 4116-4129.

RAJAN & KOPITO 2005. Suppression of wild-type rhodopsin maturation by mutants linked to autosomal dominant retinitis pigmentosa. *J Biol Chem,* Jan 14**,** 1284-91.

RAO-MIROTZNIK, R., HARKINS, A. B., BUCHSBAUM, G. & STERLING, P. 1995. Mammalian rod terminal: Architecture of a binary synapse. *Neuron,* 14**,** 561-569.

REICHENBACH & ROBINSON 1995. The involvement of Müller cells in the outer retina. *Neurobiology and clinical aspects of the outer retina,* London: Chapman & Hall**,** 395-416.

REITER, C. E. N., SANDIRASEGARANE, L., WOLPERT, E. B., KLINGER, M., SIMPSON, I. A., BARBER, A. J., ANTONETTI, D. A., KESTER, M. & GARDNER, T. W. 2003. Characterization of insulin signaling in rat retina in vivo and ex vivo. *American Journal of Physiology - Endocrinology And Metabolism,* 285**,** E763-E774.

ROHRER, B., PINTO, F. R., HULSE, K. E., LOHR, H. R., ZHANG, L. & ALMEIDA, J. S. 2004. Multidestructive Pathways Triggered in Photoreceptor Cell Death of the RD Mouse as Determined through Gene Expression Profiling. *Journal of Biological Chemistry,* 279**,** 41903-41910.

ROUAUX, C., PANTELEEVA, I., RENÉ, F., GONZALEZ DE AGUILAR, J.-L., ECHANIZ-LAGUNA, A., DUPUIS, L., MENGER, Y., BOUTILLIER, A.-L. & LOEFFLER, J.-P. 2007. Sodium Valproate Exerts Neuroprotective Effects In Vivo through CREB-Binding Protein-Dependent Mechanisms But Does Not Improve Survival in an Amyotrophic Lateral Sclerosis Mouse Model. *The Journal of Neuroscience,* 27**,** 5535-5545.

ROUNTREE, M. R., BACHMAN, K. E. & BAYLIN, S. B. 2000. DNMT1 binds HDAC2 and a new co-repressor, DMAP1, to form a complex at replication foci. *Nat Genet,* 25**,** 269-277.

RYAN, M. & PFANNER, N. 2001. Hsp70 proteins in protein translocation. *Adv Protein Chem***,** 223-42.

RYU, H., LEE, J., OLOFSSON, B. A., MWIDAU, A., DEODOGLU, A., ESCUDERO, M., FLEMINGTON, E., AZIZKHAN-CLIFFORD, J., FERRANTE, R. J. & RATAN, R. R. 2003. Histone deacetylase inhibitors prevent oxidative neuronal death independent of expanded polyglutamine repeats via an Sp1-dependent pathway. *Proceedings of the National Academy of Sciences,* 100**,** 4281-4286.

SAGAR, S. M. 1987. Somatostatin-like immunoreactive material in the rabbit retina: Immunohistochemical staining using monoclonal antibodies. *The Journal of Comparative Neurology,* 266**,** 291-299.

SAHABOGLU, A., PAQUET-DURAND, O., DIETTER, J., DENGLER, K., BERNHARD-KURZ, S., EKSTRÖM, P., HITZMANN, B., UEFFING, M. & PAQUET-DURAND, F. 2013. Retinitis pigmentosa: rapid neurodegeneration is governed by slow cell death mechanisms. *Cell Death Dis,* Feb 7**,** e488.

SAHABOGLU, A., TANIMOTO, N., KAUR, J., SANCHO-PELLUZ, J., HUBER, G., FAHL, E., ARANGO-GONZALEZ, B., ZRENNER, E., EKSTRÖM, P., LÖWENHEIM, H., SEELIGER, M. & PAQUET-DURAND, F. 2010. PARP1 Gene Knock-Out Increases Resistance to Retinal Degeneration without Affecting Retinal Function. *PLoS ONE,* 5**,** e15495.

SALIBA, R. S., MUNRO, P. M. G., LUTHERT, P. J. & CHEETHAM, M. E. 2002. The cellular fate of mutant rhodopsin: quality control, degradation and aggresome formation. *Journal of Cell Science,* 115**,** 2907-2918.

SANCHO-PELLUZ, J., ALAVI, M., SAHABOGLU, A., KUSTERMANN, S., FARINELLI, P., AZADI, S., VAN VEEN, T., ROMERO, F., PAQUET-DURAND, F. & EKSTRÖM, P. 2010. Excessive HDAC activation is critical for neurodegeneration in the rd1 mouse. *Cell Death Dis*.

SANCHO-PELLUZ, J., ARANGO-GONZALEZ, B., KUSTERMANN, S., ROMERO, F., VEEN, T., ZRENNER, E., EKSTRÖM, P. & PAQUET-DURAND, F. 2008. Photoreceptor Cell Death Mechanisms in Inherited Retinal Degeneration. *Molecular Neurobiology,* 38**,** 253-269.

SANYAL, S. & BAL, A. 1973. Comparative light and electron microscopic study of retinal histogenesis in normal and rd mutant mice. *Z Anat Entwicklungsgesch,* Oct 31**,** 219-38.

SANZ, M. M., JOHNSON, L. E., AHUJA, S., EKSTRÖM, P. A. R., ROMERO, J. & VAN VEEN, T. 2007. Significant photoreceptor rescue by treatment with a combination of antioxidants in an animal model for retinal degeneration. *Neuroscience,* 145**,** 1120-1129.

SCHIESSER, S., HACKNER, B., PFAFFENEDER, T., MÜLLER, M., HAGEMEIER, C., TRUSS, M. & CARELL, T. 2012. Mechanism and Stem-Cell Activity of 5-Carboxycytosine Decarboxylation Determined by Isotope Tracing. *Angewandte Chemie International Edition,* 51**,** 6516-6520.

SCHNITZER, J. 1988. Astrocytes in the guinea pig, horse, and monkey retina: Their occurrence coincides with the presence of blood vessels. *Glia,* 1**,** 74-89.

SCHREIBER, V., DANTZER, F., AME, J. & DE MURCIA, G. 2006. Poly(ADP-ribose): novel functions for an old molecule. *Nat Rev Mol Cell Biol,* Jul**,** 517-28.

SCROGGINS, B. T., ROBZYK, K., WANG, D., MARCU, M. G., TSUTSUMI, S., BEEBE, K., COTTER, R. J., FELTS, S., TOFT, D., KARNITZ, L., ROSEN,

N. & NECKERS, L. 2007. An Acetylation Site in the Middle Domain of Hsp90 Regulates Chaperone Function. *Molecular Cell,* 25**,** 151-159.

SERNAGOR, E., EGLEN, S. J. & WONG, R. O. L. 2001. Development of Retinal Ganglion Cell Structure and Function. *Progress in Retinal and Eye Research,* 20**,** 139-174.

SHEN, H.-Y., HE, J.-C., WANG, Y., HUANG, Q.-Y. & CHEN, J.-F. 2005. Geldanamycin Induces Heat Shock Protein 70 and Protects against MPTP-induced Dopaminergic Neurotoxicity in Mice. *Journal of Biological Chemistry,* 280**,** 39962-39969.

SHINDE, V. M., SIZOVA, O. S., LIN, J. H., LAVAIL, M. M. & GORBATYUK, M. S. 2012. ER Stress in Retinal Degeneration in S334ter Rho Rats. *PLoS ONE,* 7**,** e33266.

SIEVING, P. A., CARUSO, R. C., TAO, W., COLEMAN, H. R., THOMPSON, D. J. S., FULLMER, K. R. & BUSH, R. A. 2006. Ciliary neurotrophic factor (CNTF) for human retinal degeneration: Phase I trial of CNTF delivered by encapsulated cell intraocular implants. *Proceedings of the National Academy of Sciences of the United States of America,* 103**,** 3896-3901.

SIFFROI-FERNANDEZ, S., FELDER-SCHMITTBUHL, M.-P., KHANNA, H., SWAROOP, A. & HICKS, D. 2008. FGF19 Exhibits Neuroprotective Effects on Adult Mammalian Photoreceptors In Vitro. *Invest Ophthalmol Vis Sci,* 49**,** 1696-1704.

SOHOCKI, M. M., DAIGER, S. P., BOWNE, S. J., RODRIQUEZ, J. A., NORTHRUP, H., HECKENLIVELY, J. R., BIRCH, D. G., MINTZ-HITTNER, H., RUIZ, R. S., LEWIS, R. A., SAPERSTEIN, D. A. & SULLIVAN, L. S. 2001. Prevalence of mutations causing retinitis pigmentosa and other inherited retinopathies. *Human Mutation,* 17**,** 42-51.

SPARROW, D, H. & CP, H. 2010. The retinal pigment epithelium in health and disease. *Curr Mol Med,* Dec**,** 802-23.

STEENSMA, D. P. 2009. Decitabine treatment of patients with higher-risk myelodysplastic syndromes. *Leukemia Research,* 33, Supplement 2**,** S12-S17.

STEFANI, I., WRIGHT, D., POLIZZI, K. & KONTORAVDI, C. 2012. The role of ER stress-induced apoptosis in neurodegeneration. *Curr Alzheimer Res,* Mar**,** 373-87.

STEINBERG, R. H., LINSENMEIER, R. A. & GRIFF, E. R. 1983. Three light-evoked responses of the retinal pigment epithelium. *Vision Research,* 23**,** 1315-1323.

STERLING, P. & MATTHEWS, G. 2005. Structure and function of ribbon synapses. *Trends in Neurosciences,* 28**,** 20-29.

STONE, J. & DREHER, Z. 1987. Relationship between astrocytes, ganglion cells and vasculature of the retina. *The Journal of Comparative Neurology,* 255**,** 35-49.

STRAUSS, O. 2005. The Retinal Pigment Epithelium in Visual Function. *Physiological Reviews,* 85**,** 845-881.

STREILEIN, J. W., MA, N., WENKEL, H., FONG NG, T. & ZAMIRI, P. 2002. Immunobiology and privilege of neuronal retina and pigment epithelium transplants. *Vision Research,* 42**,** 487-495.

STRESEMANN, C. & LYKO, F. 2008. Modes of action of the DNA methyltransferase inhibitors azacytidine and decitabine. *International Journal of Cancer,* 123**,** 8-13.

STRETTOI, E. & MASLAND, R. 1995. The organization of the inner nuclear layer of the rabbit retina. *The Journal of Neuroscience,* 15**,** 875-888.

SUGIURA, H., YOSHIDA, T., MITOBE, M., YOSHIDA, S., SHIOHIRA, S., NITTA, K. & TSUCHIYA, K. 2010. Klotho reduces apoptosis in experimental ischaemic acute kidney injury via HSP-70. *Nephrol Dial Transplant,* 25**,** 60-68.

SUNG, C.-H. & CHUANG, J.-Z. 2010. The cell biology of vision. *The Journal of Cell Biology,* 190**,** 953-963.

SUNG, C.-H. & TAI, A. W. 2000. Rhodopsin Trafficking and its Role in Retinal Dystrophies. *In:* KWANG, W. J. (ed.) *International Review of Cytology.* Academic Press.

SUNG, C. H., SCHNEIDER, B. G., AGARWAL, N., PAPERMASTER, D. S. & NATHANS, J. 1991. Functional heterogeneity of mutant rhodopsins responsible for autosomal dominant retinitis pigmentosa. *Proc Natl Acad Sci U S A,* 88**,** 8840-8844.

TAI, A. W., CHUANG, J.-Z., BODE, C., WOLFRUM, U. & SUNG, C.-H. 1999. Rhodopsin's Carboxy-Terminal Cytoplasmic Tail Acts as a Membrane Receptor for Cytoplasmic Dynein by Binding to the Dynein Light Chain Tctex-1. *Cell,* 97**,** 877-887.

TAM, L. C. S., KIANG, A.-S., CAMPBELL, M., KEANEY, J., JANE FARRAR, G., HUMPHRIES, M. M., KENNA, P. F. & HUMPHRIES, P. 2010. Prevention of autosomal dominant retinitis pigmentosa by systemic drug therapy targeting heat shock protein 90 (Hsp90). *Human Molecular Genetics,* 19**,** 4421-4436.

TOMITA, H., SUGANO, E., FUKAZAWA, Y., ISAGO, H., SUGIYAMA, Y., HIROI, T., ISHIZUKA, T., MUSHIAKE, H., KATO, M., HIRABAYASHI, M., SHIGEMOTO, R., YAWO, H. & TAMAI, M. 2009. Visual properties of transgenic rats harboring the channelrhodopsin-2 gene regulated by the thy-1.2 promoter. *PLoS One,* Nov 5**,** e7679.

TRAVIS, G. H., SUTCLIFFE, J. G. & BOK, D. 1991. The retinal degeneration slow (rds) gene product is a photoreceptor disc membrane-associated glycoprotein. *Neuron,* 6**,** 61-70.

TRIFUNOVIĆ, D., DENGLER, K., MICHALAKIS, S., ZRENNER, E., WISSINGER, B. & PAQUET-DURAND, F. 2010. cGMP-dependent cone photoreceptor degeneration in the cpfl1 mouse retina. *The Journal of Comparative Neurology,* 518**,** 3604-3617.

TURNER, D. L. & CEPKO, C. L. 1987. A common progenitor for neurons and glia persists in rat retina late in development. *Nature,* 328**,** 131-136.

USHER 1914. On the inheritance of Retinitis pigmentosa with notes of cases. *Roy. Lond. Ophthalmol. Hosp. Rep. ,* 19**,** 130–236.

VANEY, D. I. & YOUNG, H. M. 1988. GABA-like immunoreactivity in cholinergic amacrine cells of the rabbit retina. *Brain Research,* 438**,** 369-373.

VECSEY, C. G., HAWK, J. D., LATTAL, K. M., STEIN, J. M., FABIAN, S. A., ATTNER, M. A., CABRERA, S. M., MCDONOUGH, C. B., BRINDLE, P. K., ABEL, T. & WOOD, M. A. 2007. Histone Deacetylase Inhibitors Enhance Memory and Synaptic Plasticity via CREB: CBP-Dependent Transcriptional Activation. *The Journal of Neuroscience,* 27**,** 6128-6140.

VISHNIVETSKIY, S. A., SCHUBERT, C., CLIMACO, G. C., GUREVICH, Y. V., VELEZ, M.-G. & GUREVICH, V. V. 2000. An Additional Phosphate-binding Element in Arrestin Molecule. *Journal of Biological Chemistry,* 275**,** 41049-41057.

WAGNER, M., HERMANNS, I., BITTINGER, F. & KIRKPATRICK, C. J. 1999. Induction of stress proteins in human endothelial cells by heavy metal ions and heat shock. *American Journal of Physiology - Lung Cellular and Molecular Physiology,* 277**,** L1026-L1033.

WALD, G. 1968. The Molecular Basis of Visual Excitation. *Nature,* 219**,** 800-807.

WALLACE, D. M., DONOVAN, M. & COTTER, T. G. 2006. Histone Deacetylase Activity Regulates Apaf-1 and Caspase 3 Expression in the Developing Mouse Retina. *Investigative Ophthalmology & Visual Science,* 47**,** 2765-2772.

WALLEN, E., BUETTNER, G. & MOSELEY, P. 1997. Oxidants differentially regulate the heat shock response. *Int J Hyperthermia,* Sep-Oct**,** 517-24.

WANG, Y., WANG, S.-Y., ZHANG, X.-H., ZHAO, M., HOU, C.-M., XU, Y.-J., DU, Z.-Y. & YU, X.-D. 2007. FK228 inhibits Hsp90 chaperone function in K562 cells via hyperacetylation of Hsp70. *Biochemical and Biophysical Research Communications,* 356**,** 998-1003.

WASSLE, H. & BOYCOTT, B. B. 1991. Functional architecture of the mammalian retina. *Physiological Reviews,* 71**,** 447-480.

WÄSSLE, H., HEINZE, L., IVANOVA, E., MAJUMDAR, S., WEISS, J., HARVEY, R. J. & HAVERKAMP, S. 2009. Glycinergic transmission in the mammalian retina. *Frontiers in Molecular Neuroscience,* 2.

WEN, X. R., LI, C., ZONG, Y. Y., YU, C. Z., XU, J., HAN, D. & ZHANG, G. Y. 2008. Dual inhibitory roles of geldanamycin on the c-Jun NH2-terminal kinase 3 signal pathway through suppressing the expression of mixed-lineage kinase 3 and attenuating the activation of apoptosis signal-regulating kinase 1 via facilitating the activation of Akt in ischemic brain injury. *Neuroscience,* 156**,** 483-497.

WERT, K. J., DAVIS, R. J., SANCHO-PELLUZ, J., NISHINA, P. M. & TSANG, S. H. 2013. Gene therapy provides long-term visual function in a pre-clinical model of retinitis pigmentosa. *Human Molecular Genetics,* 22**,** 558-567.

WILLBOLD, E. & LAYER, P. 1992. A Hidden Retinal Regenerative Capacity from the Chick Ciliary Margin is Reactivated In Vitro, that is Accompanied by Down-regulation of Butyrylcholinesterase. *Eur J Neurosci,* 4(3)**,** 210-220.

WOOD, J., ROGINA, B., LAVU, S., HOWITZ, K., HELFAND, S., TATAR, M. & SINCLAIR, D. 2004. Sirtuin activators mimic caloric restriction and delay ageing in metazoans. *Nature,* Aug 5**,** 686-9.

WU, X., GE, H., GUPTE, J., WEISZMANN, J., SHIMAMOTO, G., STEVENS, J., HAWKINS, N., LEMON, B., SHEN, W., XU, J., VENIANT, M. M., LI, Y.-S., LINDBERG, R., CHEN, J.-L., TIAN, H. & LI, Y. 2007. Co-receptor Requirements for Fibroblast Growth Factor-19 Signaling. *J Biol Chem,* 282**,** 29069-29072.

WU, X., REITER, C. E. N., ANTONETTI, D. A., KIMBALL, S. R., JEFFERSON, L. S. & GARDNER, T. W. 2004. Insulin Promotes Rat Retinal Neuronal Cell Survival in a p70S6K-dependent Manner. *Journal of Biological Chemistry,* 279**,** 9167-9175.

YAMAMOTO, M., CLARK, J. D., PASTOR, J. V., GURNANI, P., NANDI, A., KUROSU, H., MIYOSHI, M., OGAWA, Y., CASTRILLON, D. H., ROSENBLATT, K. P. & KURO-O, M. 2005. Regulation of Oxidative Stress by the Anti-aging Hormone Klotho. *J Biol Chem,* 280**,** 38029-38034.

YI, T., LI, J., HAN, X., GUO, J., QU, Q., GUO, L., SUN, H. & TAN, W. 2012. DNMT inhibitors and HDAC inhibitors regulate E-cadherin and Bcl-2 expression in endometrial carcinoma in vitro and in vivo. *Chemotherapy,* 58(1)**,** 19-2.

YOUNG, J. C. 2010. Mechanisms of the Hsp70 chaperone systemThis paper is one of a selection of papers published in this special issue entitled “Canadian Society of Biochemistry, Molecular & Cellular Biology 52nd Annual Meeting — Protein Folding: Principles and Diseases” and has undergone the Journal's usual peer review process. *Biochemistry and Cell Biology,* 88**,** 291-300.

YU, D.-Y. & CRINGLE, S. J. 2005. Retinal degeneration and local oxygen metabolism. *Experimental Eye Research,* 80**,** 745-751.

ZEISS, C. J., NEAL, J. & JOHNSON, E. A. 2004. Caspase-3 in Postnatal Retinal Development and Degeneration. *Investigative Ophthalmology & Visual Science,* 45**,** 964-970.

ZENCAK, D., SCHOUWEY, K., CHEN, D., EKSTRÖM, P., TANGER, E., BREMNER, R., VAN LOHUIZEN, M. & ARSENIJEVIC, Y. 2013. Retinal degeneration depends on Bmi1 function and reactivation of cell cycle proteins. *Proceedings of the National Academy of Sciences,* 110**,** E593–E601.

ZSCHOCKE, J., MANTHEY, D., BAYATTI, N., VAN DER BURG, B., GOODENOUGH, S. & BEHL, C. 2002. Estrogen Receptor α-mediated Silencing of Caveolin Gene Expression in Neuronal Cells. *Journal of Biological Chemistry,* 277**,** 38772-38780.

8. Summary in German

Retinitis Pigmentosa (RP) gehört zu einer Familie von neurodegenerativen Erkrankungen der Netzhaut, die gegenwärtig nicht behandelbar sind. Das Ziel dieser Doktorarbeit war es neue Marker für Netzhautdegeneration zu finden und zu erforschen, um so die Krankheit besser verstehen und die Entwicklung von neuroprotektiven Behandlungen vorantreiben zu können. In der Arbeit wurden vier verschiedene Nagermodelle für RP verwandt (*rd1* und *rd2* Mäuse; S334ter und P23H Ratten), welche es erlaubten mehrere neue Faktoren bei erblicher Netzhautdegeneration zu identifizieren. Dazu wurden eine Reihe von unterschiedlichen biochemischen, molekularbiologischer, und mikroskopischen Techniken verwandt und organotypische Kulturen untersucht. Die wichtigsten Ergebnisse dieser Doktorarbeit können wie folgt zusammengefasst werden:

1. α-Klotho war in absterbenden Photorezeptoren, in allen vier RP-Modellen, hochreguliert. Zugabe der ecto-domäne von α-Klotho zu organotypischen Netzhautkulturen verhinderte den normalen Aufbau der Netzhaut. Zudem war FGF15 in der *rd1* und *rd2* Netzhaut runterreguliert, was ein Ungleichgewicht in der α-Klotho/FGF15 Achse andeutet.

2. Klasse I und II Histondeacetylasen (HDAC) waren überaktiviert und spielten eine entscheidende Rolle für die Zelltodwege in der *rd1* Netzhaut. Inhibition der Klassen I und II dieser Enzymfamilie mit Trichostatin A (TSA) schützte Photorezeptoren *in vitro*.

3. Verstärkte DNA-Methylierung wurde in allen vier RP-Nager-Modellen gefunden. Kurzzeit-Behandlung mit Decitabine, einem spezifischen DNA-methyl-transferase (DNMT) Inhibitor, verlangsamte das Absterben von Photorezeptoren.

4. Erhöhte Expression von Hsp70 wurde in *rd1* Mäusen und S334ter Ratten gefunden und könnte auf frühe endogene neuroprotective Prozesse hindeuten. Da Hsp70 nicht mit späten Stressmarkern überlappte, könnte seine Expression Photorezeptoren schützen. Somit könnte die Induktion von Hsp70 Expression ein neuroprotektives Potenzial besitzen.

Zusammengefasst, hat diese Arbeit vier verschiedene und bislang unbekannte Faktoren bei erblicher Netzhautdegeneration aufgedeckt: Klotho, HDAC, DNMT und Hsp70. Diese Faktoren sind in verschiedenen RP Modellen entweder überexprimiert oder überaktiviert. Damit erhalten wir 1. Neue Einblicke in die Komplexität der degenerativen Prozesse, 2. Unterstützung für die Idee, dass unterschiedliche Mutationen in gemeinsame Zelltod-Stoffwechselwege münden können, 3. Ideen dafür wie neuartige neuroprotektive Strategien die nicht nur auf einzelnen Mutationen abzielen, entwickelt werden können.

9. Own contribution

Chapter 4.1

Perfomed all of the experiments and analysis except for qRT-PCR.

Chapter 4.2

Performed immunofluorescence on *wt* and *rd1* mice for acetyl-lysines and poly (ADP-ribose) polymers.

Chapter 4.3

Performed all of the experiments and analysis except for qRT-PCR and HPLC/MS/MS.

Chapter 4.4

Performed all of the experiments and analysis except for mathematical model of Hsp70 expression

10. Acknowledgements

Four years of hard work, with ups and downs, rare cheerful moments (rapidly brought back down to normal), and plenty waiting time, failed attempts and discouraging days (which never depressed me!). I have been annoyed at things a lot of the time. But the fact that I am here, trying to acknowledge a long list of people, means that I am very close to the end. Successfully? We will find out.

I am grateful to the Medical Faculty of the University of Lund and the Medical Faculty of the University of Tübingen that they have provided a frame for this thesis by making an Agreement of Cooperation ("EARNRET") with an exchange program that made this collaborative thesis work Tistou and Charlotte Kerstan Foundation, Tübingen.

My supervisors

Thank you Prof. **Eberhart Zrenner**. Being supervised by you is a huge privilege!

Per Ekström. I don't know why you hired me, I don't want to know. I am just very grateful and I hope you don't regret your decision. Thank you for being a wonderful person beyond an excellent boss. For being a friend and sometimes a sort of uncle. For being a colleague even before science days and sharing with me your passion for music. Thank you for supporting me and my new little family. There are all the makings of collaboration in the near future. I hope we will manage! For everything you have done for me with your praiseful discretion and I haven't even realized. Grazie Per!

People of Lund

Living in Lund has made me grow as a person. But in all honesty it hasn't been a piece of cake, especially in the first year. On the other hand, my life in the lab has always been great, fun and stimulating. To the people I met in the Division of Ophthalmology, Tack så mycket! And my apologies for not having learnt sufficiently your language.

Thank you to **Sten Andreasson**, one of the most gentle people I have ever met in my life. Thank you for inviting my girlfriend (now wife) to the dinner party and for regularly asking for news about our daughter. A special thanks goes to **Satpal Ahuja**, my first office mate for nearly 3 years. Thank you for teaching me many things and for your kindness. What can I say about **Maithe Perez**? So much knowledge in one Brazilian body. We had lovely and long chats about everything, from science to football, from cooking to politics. Is there anything we didn't talk about? Thank you for having three children (two of which are twins), it made my fatherhood less traumatic! I say thank you to **Frederik Ghosh**, for your funny attempts of speaking Italian. I will miss your "Arrivederci Roma!". A guitar player will always be my brother! Thank you **Ulrica Englund-Johansson**, for your friendship and for telling my once that I look nice even without beard (my wife doesn't think the same). The first time I met **Kirsten Wunderlich,** she seemed to me to be a stereotypical scientist and unwillingly made me think that probably I wouldn't fit in this job. Later in time, willingly, she made me understand the opposite. Thank you for being a very good friend and for inviting me to my first dinner out in Lund. A huge thank you goes to **Birgitta (Gitt) Klefbohm.** I lived in your apartment for my first two months here in Sweden. You took me sightseeing and pointed out the cheaper shops. Thank you for the priceless help in several experiments. **Hodan Adbshill**, what would have I done without you? What many people in the lab do without you? Simply indispensable! Thank you **Karin Arner**, for being a nearly inhexaustible source of suggestion, both scientific and personal. I had a very strange relationship with **Linnea Taylor**. In the beginning we totally ignored each other, then I introduce myself, but the situation didn't change much. Then we became friend on Facebook and started interacting commenting on each other status. We ended up being good friends. Thank you for sharing a bit of your excellent mind. **Gaelle (Piret)**, you became my office mate in the last part of my PhD. You became target of all my daily talking nonsense. Thank you for being a good friend to chat to and my congratulation for maintaining your sanity. Thank you **Erika Söderstjerna** for revealing yourself as the lovely person you are

People of Tübingen

I would like to turn my mind to **Theo van Veen**. During the few months before his retirement I had to do with him, I met a very smart, fun and sweet man. I would have been happy to talk more with you. Wherever you are, have a nice one! Thank you **Francois Paquet-Durand**. Despite few arguments we had (that we worked out) I always had, and still have, great regard of you. Thank you for teaching me many things, for being patient even when I behaved like a jerk. Thank you for hosting me in your beautiful house in the countryside and for introducing me to Leningrad Cowboys!

All my friends and colleagues in Tubingen must be acknowledge. **Blanca (Nena) Arango-Gonzalez** and **Jasvir Kaur** for being beautiful people and for their support in two of my projects. It was great to stroll around in Fort Lauderdale with you. **Tao Wei**, you are the most fun Chinese guy I have ever met (man man man man); unforgettable our basketball afternoons. **Wadood Haq**, I will always remember of you for your politeness, our long walk from the conference centre, through the beach to the hotel and your imitation of the Big Lebowsky. **Dragana Trifunovic**, grazie di avermi fatto respirare un po' della mia lingua! **Javier Sancho-Pelluz**, for being so different and so extraordinary! **Ronald Carpio**, well, you are living in Lund now. Anyway, you have been the first person I had a conversation with in Tubingen, thank you for your help anytime I asked you something. **Ayse Sahaboglu Tegkoz**, many times we tried to help each other: thank you for being a very honest person!

Friends at work

In Lund, not strictly belonging to my lab, there are several people I should say thank you. First in the list, I hope you don't mind, is **Emanuela Monni**: for being a great friend to me, Katie and Rowen as well. For supporting us personally and professionally. The door of our home will be always wide open for you! Thank you to **Marco Ledri**, the long chap! We have got many things in common (music and beer for instance, even if I cannot drink more than two), but getting along with you is the simplest and more natural thing. Rock & roll! **Shai Mulinari**, thank you for being my first real friend in Lund. Later on our roads strangely diverged in the same direction (fatherhood), but I will always remember as one of the brightest mind I have ever

met! A massive thanks to **Karthikeyan Devaraju**, for your friendship. Your support (and Monni's) has been extremely valuable for the qPCR. Thanks to **Zaza Kokaia**, for allowing me to use of the RNA bench. Thank you **Magnus Hillman**, you are a role model: the only man I know that has to deal with five women, that's brave! Anyway, thank you for your help with the spectrophotometer. **Dusan Zencak**, you came in Lund for a short period and we immediately became friends. Now you are on the other side of the world and our friendship in still strong. As I already mentioned, if I will go where I believe and you won't drop by, I will stop talking to you!

Friends outside work

Within the closest friends I have collected in Lund, the first mention belongs undoubtedly to **Carlo Proietti**. From a perfect unknown to my best friend or, as someone would remember, my wife. Lund gave me one of the funniest people existing as a friend. La grande arte! **Stefano Macrelli**, from the land of Lugaresi, thank you because you never manage to be anything but nice. I will miss the reflection from your forehead! **Luca Biondi**, the handsome one of the group. It's nice having someone that raises us above the average. We will never forget your mantra:"Nooo, it has never happen to me!". **Paolo Cifani**, my respect to the great captain of the rugby team! Few words for **Eugenio Gatto**: the first Italian met in Lund and who left one month later, have fun mate! **Francesca Battista**: the woman involved in everything! **Chiara Battistini**, **Erika Manesso**, **Lisa Carloni** (thanks for lending your car) and **Ilaria Jemos** to complete the "Francesca" group.

I must mention **Natalie Landeck**: flatties once, flatties forever! **Deepti Chugh, Litsa Nikitidou** and **Kerstin Buck**. Four of Rowen's aunties. **Miguel Angel Burguillos**, you are as crazy as my cousin, and impressively resembling.

Friends in Italy

Because I know that even if I am far away and we barely see once a year, our friendship is still strong and healthy. Too many names, you know who you are. Just a particular mention to my friends of beach-volley: thank you for clearly show how indispensable I am for the team!

Families

The biggest and warmest thank you goes to my families. My parents (**Paolo** and **Ivana**), sister (**Marzia**), brother in law (**Massimo**), my super sweet nephew (**Simone**) and all my other relatives. To my family in law: **Andrew**, **Lorraine**, **Beth** and **Paul.** To all of you, thank you for loving me, in your own way!

To my new beautiful family. **Katie** and **Rowen**, what would my life be without you? Instinctively, I would say that I might be sleeping more, no? Just joking. I would honestly be rotting in front of a computer. Katie, thank you for being the first and last thing I see every day, for pushing and supporting me, for your patience and your sweetness. For your craziness and your funny faces, for becoming my wife and for following me in a new adventure. And, Rowen, thank you for showing, after 15 months, that you love me. That really fills every gap, it puts flavours on dull days, it loosens every knot and brighten grey skies. Even though you still prefer Mamma. Love you madly! Both of you! And, while the submission procedures were ongoing, **Eli** was born, the little boy of the family, love you too…

11. CV

EDUCATION AND WORKING EXPERIENCES

Post-doc, University of Lausanne **Jan.2013 - Present**
"Functional characterisation of newly discovered proteins involved in retinal dystrophies". Supevisor: Dr. Carlo Rivolta

PhD student, University of Tübingen and Lund **Sept. 2008 - Dec.2012**
"Molecular mechanisms in inherited retinal degeneration''.
Supervisors: Prof. Dr. Med. Eberhart Zrenner and Dr. Per Ekström

MSc in Biomolecular and Cellular Sciences, University of Ferrara
Thesis: Molecular analysis of the circadian clock of the hypogean fish *Phreatichthys andruzzii*.
Supervisor: Dr. Cristiano Bertolucci

BSc in Biological Sciences, University of Ferrara, Italy
Dissertation thesis: "Human breast cancer cell line MDA-MB-231 expresses endogenous A_2B adenosine receptors mediating a Ca^{2+} signal".
Supervisor: Dr. Stefania Gessi

RESEARCH TECHNIQUES

- Immunohistochemistry and immunofluorescence
- Microscopy
- Western and Dot blot
- Immunoprecipitation
- MeDIP (Methylated DNA Immunoprecipitation)
- PCR, sequencing and genome screening
- Cloning
- Immune cell isolation and Ficoll gradients
- Intracellular Ca^{2+} quantification with FURA-2
- Cell and organotypic cultures
- Animal handling

ORAL PRESENTATIONS

Young Researchers Vision Camp, Leibertingen, Germany, June 2010.
Epigenetic markers in retinal degeneration.

Invited speaker at the department of evolution and genetics, University of Ferrara, March 2010
Excessive HDAC activation is critical for neurodegeneration in the *rd1* mouse.

POSTER PRESENTATIONS

Farinelli P, Paquet-Durand F, Zrenner E, Ekstrom P (2012). HSP70 may be involved in neuroprotective responses on *rd1* photoreceptors. ISER 2012. Program: 60. Tuesday, July 24

Farinelli P, Arango-Gonzalez B, Kaur J, Zrenner E, Paquet-Durand F, Ekstrom PA (2011). Enhanced detection of the antiaging protein α-Klotho in several rodent models of retinitis pigmentosa. *ARVO 2011*, Program#: 1814 Monday, May 02, 2011.

Farinelli P, Arango-Gonzalez B, Kaur J, Paquet-Durand F, Ekstrom PA (2010). Increased DNA Methylation in Several Animal Models of Retinitis Pigmentosa. *ARVO 2010*, Program#: 2234 Monday, May 03, 2010.

- *Awarded with travel grant from "Fondazione G.B. Bietti per l'oftalmologia".*

LANGUAGES

Native Italian speaker. Fluent in English. Basic French and Swedish.

PUBLICATIONS

Farinelli P, Arango-Gonzalez B, Zrenner E, Paquet-Durand F, Ekström P. Hsp70 temporarily protects photoreceptors in *rd1* mouse (2013) *(Manuscript in preparation).*

Farinelli P, Arango-Gonzalez B, Michalakis S, Perera A, Biel M, Zrenner E, Paquet-Durand F, Ekström P. (2013) Dying photoreceptors of murine models of RP display increased methylation of the DNA. *(Manuscript in preparation).*

Arango-Gonzalez B, Trifunović D, Sahaboglu A, Kranz K, Michalakis S, **Farinelli P**, Koch S, Koch F, Cottet S, Janssen-Bienhold U, Dedek K, Biel M, Zrenner E, Euler T, Ekström P, Ueffing M, Paquet-Durand F. (2013) Hereditary retinal degeneration: Prevalence of non-apoptotic over apoptotic cell death mechanisms (*Submitted*)

Farinelli P, Arango-Gonzalez B, Völkl J, Alesutan I, Lang F, Zrenner E, Paquet-Durand F, Ekström P. (2013) Retinitis Pigmentosa: Over-expression of anti-ageing protein Klotho in degenerating photoreceptors. (*Accepted*) *J Neurochem*. Jun 24.

Kaur J, Mencl S, Sahaboglu A, **Farinelli P**, van Veen T, Zrenner E, Ekstrom E, Paquet-Durand F, Arango-Gonzalez B (2011). Calpain and PARP Activation during Photoreceptor Cell Death in P23H and S334ter Rhodopsin Mutant Rats. *PLoS One*.

Sancho-Pelluz J, Alavi MV, Sahaboglu A, Kustermann S, **Farinelli P**, Azadi S, van Veen T, Romero FJ, Paquet-Durand F, Ekström P (2010). Excessive HDAC activation is critical for neurodegeneration in the *rd1* mouse. *Cell Death and Disease*, E-published February 11